THE UNIVERSITY OF CHICAGO

DYNAMIC STRUCTURE OF FUNCTIONAL NETWORKS DURING REACHING

A DISSERTATION SUBMITTED TO

THE FACULTY OF THE DIVISION OF THE BIOLOGICAL SCIENCES

AND THE PRITZKER SCHOOL OF MEDICINE

IN CANDIDACY FOR THE DEGREE OF

DOCTOR OF PHILOSOPHY

COMMITTEE ON COMPUTATIONAL NEUROSCIENCE

BY

MARINA JANELLE MORALES SUNDIANG

CHICAGO, ILLINOIS

MARCH 2023

COPYRIGHT

TABLE OF CONTENTS

LIST OF FIGURES

ACKNOWLEGEMENTS

Past and present members of the Hatsopoulos and MacLean Labs

Tony, Pat, Jo, Leon, Rosa, Betsy, Jeli, Midge, Ham, Rockstar, Raju, Iris, Zizou, and Jim

Animal Resources Center

Chicago Materials Research Center

The Neuroscience Institute, and The Department of Organismal Biology and Anatomy

Nicho Hatsopoulos. Jason MacLean, Matt Kaufman, and Dan Margoliash

ABSTRACT

Individual neurons are interconnected, resulting in coordinated patterns of activity and emergent population dynamics that underlie complex behavior. I investigated the time-varying co-activity of neural populations, summarized as functional networks (FN), and their relation to motor behavior. First, I found that the structure of FNs in the primary motor cortex of macaques performing an instructed-delay reaching task was specific to the instructed reach, and that FNs constructed from trials with closer reach directions are also closer in network space. I extended this analysis by computing co-activity within a short interval across time to construct temporal FNs. This revealed that reach-specific differences in FNs emerge shortly after instruction and, consequently, become decodable for reach direction. In fact, FNs provide an additional source of information about behavior beyond what is carried by firing rates alone. Next, in the sensorimotor cortex of a marmoset performing a self-initiated virtual prey capture task, FNs at specific task events (such as trial start, target presentation, etc.) can be discriminated based on its nearest neighbors using either a low-dimensional metric (distance in an embedding space) or a network alignment score. Partitioning temporal FNs based on structure showed FN states that corresponded to specific behaviors such as arm extension or licking, and that successful trials involve a stereotyped sequence of these states. These results suggest that FNs can provide novel insight on the statistical regularities of neural co-activity that produce neural population dynamics during voluntary goal-directed reaching behavior.

CHAPTER I. Introduction

Motor control as an insight into neural computation

Generating movements is a computational feat that the nervous system has evolved to accomplish flexibility and with little difficulty [1]. Within fractions of a second, we evaluate our environment and interpret sensory data, choose the best course of action, and then execute motor commands to precisely control our bodies to perform a task. We can learn new motor skills without forgetting already learned skills in our repertoire. Artificial systems which have surpassed human performance in single-tasks [2], are still eclipsed by the nervous systems' ability to generalize and flexibly switch from task to task using the same circuit. Understanding how a set of interconnected neurons form functional and versatile circuits has been an important endeavor in neuroscience and in the growing field of artificial general intelligence. Movement is a physical manifestation of the output of neural computations and therefore the study of sensorimotor control has the potential to uncover insight about the nature and workings of these computations.

The search for the neural correlates of movement started in the 19th century when the seminal experiment of Fritsch and Hitzig revealed that stimulation of parts of the cortex found that a) the cortex is excitable and b) that certain parts of the cortex, when stimulated, evoked muscle spasms from different parts of the body. This led to the discovery that there are anatomical delineations in the cortex that localize function; ie, the discovery of the "motor cortex" [3]. These experiments succeeded and confirmed the observations by John Hughlings-Jackson in 1873 that

[1] Wolpert, Diedrichsen, and Flanagan, "Principles of Sensorimotor Learning."
[2] Silver et al., "A General Reinforcement Learning Algorithm That Masters Chess, Shogi, and Go through Self-Play"; Schmidt and Schmied, "Fast and Data-Efficient Training of Rainbow"; OpenAI et al., "Dota 2 with Large Scale Deep Reinforcement Learning"; Baker et al., "Video PreTraining (VPT)."
[3] Taylor and Gross, "Twitches versus Movements: A Story of Motor Cortex."

patients with epilepsy exhibited seizures that would progress from one area to another in a systematic way [4] suggesting anatomical organization in the cortex.

A few years later, near the end of the century, Ramon y Cajal discovered that the nervous system is composed of individual neurons rather than a reticulum, a concept known as the neuron doctrine [5]. In the mid-20th century, single cell recordings techniques were developed [6], and the first experiments that related cell activity to movement took place. In a trilogy of experiments, Edward Evarts [7] recorded from pyramidal tract neurons during wrist movements and found that PTN activity showed a relationship to the presence and absence of movements, that responses to a stimulus preceded wrist movements, were related to force changes. These field-defining experiments were early examples of "representational" models which linked the activity of single neurons to specific aspects of the sensory input or the motor output.

Representational models suggest that aspects of the computation, such as encoding sensory information or producing descending motor commands, are reflected in the responses of single neurons, and, in order for movement to be generated, a series of transformations between different representation coordinates(input to output) must be performed. Subsequent studies following Evarts' findings aimed to link single-cell activity to different movement parameters and support

[4] Taylor and Gross.
[5] López-Muñoz, Boya, and Alamo, "Neuron Theory, the Cornerstone of Neuroscience, on the Centenary of the Nobel Prize Award to Santiago Ramón y Cajal."
[6] Li and Jasper, "Microelectrode Studies of the Electrical Activity of the Cerebral Cortex in the Cat"; Hubel, "Tungsten Microelectrode for Recording from Single Units."
[7] "Relation of Discharge Frequency to Conduction Velocity in Pyramidal Tract Neurons"; "Pyramidal Tract Activity Associated with a Conditioned Hand Movement in the Monkey."; "Relation of Pyramidal Tract Activity to Force Exerted during Voluntary Movement."

the representationalist view. The responses of single neurons in the motor cortex were associated with force [8], movement direction [9], velocity [10], among others.

WT Thach [11] investigated the correlation of single neuron discharge patterns to muscle activation, wrist angle, and intended direction simultaneously. A series of eight hold positions were designed to dissociate the three parameters. He found that neurons in M1 were associated strongly to one of the parameters, however neurons that were related to wrist angle tend to also correlate with the following movement direction. This illustrates a few drawbacks in the representational view of coding: neurons can show partial correlations to multiple parameters and some movement parameters themselves can be spatially and temporally correlated due to biomechanics [12]. Indeed, responses of single neurons in M1 and premotor cortex were found to have temporally complex activity profiles, and time-varying and context-dependent relationships to movement [13]

This brings us back to the neuron doctrine. The unambiguous proof that the nervous system is made up of discrete neurons (and consequently debunking the reticular theory) was the structural confirmation of the synapse [14] provided by the development of electron microscopy in the 1950s. The concept of the synapse was first introduced by Sherrington much earlier: *"The lack of*

[8] Hepp-Reymond, Wyss, and Anner, "Neuronal Coding of Static Force in the Primate Motor Cortex"; Cheney and Fetz, "Functional Classes of Primate Corticomotoneuronal Cells and Their Relation to Active Force"; Kalaska et al., "A Comparison of Movement Direction-Related versus Load Direction-Related Activity in Primate Motor Cortex, Using a Two-Dimensional Reaching Task."
[9] Georgopoulos et al., "On the Relations between the Direction of Two-Dimensional Arm Movements and Cell Discharge in Primate Motor Cortex."
[10] Moran and Schwartz, "Motor Cortical Representation of Speed and Direction During Reaching."
[11] "Correlation of Neural Discharge with Pattern and Force of Muscular Activity, Joint Position, and Direction of Intended next Movement in Motor Cortex and Cerebellum."
[12] Kalaska, "From Intention to Action"; Kalaska, "Emerging Ideas and Tools to Study the Emergent Properties of the Cortical Neural Circuits for Voluntary Motor Control in Non-Human Primates"; Reimer and Hatsopoulos, "The Problem of Parametric Neural Coding in the Motor System"; Scott, "Inconvenient Truths about Neural Processing in Primary Motor Cortex."
[13] Churchland and Shenoy, "Temporal Complexity and Heterogeneity of Single-Neuron Activity in Premotor and Motor Cortex"; Wu and Hatsopoulos, "Evidence against a Single Coordinate System Representation in the Motor Cortex."
[14] Palay and Palade, "THE FINE STRUCTURE OF NEURONS"; Palay, "SYNAPSES IN THE CENTRAL NERVOUS SYSTEM"; De Robertis and Bennett, "SOME FEATURES OF THE SUBMICROSCOPIC MORPHOLOGY OF SYNAPSES IN FROG AND EARTHWORM."

continuity between the material of the arborization of one cell and that of the dendrite (or body) of the other offers the opportunity for some change in the nature of the nervous impulse as it passes from one cell to the other." [15] Thus, in confirming the neuron doctrine, another idea was advanced: neurons interact with and influence one another via synaptic connections. The word *synapse* means "joining together". Eberhard Fetz writes,

> *"The basic reason that movement parameters need not be explicitly coded in the activity of single neurons is that movement is the consequence of large populations of interacting cells, which can generate an output without requiring any one cell to fire in proportion to the resultant movement parameters. Instead, the activity that is appropriate for a given cell is determined largely by its connections with the rest of the network rather than by any need to code an output parameter explicitly."* [16]

For many decades the neuron has been considered the structural and functional unit of neural computation [17]. Studies in the control of movement has shown evidence that single neuron discharges can be correlated with movement parameters. This has given us valuable insight on the response profiles of neurons in M1, and their correlation with movement parameters further supported the role of M1 in movement. However, the representationalist view does not fully account for the heterogeneity, non-stationarity, and temporal complexity of neural responses in M1. Single neurons are not merely feature detectors and observers but a part of a complex network of cells, and their correlation to movement parameters is a consequence of their interactions. In the next section, I discuss the alternative hypothesis: that single neurons are part of a larger circuit where computation is distributed across the neural population.

---

[15] Sherrington, *Man On His Nature*.
[16] Fetz, "Are Movement Parameters Recognizably Coded in the Activity of Single Neurons?"
[17] Saxena and Cunningham, "Towards the Neural Population Doctrine"; Yuste, "From the Neuron Doctrine to Neural Networks."

Emergent properties of cortical populations

The "cell assembly" hypothesis and early evidence

Representational models gained traction largely in part due to the compelling evidence provided by single cell microelectrode recordings [18]. Theories of neural cooperation preceded any multi-cell recording technologies that were able to confirm it [19]. Donald Hebb, in his book Organization of Behaviour [20], postulated the existence and emergence of "cell assemblies":

> *"any frequently repeated, particular stimulation will lead to the slow development of a 'cell assembly', a diffuse structure comprising of cells in the cortex and diencephalon [...], capable of acting briefly as a closed system, delivering facilitation to other such systems and usually having a specific motor facilitation."*

Sherrington also states similar ideas: "*Activity of the brain involves great numbers, not to say vast numbers, of nerve-cells co-operating. Yet the means of securing that co-operation is by impulses via nerve-fibres connecting cells."* [21] It was not until the 1960s that evidence of cooperation was shown from simultaneously recorded cells [22]. Using pairs of simulated neurons, Gerstein and Perkel [23] presented a way to visualize the simultaneous co-activity of two neurons, the joint peri-stimulus-time (jPST) scatter diagram (an update on [24]). The diagram produces a square diagram where the horizontal x-axis corresponds to time points for neuron i and the vertical y-axis for neuron j. A point (xt,yt) in the diagram would represent an impulse that occurred in neuron i at

[18] Yuste, "From the Neuron Doctrine to Neural Networks."
[19] Gerstein, Bedenbaugh, and Aertsen, "Neuronal Assemblies"; Saxena and Cunningham, "Towards the Neural Population Doctrine."
[20] *The Organization of Behavior; a Neuropsychological Theory.*
[21] Sherrington, *Man On His Nature.*
[22] Gerstein and Clark, "Simultaneous Studies of Firing Patterns in Several Neurons"; Gerstein and Perkel, "Simultaneously Recorded Trains of Action Potentials."
[23] "Simultaneously Recorded Trains of Action Potentials."
[24] Perkel, Gerstein, and Moore, "Neuronal Spike Trains and Stochastic Point Processes. II. Simultaneous Spike Trains."

time xt, and neuron j at time yt. This results in a scatter plot that shows both the individual neurons' response to the stimulus as well as the cross correlation of their spike trains along the diagonal. They showed that combinations of excitatory and inhibitory connections between two simulated neurons produced distinct densities in the jPST scatter diagram. Notably, the density in the diagonal showed temporal relationships between the activity of the two neurons that are not directly observed in their individual spike trains. Next, they simultaneously recorded pairs of neurons in the cat auditory cortex using tungsten microelectrodes which were able to record multiple nearby cells. After sorting the waveforms based on shape and associating these action potentials with an individual neuron [25], they showed experimentally that some pairs of neurons show correlated activity that is not immediately observable from the individual neurons' activity. They argued that this correlated activity arose from underlying connectivity between the neurons, either from a direct connection or from common inputs. This also applied the other way: interconnected neurons exhibit statistical dependencies in their activity.

Co-activity carries information

The emergence of these interactions revealed local connectivity structure, however, at that point, its relationship to encoding stimulus and movement information was yet to be explored. In simultaneously recorded neurons in the premotor cortex of a rhesus macaque performing a sensorimotor task, Aertsen et al [26] and Vaadia et al [27] investigated the "net effect" of one neuron on another (called the "effective" or "functional connectivity"), which was normalized to remove the stimulus and movement effects of individual neurons [28]. They showed that neuronal

[25] Gerstein and Clark, "Simultaneous Studies of Firing Patterns in Several Neurons."
[26] "Neural Interactions in the Frontal Cortex of a Behaving Monkey."
[27] "Dynamics of Neuronal Interactions in Monkey Cortex in Relation to Behavioural Events."
[28] Aertsen et al., "Dynamics of Neuronal Firing Correlation"; Ahissar et al., "Dependence of Cortical Plasticity on Correlated Activity of Single Neurons and on Behavioral Context."

interactions evolve during the task and their dynamics depended on the task condition and behavioral context. In the motor cortex, spiking events in pairs of neurons that were significantly coincident (unitary events, UE; within 5 ms) were shown to increase during times where the subject expected a stimulus presentation [29]. Increased occurrences of UEs were observed to be more time-locked to expected stimuli during trials with shorter reaction times than longer reaction times. Moreover, an example of a triplet of simultaneously recorded neurons exhibited a pattern of UEs at systematic times during engagement with the task which was not present during trials that were not completed successfully. It was also shown that a fraction of the neural population showed an increase in pairwise synchrony around movement onset [30]. Moreover, the synchrony between pairs of neurons carries information about the movement direction. These results suggest that short interval co-activity between pairs (and triplets) of neurons is dynamic, carries behaviorally relevant information, and serves a functional role in neural computation.

The cell assembly scheme hypothesizes that the activity of a single neuron is the result of its interactions in the network [31]. Can the observed single neuron responses that were correlated with parameters of the feature space be explained by their functional connectivity? A study that looked at the relationship between functional connections and spiking activating in M1, premotor cortex, retina, lateral geniculate nucleus (LGN), primary visual cortex (V1), and hippocampus [32]found that when predicting the spiking activity of a neuron, models that include the activity of other simultaneously recorded neurons via their functional interactions often performed better than using canonical tuning curves only.

---

[29] Riehle et al., "Spike Synchronization and Rate Modulation Differentially Involved in Motor Cortical Function."
[30] Hatsopoulos et al., "Information about Movement Direction Obtained from Synchronous Activity of Motor Cortical Neurons."
[31] Hebb, *The Organization of Behavior; a Neuropsychological Theory.*; Harris, "Neural Signatures of Cell Assembly Organization."
[32] Stevenson et al., "Functional Connectivity and Tuning Curves in Populations of Simultaneously Recorded Neurons."

More recent studies in the visual cortex have shown that measured asymmetric partial correlations across an optically imaged population can be used to predict single trial response and variability of individual neurons [33]. Moreover, the set of measured pairwise correlations across the population summarized as a functional network (a framework that will be elaborated on further in the next sections) is specific to the direction of the visual stimulus [34]. In many classical representational models, single neurons were classified as "tuned" if their responses were correlated to an input or output parameter, and neurons that did not show this specificity were labeled as "untuned". Under the cell assembly hypothesis, single neuron responses are driven by the dynamics of the interconnected network. Therefore, "tuned" and "untuned" responses, while they may perform different functions, are both important to neural computation. Levy et al [35] showed, in fact, that "untuned" neurons not only were involved in encoding visual stimuli, they occupied a crucial role as network hubs, as integrators of information [36].

Dynamics of population activity

Hebb continues his description of the cell assembly above: *"A series of such events constitutes a 'phase sequence'[...]. Each assembly action may be aroused by a preceding assembly, by a sensory event, or-- normally -- by both.* [37]*"* As discussed above, early work in the 1960s showed that pairwise interactions are dynamic and behavioral contexts can influence the dynamics of the interaction. While the microelectrode technology at that point limited their

[33] Dechery and MacLean, "Functional Triplet Motifs Underlie Accurate Predictions of Single-Trial Responses in Populations of Tuned and Untuned V1 Neurons"; Kotekal and MacLean, "Recurrent Interactions Can Explain the Variance in Single Trial Responses."
[34] Levy, Sporns, and MacLean, "Network Analysis of Murine Cortical Dynamics Implicates Untuned Neurons in Visual Stimulus Coding."
[35] Levy, Sporns, and MacLean.
[36] Zylberberg, "The Role of Untuned Neurons In Sensory Information Coding."
[37] *The Organization of Behavior; a Neuropsychological Theory.*

recordings to pairs (up to a few neurons), Gerstein et al [38] presented an analytical framework that abstracted the neurons (simulated or recorded) as point particles placed equidistantly in a N-dimensional hypercube in order to study the dynamics of the functional connections of the population. Each neuron acquires some "particle charge" for every spike emission, which then decays at a time constant, and as a consequence, these neuron-particles would attract each other proportionally to their charge. Thus, neurons that would tend to fire at the same time (and within the set time constant) will tend to be closer together in this N-space -- their distance in the space represents their functional connectivity, and their movement in the space which results in the changing distances describes the dynamics of their connectivity. Furthermore, Gerstein et al. extends this framework to enquire about the state of the neural population:

> *"By analogy with the phase-space representation used, for example, in statistical mechanics, we can abstract a still higher level representation than the one we have described. [...]Specifically, we can incorporate the instantaneous positions and migration velocities of all N points into a single vector [...]. In an abstract space of this dimension, this vector is represented by a moving point. The trajectory of the point represents the temporal evolution of the state of the system, which in turn embodies the changing set of functional interactions among the neurons as manifested by their impulse activity. For example, approximately closed or repeating trajectories of this state point would correspond to cyclic alterations in the organization of the neuronal population. Such changes in organization could arise from actual changes in effective connectivity as well as from alterations in thresholds, membrane excitability, and the like, or from changes in input external to the observed population of neurons."*

[38] "Cooperative Firing Activity in Simultaneously Recorded Populations of Neurons."

This describes the current state of the neural population as a point in some space. The time-varying activity of the population traces a trajectory in this state space. This is consistent with a dynamical systems perspective which implies that the system is governed by a set of dynamical laws that describes such a state space wherein its current state can be determined by its previous state. In addition, external perturbations can also influence the system's states. A major consequence of the interconnectedness of the nervous system and its resulting correlated activity is that the activity of a population of neurons is lower in dimensionality than if they were all independent actors. That is , the number of variables needed to explain the population activity is less than the number of neurons [39] and it is likely that this state space is low dimensional as well [40].

Under this dynamical systems perspective, it is the collective, structured activity patterns in the brain and its evolution that computation is implemented [41]. In the motor system, there was mounting evidence that representational models are not sufficient to describe the complex activity of the observed population [42]. While the activity of some neurons may reflect the movement parameters that were previously reported under the assumption of a representational model, Shenoy et al posits "others will reflect the act of pattern generation itself."[43] A particularly striking example of this is during movement preparation. In instructed-delay tasks, where a delay period is enforced between the initial instruction and the "go" cue, preparatory activity was shown to have a functional role in the subsequent behavior [44]. Churchland et al hypothesized that different

[39] Cunningham and Yu, "Dimensionality Reduction for Large-Scale Neural Recordings."
[40] Shenoy, Sahani, and Churchland, "Cortical Control of Arm Movements: A Dynamical Systems Perspective"; Humphries, "Strong and Weak Principles of Neural Dimension Reduction."
[41] Vyas et al., "Computation Through Neural Population Dynamics."
[42] Reimer and Hatsopoulos, "The Problem of Parametric Neural Coding in the Motor System"; Scott, "Inconvenient Truths about Neural Processing in Primary Motor Cortex."
[43] Shenoy, Sahani, and Churchland, "Cortical Control of Arm Movements: A Dynamical Systems Perspective."
[44] Churchland and Shenoy, "Temporal Complexity and Heterogeneity of Single-Neuron Activity in Premotor and Motor Cortex"; Churchland et al., "Neural Variability in Premotor Cortex Provides a Signature of Motor Preparation."

movements will have a different subspace in that state space, and that preparatory activity "moves" the system towards the desired optimal subspace. There is an observed advantage to reaction time when the system is within this optimal "initial condition" [45]. Additionally, by task definition, movement is suppressed during the preparatory period. Thus, the activity of the neural population at preparation and at movement may occupy different subspaces, one that does not invoke movement, and another that can be read out by downstream effectors, respectively [46]. Elsayed et al found that the preparatory and movement subspaces were orthogonal but linked [47]. Surprisingly, the neural population reorganizes its correlation structure between these two epochs, essentially functioning as two separate circuits, however a linear transformation is able to explain the shift from one structure to another. The activity, and consequently dynamics of the population, is governed by its underlying connectivity structure. In the next section, I will discuss a network perspective that represents coordinated population activity while maintaining single cell identities, to probe the structure of the interactions between neurons.

A Functional Network Perspective

A complex system is one with many interacting elements. Although the system as a whole may have emergent dynamics and features, these properties are shaped by the underlying interactions between its elements. A tractable way to study complex systems has been to represent them as a network where the nodes (or vertices) are the elements of the system, and they are connected by links (or edges) that describe their interaction. Network science has revealed many interesting features of complex systems from characterizing the spread of disease given a particular

[45] Afshar et al., "Single-Trial Neural Correlates of Arm Movement Preparation."
[46] Kaufman et al., "Cortical Activity in the Null Space: Permitting Preparation without Movement HHS Public Access Author Manuscript."
[47] "Reorganization between Preparatory and Movement Population Responses in Motor Cortex."

social network structure [48], to uncovering novel group structures in an ecological network in the Serengeti [49]. The neocortex lends itself well to being modeled as a network, and in many different scales [50]. Nodes can represent whole sensory systems, brain areas, individual neurons, or interacting molecules within the neuron. Edges can be structural connections between the nodes (eg. synapses), or functional connections (eg. statistical dependencies between nodes) [51]. It is important to note that functional connections do not explicitly imply a physical connection. As we discussed above, synaptic connections between neurons influence their activity, however, a single neuron receives many inputs and how they converge into a response is complicated by the specific biophysical properties of that neuron and its presynaptic partners, as well as other unobserved latent variables. Moreover, depending on the metric and window of measurement used, functional connections can change faster than it takes to form physical connections, and therefore can describe neural population dynamics in short timescales [52].

In this thesis, I summarized the statistical dependencies of the time-varying activity of extracellularly recorded neurons as a Functional Network (FN) and investigated how the network structure changes in relation to motor behavior. In contrast to the dynamical systems perspective, where the underlying connectivity defines a low dimensional state space wherein neural trajectories evolve through time, the functional network perspective considers the structure of the population co-activity explicitly. Early studies looking at pairwise correlations between neurons

[48] Newman, "Spread of Epidemic Disease on Networks."
[49] Baskerville et al., "Spatial Guilds in the Serengeti Food Web Revealed by a Bayesian Group Model."
[50] Bassett and Sporns, "Network Neuroscience," February 23, 2017; Bullmore and Sporns, "Complex Brain Networks: Graph Theoretical Analysis of Structural and Functional Systems," March 4, 2009; Humphries, "Dynamical Networks: Finding, Measuring, and Tracking Neural Population Activity Using Network Science."
[51] Magrans de Abril, Yoshimoto, and Doya, "Connectivity Inference from Neural Recording Data: Challenges, Mathematical Bases and Research Directions"; Faskowitz, Betzel, and Sporns, "Edges in Brain Networks: Contributions to Models of Structure and Function."
[52] Humphries, "Dynamical Networks: Finding, Measuring, and Tracking Neural Population Activity Using Network Science."

showed dynamic cooperation that can be context-dependent [53]. More recent studies have shown that correlation structures across a recorded population are reorganized between different neural computations, here, preparatory and movement phases during a reach [54]. Therefore there is reason to believe that the structure of functional connectivity can be informative of underlying neural computations and its relation to behavior. Indeed, the structure of FNs over the presentation of different visual stimuli have been shown to be stimulus specific in the murine visual cortex [55]. In the first part of Chapter 2, I employed the same analytical framework to populations of recorded neurons in the macaque M1 while the subjects performed an instructed-delay reaching task. I found the same to be true: the structure of the set of measured mutual information between spike trains in the population across the trial was specific to the instructed reach and that FNs constructed from trials with closer reach directions are also closer in network space. However, important features of the network, such as how the correlation structure is evolving to accommodate various sorts of neural computations, may not be adequately captured by averaging interactions over long periods of time.

By computing pairwise spike time statistics across short time windows over the course of a behavioral event, I constructed temporal FNs [56] to investigate the dynamics of pairwise interactions during reaching. In Chapter 2, I extended the static FN analysis results by using temporal FNs to elucidate when the structure of functional connections begin to differentiate based on reach direction, and consequently carry decodable behavioral information. Having a

[53] Vaadia et al., "Dynamics of Neuronal Interactions in Monkey Cortex in Relation to Behavioural Events"; Aertsen et al., "Dynamics of Neuronal Firing Correlation."
[54] Elsayed et al., "Reorganization between Preparatory and Movement Population Responses in Motor Cortex."
[55] Levy, Sporns, and MacLean, "Network Analysis of Murine Cortical Dynamics Implicates Untuned Neurons in Visual Stimulus Coding."
[56] Holme and Saramäki, "Temporal Networks"; Thompson, Brantefors, and Fransson, "From Static to Temporal Network Theory: Applications to Functional Brain Connectivity"; Ju and Bassett, "Dynamic Representations in Networked Neural Systems," June 15, 2020.

stereotyped trial structure and an instructed reach direction, I am able to measure dynamics of the alignment scores between pairs of trial temporal FNs, and relate them to the distance of their instructed reach and the timing during the task. In Chapter 3, we are faced with the complexity and richness of a less constrained task [57]. In the motor areas (M1 and surrounding cortical areas; [58]) of a marmoset engaging freely with an artificial prey capture task, using the same temporal FN framework, I investigated whether the structure of functional connections during unconstrained voluntary goal-directed behaviors exhibited regularities. Partitioning temporal FNs based on structure [59] showed a stereotyped sequence of network states during successful prey captures.

[57] Walker et al., "A Platform for Semiautomated Voluntary Training of Common Marmosets for Behavioral Neuroscience"; Krakauer et al., "Neuroscience Needs Behavior: Correcting a Reductionist Bias."
[58] Walker, MacLean, and Hatsopoulos, "The Marmoset as a Model System for Studying Voluntary Motor Control"; Walker et al., "Chronic Wireless Neural Population Recordings with Common Marmosets."
[59] Masuda and Holme, "Detecting Sequences of System States in Temporal Networks"; Cao and Sayama, "Detecting Dynamic States of Temporal Networks Using Connection Series Tensors."

CHAPTER II. Dynamic structure of motor cortical neuron co-activity carries behaviorally relevant information

This work was previously published:
Sundiang, Marina, Nicholas G. Hatsopoulos, and Jason N. MacLean. 2022. "Dynamic Structure of Motor Cortical Neuron Co-Activity Carries Behaviorally Relevant Information." *Network Neuroscience*, December 1–40. https://doi.org/10.1162/netn_a_00298.

ABSTRACT

Skillful, voluntary movements are underpinned by computations performed by networks of interconnected neurons in the primary motor cortex (M1). Computations are reflected by patterns of co-activity between neurons. Using pairwise spike time statistics, co-activity can be summarized as a *functional network (FN)*. Here, we show that the structure of FNs constructed from an instructed-delay reach task in non-human primates are behaviorally specific: low dimensional embedding and graph alignment scores show that FNs constructed from closer target reach directions are also closer in network space. Using short intervals across a trial we constructed *temporal FNs* and found that temporal FNs traverse a low-dimensional subspace in a reach-specific trajectory. Alignment scores show that FNs become separable and correspondingly decodable shortly after the instruction cue. Finally, we observe that reciprocal connections in FNs transiently decrease following the instruction cue consistent with the hypothesis that information external to the recorded population temporarily alters the structure of the network at this moment.

AUTHORS' SUMMARY

It remains unclear how motor cortical neurons flexibly perform the computations necessary to generate movement. We hypothesized that neuronal co-activity contains movement information

and its dynamics can reveal how the population switches computations during a task. We quantified co-activity as a Functional Network (FN) with single neurons as nodes and population co-activity as directed weighted edges. We also constructed FNs within short epochs across a trial to determine *when* co-activity begins to carry information and to investigate the dynamic structure of these interactions. Following the instruction cue, reciprocal connections in FNs transiently decrease, and shortly after, FNs become maximally decodable for reach direction.

INTRODUCTION

Individual neurons do not function in isolation, but rather as co-active and cooperatively interacting components of spiking networks. The resulting coordinated neuronal co-activity is reflected in pairwise spike time statistics. Spike time correlations have been implicated in the propagation of spiking in networks [1] making them an intriguing signal when studying the circuit mechanisms and computations that give rise to behavior. Recent work has shown that spike time correlations provide information, in addition to that provided by changes in firing rate, as to the nature visual stimuli [2], auditory stimuli [3], and spatial location [4]. In motor cortex (M1) pairwise spike *count* correlations have similarly been shown to provide information about motor behavior beyond what is provided by firing rates alone [5], and have also been used to improve encoding

[1] Bojanek, Zhu, and MacLean, "Cyclic Transitions between Higher Order Motifs Underlie Sustained Asynchronous Spiking in Sparse Recurrent Networks"; Chambers and MacLean, "Higher-Order Synaptic Interactions Coordinate Dynamics in Recurrent Networks."
[2] Dechery and MacLean, "Functional Triplet Motifs Underlie Accurate Predictions of Single-Trial Responses in Populations of Tuned and Untuned V1 Neurons"; Kotekal and MacLean, "Recurrent Interactions Can Explain the Variance in Single Trial Responses"; Levy, Sporns, and MacLean, "Network Analysis of Murine Cortical Dynamics Implicates Untuned Neurons in Visual Stimulus Coding"; Ruda, Zylberberg, and Field, "Ignoring Correlated Activity Causes a Failure of Retinal Population Codes."
[3] Betzel et al., "Stability of Spontaneous, Correlated Activity in Mouse Auditory Cortex"; Insanally et al., "Spike-Timing-Dependent Ensemble Encoding by Non-Classically Responsive Cortical Neurons."
[4] Levy et al., "A Neuronal Code for Space in Hippocampal Coactivity Dynamics Independent of Place Fields"; Nardin et al., "The Structure of Hippocampal CA1 Interactions Optimizes Spatial Coding across Experience."
[5] Maynard et al., "Neuronal Interactions Improve Cortical Population Coding of Movement Direction."

models that predict the activity of neurons [6]. However, it remains unclear whether pairwise spike *time* correlations contain behaviorally relevant information. Consistently the temporal dynamics of spike time correlations over the course of a behavioral trial and the extent of specificity of spike time correlations to kinematic variables is underexplored.

Here, we represent pairwise spike time statistics as *Functional Networks (FN)* and use tools from network science [7] to examine the structure and information content of pairwise spike time correlated activity of active populations in M1. Given that many of the computations needed to carry out a movement happen in fractions of a second, averaging interactions over long periods of time are unlikely to capture important dynamic aspects of the network [8]. We extend the FN framework by constructing temporal FNs [9] of single trials by computing pairwise spike time statistics across short intervals to elucidate the temporal progression of pairwise correlations among a population of M1 neurons throughout a trial and to relate single-trial population dynamics to network structure.

Using temporal FNs, we evaluate whether the dynamics of pairwise correlations carry information about the instructed reach, and determine when network structure begins to carry information relative to behaviorally relevant moments during the trial. We also determine what types of network interactions are most prevalent relative to different phases of the trial. We find that temporal FNs evolve during the trial in a way that specifies the instructed reach. Using a

[6] Stevenson et al., "Functional Connectivity and Tuning Curves in Populations of Simultaneously Recorded Neurons."
[7] Bassett and Sporns, "Network Neuroscience," March 1, 2017; Bullmore and Sporns, "Complex Brain Networks: Graph Theoretical Analysis of Structural and Functional Systems," March 4, 2009; Rubinov and Sporns, "Complex Network Measures of Brain Connectivity: Uses and Interpretations."
[8] Pedreschi et al., "Dynamic Core Periphery Structure of Information Sharing Networks in Entorhinal Cortex and Hippocampus."
[9] Holme and Saramäki, "Temporal Networks"; Ju and Bassett, "Dynamic Representations in Networked Neural Systems," June 15, 2020; Thompson, Brantefors, and Fransson, "From Static to Temporal Network Theory: Applications to Functional Brain Connectivity."

perceptron decoder, we demonstrate that temporal FNs contain information about motor behavior beyond what is conveyed by firing rate changes alone. We show that the topology of temporal FNs varies systematically over the time course of a trial, becoming transiently less reciprocal after the onset of the instruction cue, coinciding with the increase in decodable behavioral information from the FNs.

METHODS

Data and code availability

The data used in this work can be found publicly at https://doi.org/10.5061/dryad.9p8cz8wm6. All code written in support of this publication is publicly available at https://github.com/hatsopoulos-lab/macaque-dynamic_functional_networks.

Data collection and reaching task

We used previously published datasets from two macaques, Monkey Rs and Monkey Rj, performing an instructed center-out reaching task [10]. Subjects were trained to hold a cursor on a center target presented on a video screen using a 2D arm exoskeleton (KINARM, Kingston, Ontario). One of eight radially positioned peripheral targets was then presented and served as an Instruction cue during which time the subjects were required to keep holding the cursor on the center target. After a 1 second delay period, the peripheral target began blinking (Go cue) instructing the subjects to move the cursor to the peripheral target (Fig 1A). Trial start was 0.5 s before the instruction cue appeared, and trial termination was 0.5 s after the peripheral target was

[10] Hatsopoulos, Joshi, and O'Leary, "Decoding Continuous and Discrete Motor Behaviors Using Motor and Premotor Cortical Ensembles"; O'Leary and Hatsopoulos, "Early Visuomotor Representations Revealed from Evoked Local Field Potentials in Motor and Premotor Cortical Areas."

acquired. Trial inclusion depended upon target acquisition falling within 1.5s following movement onset. We also only included correct trials. Movement onset is defined as the time when the hand velocity reached 5% of the peak velocity of the movement after the Go cue.

Neural data were recorded from 96-channel Utah arrays implanted in the arm/hand area of primary motor cortex (M1) on the precentral gyrus. Spike waveform snippets sampled at 30 kHz were extracted using a user-defined threshold (Cerebus BlackRock Microsystems, Salt Lake City, UT) and were sorted into individual units using Offline Sorter (Plexon, Dallas, TX).

The surgical and behavioral procedures involved in this study were approved by the University of Chicago Institutional Animal Care and Use Committee.

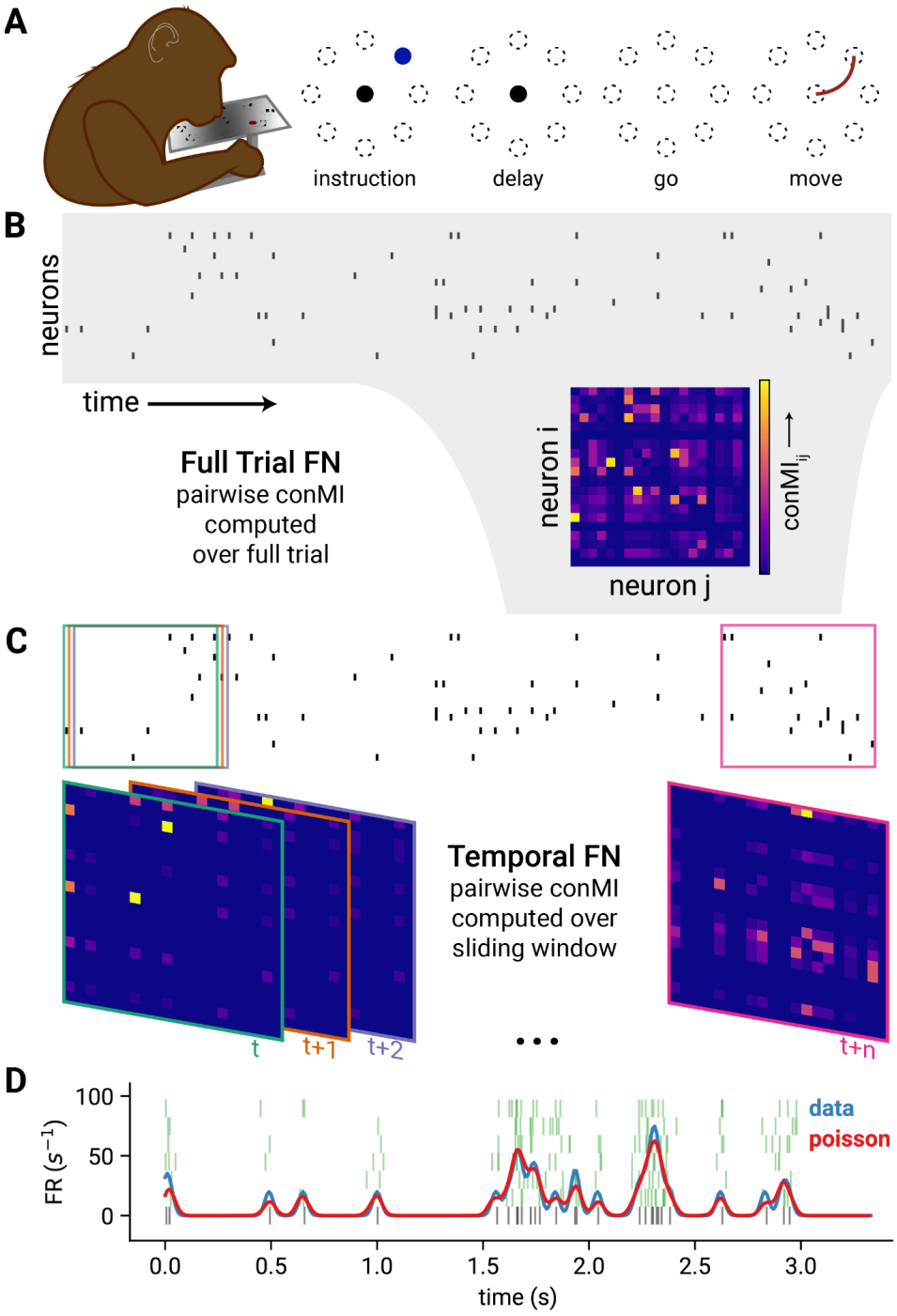

Figure II-1. Task structure and Functional Network construction.

(A) Subject using a Kinarm exoskeleton to control a cursor on a screen. The subject holds the cursor at the center target (black circle) to initiate a trial. An instruction cue (blue) appears in one of 8 target locations (indicated by the circles with broken-lines). After the delay period, the target cue begins blinking which indicates that the subject may move to the instructed target.

(Figure II-1 Continued) **(B)** A raster plot shows the binned spikes of the recorded neurons across time. The Full Trial FN is constructed by computing the confluent Mutual Information (conMI, see Methods) between the spike train for the full trial for each pair of recorded neurons. **(C)** To generate the Temporal FN, pairwise conMI were computed within a 200 ms sliding window across the trial. Boxes on the raster indicate the interval in the spike train that was considered for the corresponding FN with the same color border. **(D)** To generate rate-matched nulls, we computed the instantaneous firing rate of a unit for each single trial (blue trace) from the raw spikes (black raster plot, bottom). We used this firing rate profile to generate new spikes from an inhomogeneous Poisson process (5 example spike trains, green rasters). The mean of the instantaneous firing rates for 50 iterations of this Poisson process is shown in red.

Using pairwise spike time statistics to construct functional networks

To compute pairwise spike time statistics between recorded neurons, we binned the recorded spike trains into 10 ms bins: assigning a value of 1 if at least 1 spike occurred in that bin, and 0 otherwise. We then used the confluent mutual information (conMI) between the binned spike train [11]. conMI tells us how much information we gain from the firing state of a source neuron i at time t about the firing state of target neuron j in the same time bin t and the consecutive bin, t+1:

$$conMI = \sum_{i(t)\in\{0,1\}} \sum_{j(\widehat{t})\in\{0,1\}} p(i(t), j(\widehat{t})) \cdot log_2 \left[\frac{p(i(t), j(\widehat{t}))}{p(i(t)) \cdot p(j(\widehat{t}))} \right]$$

$$where\ j(\widehat{t}) = \begin{cases} 1, & \text{if } j(t) = 1 \text{ OR } \ j(t+1) = 1 \\ 0, & \text{otherwise} \end{cases}$$

The functional network constructed using this measure is consequently weighted and directed. We computed functional networks from either the full trial duration or from 200ms epochs. For the full trial networks, we computed the conMI between the entire spike train of the source and target neurons for a single trial (Fig 1B). We also computed the conMI for 200 ms windows that we slid in 10ms (1 bin) increments across a single trial resulting in a temporal FN

[11] Chambers et al., "Ensemble Stacking Mitigates Biases in Inference of Synaptic Connectivity."

per trial: a set of FNs each representing the measured co-activity of the recorded population during the trial at each time window (Fig 1C).

To disambiguate the structure that arises from firing rates alone and that which is the consequence of precise spike timing we computed FNs from short interval rate-matched Poisson neurons. Specifically we computed the instantaneous firing rate of each neuron on a trial by trial basis by convolving each neurons' spike train (Fig 1D, black raster) with a Gaussian kernel (σ = 20 ms). This smoothed rate-signal (Fig 1D blue trace) is then used as the probability of observing a spike for that neuron within a sampling period (10 ms) in an inhomogeneous Poisson process (Elephant[12]) which results in a spike train with the same rate-profile over the time course of a trial as the original data but the precise timing, which is crucial to compute pairwise spike time statistics is jittered within the width of the Gaussian kernel (Fig 1D, green rasters and mean instantaneous rate in red). We generate a rate-matched spike train for each neuron for every trial, and then generate the rate-matched FNs using the methods described above.

Dimensionality reduction and visualization

We vectorized each FN adjacency matrix and used the UMAP algorithm to reduce the dimensionality of the FN adjacency matrix from N-by-N (neurons, N: Rs: N=143, and Rj: N= 78) to two dimensions [13]. For the full trial FNs we used the following UMAP parameters: n_neighbors=50, min_dist=1, metric='cosine'. Each sample used to construct the low-dimensional embedding is an FN computed from an entire trial (total samples: Rs = 391, Rj = 246). We used a bivariate kernel density estimation for the (x,y) positions of the FNs to visualize the boundaries of

[12] Denker, Yegenoglu, and Grün, "Collaborative HPC-Enabled Workflows on the HBP Collaboratory Using the Elephant Framework"; Denker et al., "Elephant 0.11.2."
[13] McInnes, Healy, and Melville, "UMAP: Uniform Manifold Approximation and Projection for Dimension Reduction."

the projected FNs for each reach direction. As with the full trial FN, we embedded all the temporal FNs together but in this case each sample is a FN computed from 200ms in the trial (total samples: Rs = 103246 , Rj = 20856). For the temporal FNs, because there are significantly more samples, we used a different set of parameters in order to balance the local versus global structure of the data accordingly (n_neighbors=100, min_dist=0.1, metric='cosine'). We then used a spline to interpolate a path through the set of embedded FNs from a single trial to visualize the trajectory of the temporal FN in the low-dimensional subspace.

Graph Alignment Score

Similarity between two FNs, M and N with k neurons, was measured using a node-identity preserving Graph Alignment Score, GAS ,as described in [14] and [15]:

$$GAS = \frac{2\sum_{i=1}^{k}\sum_{j=1}^{k} min(M_{ij}, N_{ij})}{\sum_{i=1}^{k}\sum_{j=1}^{k} M_{ij} + Nij}$$

GAS measures the ratio of overlapping edges over the total number of edges. In the weighted case, the numerator represents the sum of the minimum edge weight between each pair of nodes, and the denominator is the total sum of the edge weights. Alignment scores were grouped according to the degree difference between the instructed target in a trial. Specifically, we evaluated the GAS distributions for FNs from the same (**Δ**0°), neighboring (**Δ**45°) and opposite (**Δ**180°) reach directions. For the temporal networks, we computed the alignment scores between pairs of FNs within the same 200ms time window aligned to the trial cues (Instruction and Go), and to movement onset.

[14] Levy, Sporns, and MacLean, "Network Analysis of Murine Cortical Dynamics Implicates Untuned Neurons in Visual Stimulus Coding."
[15] Gemmetto et al., "Multiplexity and Multireciprocity in Directed Multiplexes."

Decoding

A multilayer perceptron classifier (MLPC) was trained to decode the trial target direction from either the FN, the firing rates, both the FNs and firing rates, or the rate-matched Poisson FNs. The MLPC architecture has one hidden layer with 100 rectified linear activation units, linear output units, and a constant learning rate (step size = 0.001). The MLPC was trained for 200 iterations or until convergence, whichever happened first. We trained a different decoder for each time point and feature set (75% of the data is used for training) and tested on held out data (remaining 25%). We trained and tested 50 decoders for each feature set in order to get a distribution of performance scores (Fig 5)

Reciprocity

We computed the weighted reciprocity of FNs using a method described in [16]. First, we used a range of percentiles, from 85th to 90th (i.e. top 15th to 10th percent of magnitudes), to threshold the FNs in order to isolate the most reliable interactions in the population. In order to measure the overlapping or reciprocal edges, we take the minimum weight between neuron i and j:

$$w^{\leftrightarrow}_{i,j} \equiv min[w_i, w_j] = w^{\leftrightarrow}_{j,i}$$

The reciprocity of a network is the ratio between the sum of the reciprocal edge weights and the total sum of edge weights:

$$\overleftrightarrow{W} \equiv \sum_i \sum_{j \neq i} w^{\leftrightarrow}_{i,j}$$

$$W \equiv \sum_i \sum_{j \neq i} w_{i,j}$$

[16] Squartini et al., "Reciprocity of Weighted Networks."

$$r \equiv \frac{\overleftrightarrow{W}}{W}$$

We normalized the value to the average reciprocity of 45 rate-matched networks ($\bar{r}$) using the equation described in [17] for binary networks and adapted by [18] for weighted networks:

$$\rho = \frac{r - \bar{r}}{1 - \bar{r}}$$

Thus when the value is positive, the FNs from the data are more reciprocal than what is expected from chance correlations due to firing rates, and negative when it is less reciprocal. The mean reciprocity was computed between the presentation of the instruction cue to 100ms post instruction for every trial. This resulted in a distribution of scores that we defined as the baseline distribution. We compared the distribution of reciprocity scores at the time when the mean reciprocity over trials is at its minimum to determine whether the reciprocity of the FNs significantly changed during the trial relative to the baseline.

RESULTS

We analyzed single-unit recordings from M1 while two macaques (Monkey Rs and Monkey Rj) performed a center-out reaching task in the horizontal plane. Subjects were trained to control a cursor on a screen by moving a handle on a 2D arm exoskeleton (KINARM, Kingston, Ontario). The task was to hold the cursor in the center position during an instructed delay period while an instruction cue was presented that indicated one of 8 target reach locations positioned radially around the center. After the end of the delay period (1s), a go cue appeared instructing the subjects to initiate a reaching movement (Fig 1A).

[17] Garlaschelli and Loffredo, "Patterns of Link Reciprocity in Directed Networks."
[18] Squartini et al., "Reciprocity of Weighted Networks."

We summarized neuronal population activity during the task as a functional network (FN, Fig 1B-C). The FN is composed of nodes, which are the spiking single units, and edges between nodes, which correspond to the pairwise spike time statistics and not anatomical connectivity (Rs: 142 single units, Rj: 78 single units). Specifically, edges are computed using a mutual information measure (conMI, Methods; [19]. Confluent mutual information (conMI) computes the mutual information between the binned activity of neuron i at time t, and of neuron j at time t and the adjacent time bin, t+1 (where bins are 10ms) and is positive, by definition. The reliability of the co-activity between neuron i and j during a specified time window resulted in a weight. The resultant FN is both weighted and directed corresponding to the reliability and the directionality of the pairwise spike time correlation between units. We assessed whether the conMI between i and j is strongly influenced by their firing rates. We found that the relationship between conMI and pairwise FR (geometric mean) is not a simple linear correlation (Supplementary Figure 1). Notably, the relationship between conMI and the FR is similar in both the data and the rate-matched null.

Correlational structure in population activity are specific to reach direction

We first determined whether FNs during the entirety of single reach trials are specific to reach target direction. We did so in two ways: low-dimensional embedding of FNs and a graph similarity metric. Both approaches showed that FNs constructed from closer reach target directions are also closer in network space. First, we embedded the FNs in a low dimensional manifold that optimizes the distances between data points according to the original high-dimensional similarity. Consequently, FNs that are more similar to each other will lie closer together on the low

[19] Chambers et al., "Ensemble Stacking Mitigates Biases in Inference of Synaptic Connectivity."

dimensional manifold, and conversely, FNs that are structurally different will be more distant. Specifically, we used UMAP to project the high dimensional FNs into a lower dimensional space (see Methods). We found that networks from reaches to neighboring directions are close together in the low-dimensional manifold. In fact, the embedding produced a radial arrangement of data points that reflected the radial arrangement of the target locations (Fig 2A-D).

To further evaluate the similarities and differences between FNs according to reach direction as well as control for similarities and differences resulting from firing rates we compared FNs and single trial rate matched FN nulls using Graph Alignment Scores (GAS, see Methods). GAS allows for a quantitative comparison of FNs by identifying common edges between graphs [20]. This metric preserves node identities and reflects the fraction of similar edges out of all the existing edges between two networks. Therefore, a value of 1 means that the two networks are exactly the same. We measured alignment between each pair of FNs constructed from single trials. We then grouped the measured GAS according to the degree difference between the respective instructed reach targets: same (**Δ**0°), neighboring (**Δ**45°) and opposite (**Δ**180°). We observe that pairs of FNs from trials with the same reach target have higher alignment scores (**Δ**0° Rs = 0.399 ± 0.014, Rj = 0.393 ± 0.011, mean ± std) than those from neighboring reach directions (**Δ**45: Rs = 0.388 ± 0.015, Rj = 0.389 ± 0.011; p<=1.865e-89, Mann-Whitney U (MWU) two-sided test, mean ± std). Alignment scores were lowest when computed using FNs from opposite reach targets (**Δ**180°: Rs = 0.363 ± 0.015, Rj = 0.385 ± 0.012; p<=1.882e-236 , MWU two-sided test, mean ± std) indicating that the shared correlational network structure, in this case summarized as FNs, are informative of the instructed reach (Fig 2E-F). Additionally, while the rate-matched networks also exhibited differences in these distributions, GAS from the data were higher for all three

[20] Gemmetto et al., "Multiplexity and Multireciprocity in Directed Multiplexes."

distributions suggesting that FNs are more consistent than firing rates trial to trial (Rs = 0.363 ± 0.016, 0.353 ± 0.016, 0.331 ± 0.016 ; Rj = 0.380 ± 0.012, 0.378 ± 0.012, 0.374 ± 0.014; GAS for pairs of rate-matched FNs for same, neighboring, and opposite trials, respectively, $p<0.001$, MWU two-sided test for all data and rate-matched comparisons, mean ± std). Together both measures, UMAP and GAS, demonstrated that there were differences in the pairwise spike time correlation structure within the recorded population across different reach directions, and that there was additional structure resulting from pairwise spike time statistics of the populations that was not accounted for by firing rate correlations.

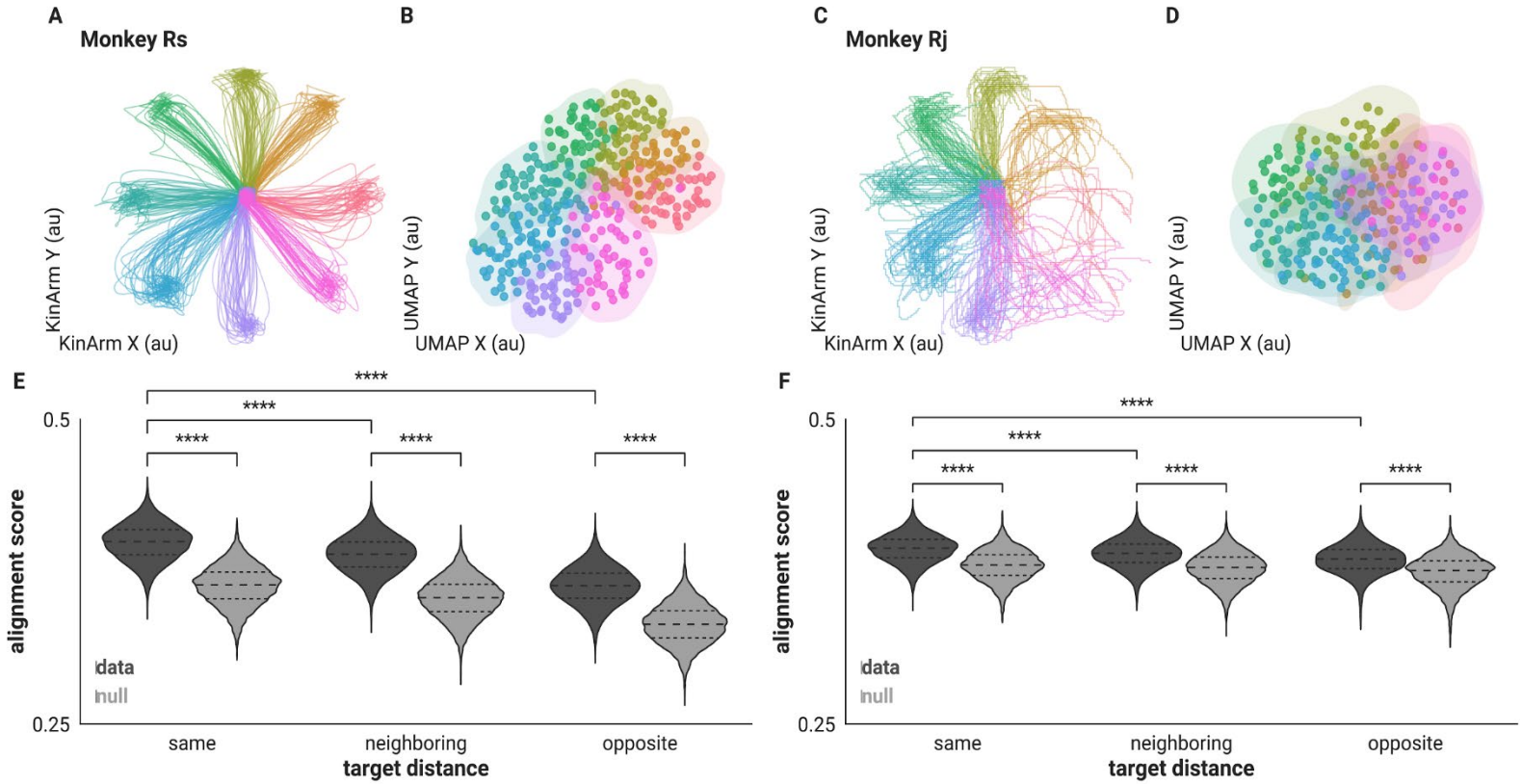

Figure II-2 Correlational structure of full trial FNs are specific to reach target direction.

(A,C) Hand trajectories of included trials colored by reach direction. **(B,D)** Low-dimensional embedding of full trial FNs preserve reach target direction. Colored the same as A,C. Shaded contour is the bivariate Kernel Density Estimation (see Methods) for the (x,y) positions of the FNs to visualize the boundaries of the projected FNs of each direction. **(E,F)** Distribution of alignment scores between each pair of FNs separated by target distance in dark gray and score distributions for corresponding rate-matched FNs shown in light gray (**** = $p < 1.00e-04$, Mann-Whitney U two-sided test). Dashed lines indicate quartiles.

Temporal progression of pairwise spike time statistics on single trials are specific to reach direction

Correlations between neurons are dynamic [21] and can vary over a behavioral trial depending on task condition [22]. Thus, we next evaluated the time varying spike time correlational structure by constructing FNs from short epochs (200 ms) of trial time. These "snapshots" of the network across time, *temporal FNs,* allowed us to evaluate how the network evolves over the time course of single trials and to determine when, during a trial, the reach-specific differences in the FNs first occur and are most pronounced. Again we examined the differences between FNs in two ways. First, we embedded the FNs into a lower-dimensional subspace using UMAP as we had done with the full trial FNs. This allowed us to use the embedding to track the progression of temporal FNs relative to trial structure and reach direction. We found that the temporal FNs progressed along trajectories through the subspace in a reach-specific path (Fig 3); Temporal FNs are initially close together in the computed subspace (Fig 3A) and then increasingly separate according to the instructed reach direction as the trial progresses (Fig 3B), separating maximally after the *go* cue and during movement (Fig 3C). Again, we used an unsupervised method of dimensionality reduction and therefore did not include information about the behavior of the subject in the embedding. Consequently, any separation in the embedding of the temporal FNs is the result of the differences in the pairwise spike time statistics of the neural population and not from any training labels.

[21] Aertsen et al., "Dynamics of Neuronal Firing Correlation: Modulation of 'Effective Connectivity.'"
[22] Vaadia et al., "Dynamics of Neuronal Interactions in Monkey Cortex in Relation to Behavioural Events."

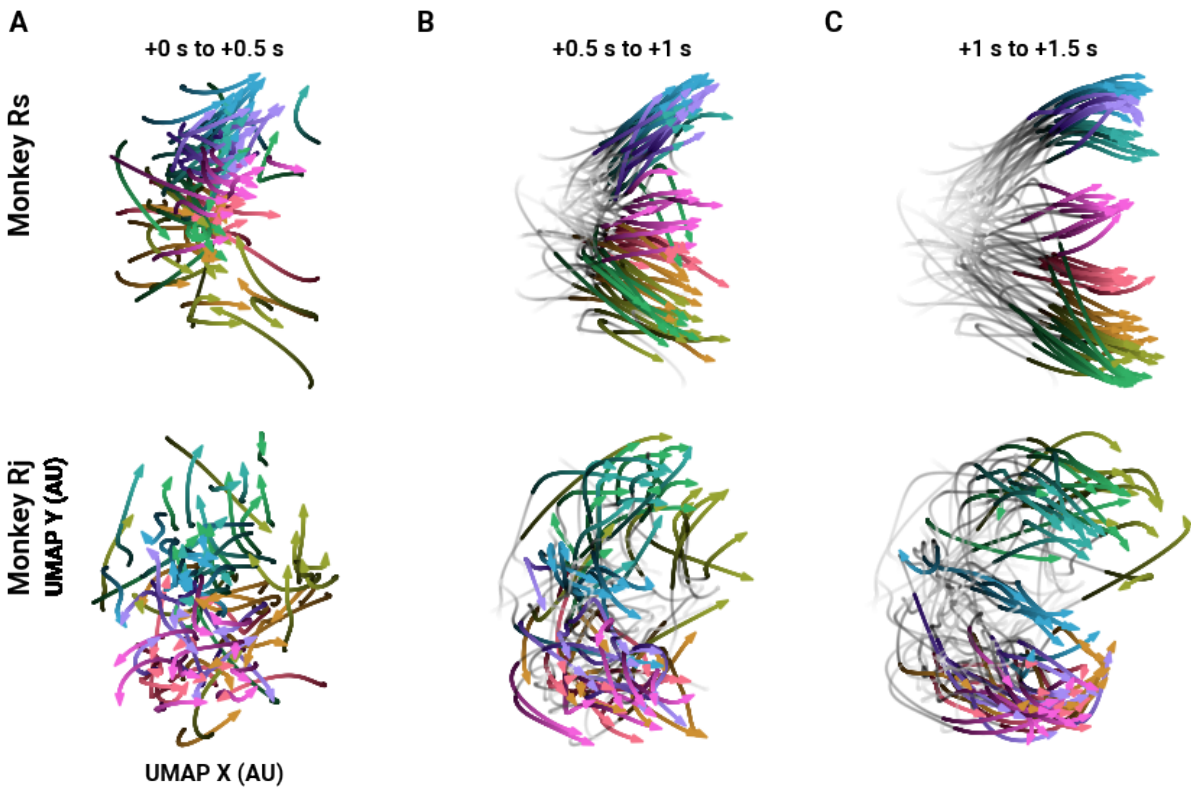

Figure II-3 Trajectories of single trial temporal FNs through a low-dimensional subspace

Example trajectories of single trial temporal FNs across a low-dimensional subspace (10 trials per direction). Times (in seconds) indicate the time post-instruction. **(A)** Trajectories from instruction (0s) to 0.5 s after instruction. Trajectory begins with the darkest hue. Color legend the same as Fig 2a-d. **(B)** The same trajectories from (A) later in time: the gray, low-opacity tails show the trajectory from instruction, and the colored and opaque section show the trajectory at 0.5 s post-instruction to Go cue (1s post-instruction). **(C)** the same as (B) but for after Go (1 s) and through the end of the trial.

As with the full trial FNs, we next computed the extent to which the structure of the temporal FNs indicated the instructed reach and compared the temporal FNs to the rate-matched FNs. At each time window, we measured the GAS of every pair of FNs and sorted the scores according to difference in target direction. We then evaluated the distribution of graph alignment scores for the same, neighboring, and opposite reach directions across the time course of the trial

(Fig 4). Before and shortly after instruction, the FNs are not informative as to reach direction as indicated by similar GAS values (MWU two sided test, p >= 4.045e-3, Bonferroni corrected between all scores from data FNs). The score distributions of neighboring and opposite reach-directions became significantly different from scores of FNs from the same reach trials post-instruction cue consistent with the embedding result (Fig 4A; **Δ**0° vs **Δ**180°: MWU two sided test, p <= 1.576e-6, Bonferroni corrected from 160 ms post instruction for Rs, and 180 ms post instruction for Rj. **Δ**0° vs **Δ**45°: MWU two sided test, p <= 3.106e-4, Bonferroni corrected from 210 ms post instruction for Rs, and 230 s post instruction for Rj). The scores remained significantly different for the remainder of the trial and also at movement onset (Fig 4B-C). Notably, the scores between the same and the opposite reach directions diverge first before scores from the same and neighboring reach directions, again suggesting that FNs generated from nearby reach directions are also more similar in network space. We also note that while the rate-matched FNs exhibited differences between distributions (**Δ**0° vs **Δ**180°: MWU two sided test, p <= 2.305e-4, Bonferroni corrected from 160 ms post instruction for Rs and Rj. **Δ**0° vs **Δ**45°: MWU two sided test, p <= 8.688e-4, Bonferroni corrected from 220 ms post instruction for Rs, and 229 ms post instruction for Rj), the GAS between pairs of FNs computed from pairwise spike time statistics from the data are consistently higher indicating that the structure of pairwise spike timing is conserved from trial to trial. Additionally, if the temporal evolution in alignment scores are due to rates alone and that the GAS values for the data is merely offset by some value, we would expect that the normalized GAS (Supplementary Figure 2) would not show a) changes across time and b) significant differences in the GAS values between reach directions. We show that when we normalize the GAS we still find that for RS, GAS between **Δ**0 and **Δ**45 are significantly different at 210 ms. For Rj, while the mean normalized GAS for **Δ**0 is consistently higher than the mean for

Δ45 starting at 110 ms, the scores are significantly different at 380 ms. However, it must also be noted that the scores were significantly different between **Δ**0 and **Δ**90 starting at 220 ms for Rj.

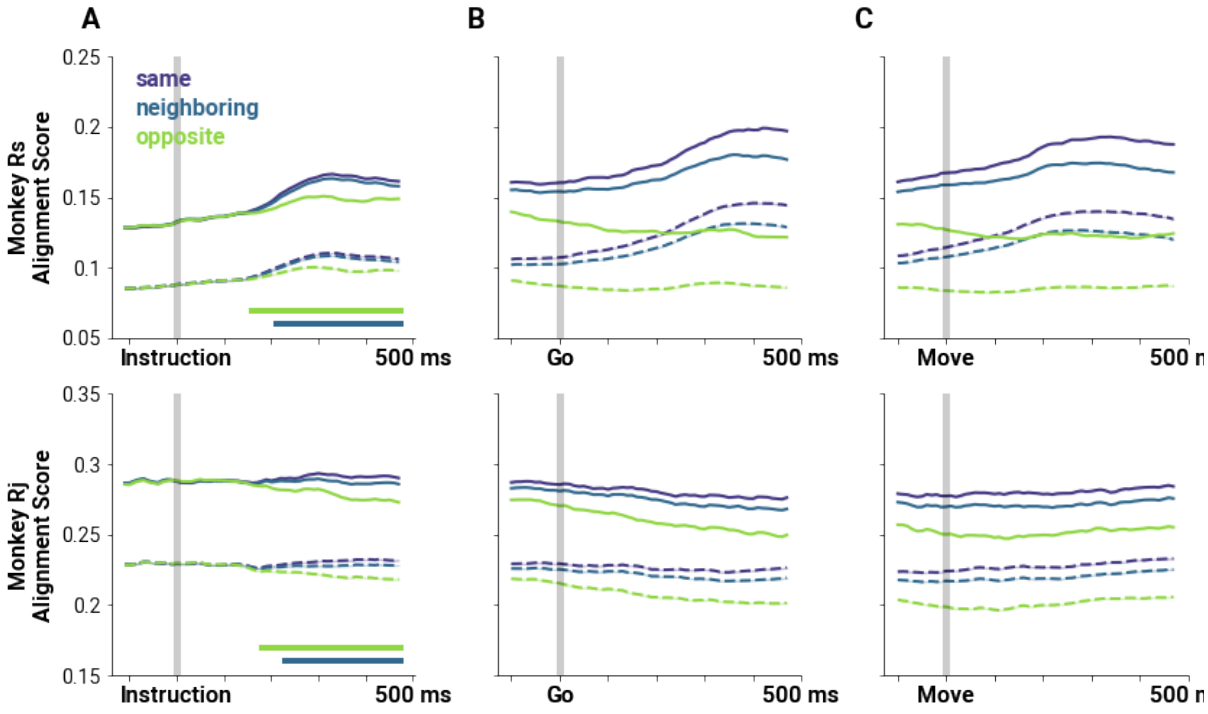

Figure II-4 Graph alignment scores between FNs reflect distance of reach targets.

(A) Mean alignment scores between pairs of FNs at each sliding window (solid lines), and corresponding scores for rate-matched FNs (broken lines) aligned to the instruction cue. The shaded region indicates the SEM of the GAS distribution, which is very small. Alignment scores are separated based on reach target difference: same (violet), neighboring (blue), and opposite (green) reach targets. Straight horizontal lines on the lower left of the plot indicate when the score distributions from neighboring or opposite locations (blue and green, respectively) become significantly different from the score distributions between FNs of the same direction ($p<0.01$ MWU two-sided test, Bonferroni corrected). **(B)** same as (A) but aligned to Go cue. Differences between distributions are significant throughout the plotted window ($p<0.01$ MWU two-sided test, Bonferroni corrected). **(C)** same as (A) but aligned to movement onset. Differences between distributions are significant throughout the plotted window ($p<0.01$ MWU two-sided test, Bonferroni corrected).

Decoding behavior from functional networks

Temporal FNs became increasingly differentiable during the trial with the differences following a stereotyped time course relative to trial structure, indicating that there is information

about motor behavior in the temporal FN. We next asked if this information can be used to decode reach target direction. Since GAS analysis indicated that the differences in the temporal FN depended on time, we also measured when the temporal FNs were decodable relative to trial structure and movement onset, and when they were maximally decodable. To do so, we employed multilayer perceptron decoders trained on different features of the data to predict the reach target of a 200 ms sample window of a single trial (see Methods). We then compared the performance of the decoders based on the features on which they were trained. Specifically, decoders were trained on either the set of pairwise spike time statistics between neurons generated in the time window (FN decoder, Fig 5 green), or the firing rates of the neurons during the window (FR decoder, Fig 5, blue). To determine whether pairwise spike time statistics carry additional information beyond firing rates, we also examined decoding performance when both firing rate and the temporal FNs were included in decoder training (FRFN decoder, Fig 5, red). Comparing the decoding performance of the FN and FR decoders to the full FRFN decoder allowed us to establish the contribution of each held out feature to the overall decoding performance. Finally, in order to rule out the effect of spurious correlations due to firing rate dynamics, we generated FNs from trial by trial Poisson rate matched neurons and similarly evaluated decoding performance (null FN decoder, Fig 5 purple; see Methods).

As expected, before the instruction cue, all four decoders performed at chance level (Fig 5A, 12.5% performance indicated by dashed line). At 147 ± 9 ms following the instruction cue, decoding performance increased above chance for the FN, FR and FRFN decoders (1 sample t-test, $p <= 9.550e-4$, Bonferroni corrected, mean ± std). The null FN decoders achieved performance above chance about 50 ms later, at 205 ± 44 ms (mean ± std). All four decoders reached an initial peak around 364 ± 48 ms (defined as the maximum performance within 500 ms

of the instruction, indicated by the black triangle on every performance trace in Fig 5). At this peak, the FRFN decoders performed better than the FR decoder (Rs: 45.10% vs 37.67%, Rj: 58.03% vs 51.03%, respectively, p <= 6.438e-05, MWU two-sided test), suggesting that the inclusion of pairwise spike time statistics provides additional information about the reach direction. In fact, the FRFN decoder performance was significantly higher than the performance of the FR decoder beginning 170 ms for Rs and 180 ms for Rj and remained significantly higher throughout the rest of the trial, as well as during movement (MWU two sided test, p <= 9.888e-04, Bonferroni corrected between FRFN and FR performance scores). We note that the FR decoder performed better than the FN decoder for Rj (51.03% vs 40.85% at their initial peaks, respectively). However, the increase in performance in the combined FRFN decoder compared to the FR decoder indicates that precise spike time correlations contain additional information about the reach target beyond firing rates alone.

We also observed that at the initial peak, the FN decoders performed significantly better than the rate-matched FNs (Rs: 42.39% vs 33.37%, Rj: 40.85% vs 27.28%, respectively, p<=3.562e-04, MWU two-sided test). For Rj, this performance difference was significant from 170 ms throughout the rest of the trial (MWU two sided test, p<=3.3845e-04, Bonferroni corrected). For Rs, this difference was significant beginning 240ms (MWU two sided test, p<=8.853e-04, Bonferroni corrected) and sporadically thereafter. This highlights that there is information about the instructed reach in the pairwise spike time statistics in the data that does not arise from chance correlations due to firing rates.

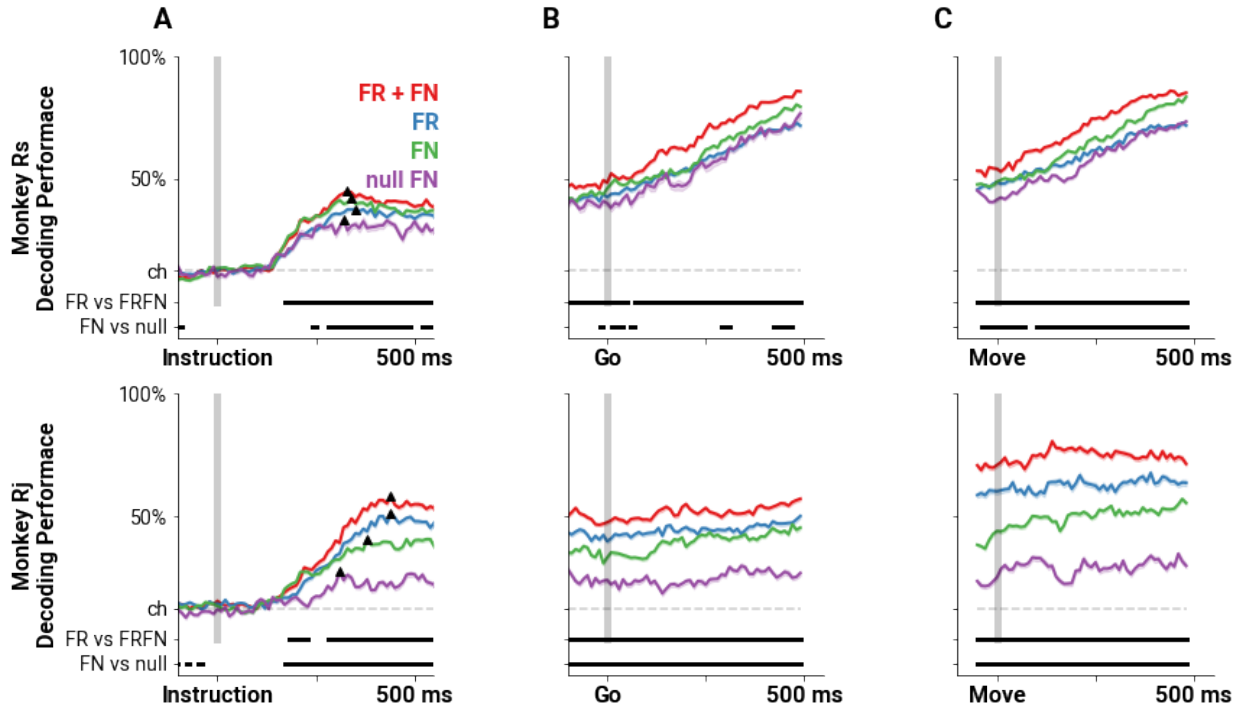

Figure II-5 Decoders that incorporate pairwise spike time statistics predict reach direction more accurately.

Mean performance perceptron decoders trained on either firing rates (FR, blue), the set of pairwise correlations as FNs (FN, green), both firing rates and correlations (FR + FN, red), or correlations from rate-matched nulls (null FN, purple) aligned on Instruction cue **(A)**, Go cue **(B)**, and movement onset **(C)**. Dashed gray line indicates chance level (1 in 8), and the two bars on the bottom of each panel indicate the times during which performance of the FR and FRFN, or the FN and null FN decoders are significantly different from each other ($p<0.01$ MWU two-sided test, Bonferroni corrected). The triangles in panel A mark the initial peak in performance for the decoders. The shading represents the SEM of the decoder performance.

Reciprocity in the network varies systematically during the trial

One of the strengths of representing cortical population activity as a weighted and directed temporal FN, is that not only can we investigate the dynamics of pairwise spike time statistics across the population (as weighted edges), we can also consider the changes to network architecture. Doing so has the potential to provide insights into information propagation and computation. Here, we focus on the most reliable reciprocal connections in the temporal FN. We

thresholded the temporal FNs according to weight percentile, in order to isolate the most reliable edges and then measured the normalized reciprocity of the temporal FNs throughout the trial (see Methods). Reciprocity tells us how likely two units in the temporal FN are mutually linked [23] as well as the importance of the direction of the interaction between neurons: a fully reciprocal FN means that units are co-active symmetrically in contrast to a less reciprocal FN where the direction of the interaction is important in characterizing the network. In the temporal regime, reciprocity may influence the state of the FNs in the next time point. We investigated whether and when the reciprocity of the temporal FN changes over the time course of the trial. We compared the distribution of reciprocity scores at the time when the mean reciprocity over trials is at its minimum (Fig 6, indicated by ★) with the instructed delay period with the distribution of mean scores of each trial from instruction to 100 ms post-instruction (Fig 6, gray shaded region). The minima occurred at 291 ± 31 ms after instruction cue (mean ± std). We compared the distribution of mean scores of each trial from instruction to 100 ms post-instruction (Fig 6, gray shaded region) with the distribution of scores at each time point during the delay period. Reciprocity significantly decreases at 156 ± 11.1 ms for Rs and 267 ± 4.7 ms for Rj ($p<=7.46e-03$ and $p<=9.83e-03$, respectively). The significant decrease in reciprocity lasts until 358 ± 91.4 ms for Rs and 303 ± 12.5 ms for Rj.

We also compared the distribution of reciprocity scores at the time when the mean reciprocity over trials is at its minimum (Fig 6, indicated by ★). The minima occurred at 291 ± 31 ms after instruction cue (mean ± std). We found that reciprocity is significantly decreased at the minima for the networks thresholded at 85th to 87th percentile for both RS and RJ (Fig 6, independent sample t-test, $p <= 3.773e-4$). There is a significant decrease in reciprocity with RS

[23] Squartini et al., "Reciprocity of Weighted Networks."

at the higher threshold levels (88th to 90th percentile of edge weights), and significant decrease in reciprocity scores with RJ at lower thresholds (75th to 85th percentiles, see Supplementary Figure 3). The difference in significant threshold levels is due to the differences in the density and size of the FNs. Nevertheless, this decrease is present in both subjects. At moments when inputs external to the recorded population would be most likely, the network structure becomes less reciprocal.

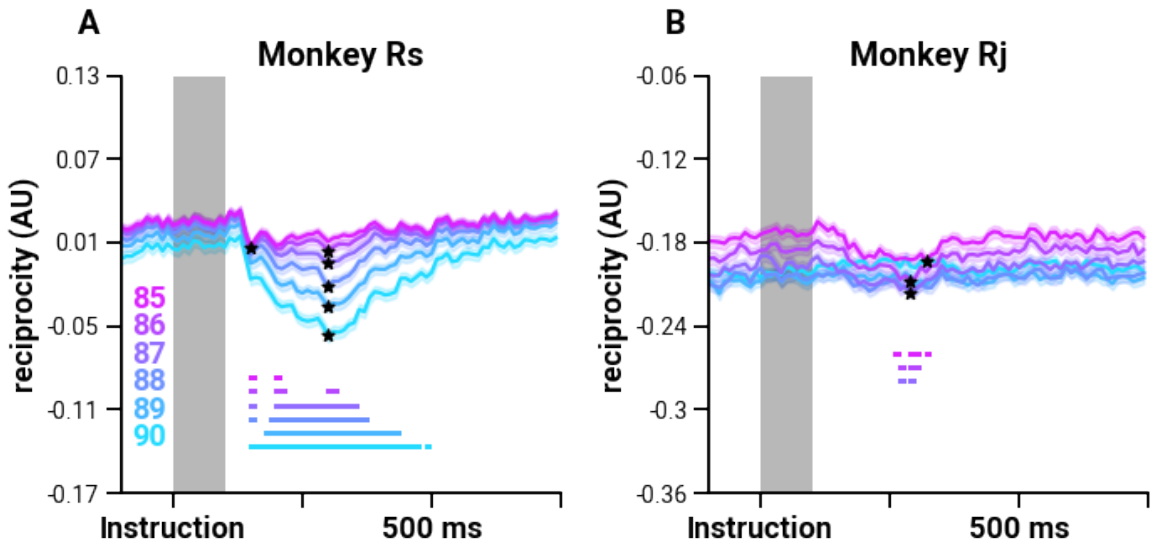

Figure II-6 Reciprocity decreases shortly after instruction.

Mean normalized reciprocity scores (lines, the shaded region shows the SEM) from thresholded FNs based on weight percentile values for monkeys Rs **(A)** and Rj **(B)** indicated by the color legend in the lower left**.** The mean reciprocity for the shaded region (Instruction to 100 ms post instruction) is computed for each trial resulting in a distribution of reciprocity scores, which is then compared to the scores at each time point and at the minima to determine if there is a decrease in reciprocity. Stars indicate whether the distributions at the minima decrease significantly ($p<0.01$, independent sample t-test). Solid straight lines at the bottom of the plot show the times that are significantly different from the baseline ($p<0.01$, independent sample t-test, Bonferroni Corrected)

DISCUSSION

We show that pairwise spike time statistics between neurons, summarized as Functional Networks (FNs), are informative of reach direction and are dynamic over the course of a single

task trial. Previous studies have shown that firing rate correlations between neurons provide additional information about behavior or the environment that is not gleaned from observing each neuron independently [24]. Moreover, the dynamics of pairwise firing rate correlations are indicative of behavioral conditions that are otherwise unobservable from individual neuron firing rates or from trial-averaged cross-correlations [25]. These previous studies measured correlations of spike counts across trials and over broad time scales. In contrast we focused on spike time correlations over short intervals. Earlier work has documented fine time-scale synchrony between pairs of M1 neurons that emerges predominantly at movement onset and carries information about reach direction [26]. Our results are consistent with this earlier work but extends it in several ways. First and foremost, our focus here was on characterizing the FN structure among the entire recorded neuronal population as opposed to multiple, individual pairwise interactions. Second, by using conMI, we could distinguish directed functional interactions as opposed to synchronous interactions. This allowed us to analyze the temporal dynamics of reciprocal versus non-reciprocal interactions across the duration of the reach. Third, we documented the emergence of information-bearing interactions early during movement preparation in the instructed-delay period which was not evident in the earlier work.

Since movement is the culmination of multiple computations, many of which happen at short timescales, we hypothesized that task-relevant information must be represented in the short time scale pairwise spike time statistics. Our work substantiates this hypothesis, since we find evidence that temporal FNs constructed from short intervals during single trials carry a representation of the instructed movement. Specifically, we found that the similarity between pairs

[24] Maynard et al., "Neuronal Interactions Improve Cortical Population Coding of Movement Direction."
[25] Vaadia et al., "Dynamics of Neuronal Interactions in Monkey Cortex in Relation to Behavioural Events."
[26] Hatsopoulos et al., "Information about Movement Direction Obtained from Synchronous Activity of Motor Cortical Neurons."

of temporal FNs from single trials reflected the distance between their respective target directions and are correspondingly decodable. The temporal FN framework also allows us to identify *when* correlations begin to be indicative of reach direction, which in turn has the potential to provide insight into corresponding computations. We find that FNs become decodable above chance 140 ± 10 ms after the instruction cue appeared. Notably an increase in timing precision of spiking in individual neurons across trials has been found around this time (~100 ms), and mutual information increases between target location and spike counts of single neurons at this time [27]. The modulation of firing rates across the population and the stronger relationship between spike count and target location suggests that information about the target arrives at M1 at this time lag. Consistently, we find that precise spike timing *between* neurons in single trials, as reflected in their correlation, is additionally informative of target direction. Moreover, alignment scores between temporal FNs constructed from single trials of the same target direction are higher than alignment between temporal FNs that correspond to neighboring and opposite directions, suggesting that there is consistent and informative spike timing between neurons on a trial-to-trial basis that is specific to reach direction.

Local connectivity patterns shape the activity patterns and consequently, the dimensionality and behavior of a recurrent network [28]. In this work, we focused on measuring reciprocal connections because they serve as building blocks for higher-order (beyond pairwise) structures. When external inputs impinge on local circuitry, they must be integrated into ongoing activity and processed across the network. A recent study which inferred single trial M1 dynamics using LFADS found it was necessary to include external inputs in order to maximize model

[27] Reimer and Hatsopoulos, "Periodicity and Evoked Responses in Motor Cortex."
[28] Recanatesi et al., "Dimensionality in Recurrent Spiking Networks: Global Trends in Activity and Local Origins in Connectivity."

accuracy[29]. They found that large input transients were disproportionately necessary at ~150 ms after target presentation compared to other times in the trial. Here we find that reciprocal connections begin to decrease with similar latencies to the target appearance as the inferred input transients (significantly at 156 ± 11.1 ms for Rs and 267 ± 4.7 ms for Rj). Also at this time, decoding performance improves above chance (147 ± 9 ms), and GAS values between the same and opposite directions begin to diverge (170 ± 10 ms). This shift in structure may be an indication of the network integrating and propagating information about inputs external to the recorded population, such as visual stimulus related to the instructed target direction. Interestingly, this topology is transient; the network returns to its baseline level of reciprocity, but it is important to note that the information about the reach target is maintained in the FN after this transient topological shift since decodability of the FNs remains stable for the remainder of the delay period. Previous studies have shown that the population activity during the preparatory and the movement phase are dynamic [30], that they occupy orthogonal subspaces [31], and that these subspaces can be linked [32]. Consistent with this work on computation through population dynamics, we show that the patterns of coordinated activity of the neural population evolve during the reach trial in a systematic way. Our findings provide evidence that the network transiently reorganizes to a less reciprocal topology which may facilitate processing external inputs setting the state of the population according to the instructed movement and may enable the reported transition from the preparatory subspace to the movement subspace.

[29] Malonis et al., "M1 Dynamics Share Similar Inputs for Initiating and Correcting Movement."
[30] Churchland et al., "Neural Population Dynamics during Reaching"; Shenoy, Sahani, and Churchland, "Cortical Control of Arm Movements: A Dynamical Systems Perspective"; Vyas et al., "Computation Through Neural Population Dynamics."
[31] Kaufman et al., "Cortical Activity in the Null Space: Permitting Preparation without Movement."
[32] Elsayed et al., "Reorganization between Preparatory and Movement Population Responses in Motor Cortex."

In this study we did not try to classify the single units functionally or into putative cell classes. Future work would clearly benefit from data in which individual classes of neurons are considered separately. The FN framework can be extended to include labels on nodes and edges such as cell type, or functional properties [33]. Notably an impressive census of cell types in motor cortex has recently been published by the The BRAIN Initiative Cell Census Network [34] highlighting the potential for an analytical approach, such as FNs, which can both incorporate cell information and network dynamics. For example, in the visual cortex, the topology of single trial FNs depends on the visual stimulus and untuned neurons act as hubs in the network serving an integral role in stimulus coding [35]. A functional network framework revealed that fronto-parietal areas in the grasping motor network has modular organization that is not constrained to anatomical boundaries, and a rich-club of oscillatory neurons that may be key to synchronizing the network and generating grasping behavior [36]. Previous work has shown that modeling functional connections can predict neural responses in M1 more accurately than canonical tuning curves suggesting that the tuning properties of individual neurons is in part a result of network interactions [37]. Additionally, tuning properties are not stationary such that single cortical neurons in M1 encode temporally extensive movement fragments or trajectories, as opposed to single movement parameters such as direction [38]. The temporal FN framework that we introduce in this paper has

[33] Faskowitz, Betzel, and Sporns, "Edges in Brain Networks: Contributions to Models of Structure and Function."
[34] BRAIN Initiative Cell Census Network (BICCN), "A Multimodal Cell Census and Atlas of the Mammalian Primary Motor Cortex."
[35] Levy, Sporns, and MacLean, "Network Analysis of Murine Cortical Dynamics Implicates Untuned Neurons in Visual Stimulus Coding."
[36] Dann et al., "Uniting Functional Network Topology and Oscillations in the Fronto-Parietal Single Unit Network of Behaving Primates," August 15, 2016.
[37] Stevenson et al., "Functional Connectivity and Tuning Curves in Populations of Simultaneously Recorded Neurons."
[38] Hatsopoulos, Xu, and Amit, "Encoding of Movement Fragments in the Motor Cortex."

the potential to link dynamically changing network interactions across the trial to time-varying preferred movement trajectory tuning.

Aside from containing information about the instructed reach, upon visual inspection of the low-dimensional embeddings, we found that FNs carry kinematic information. For example, in the full trial and temporal embeddings of FNs from Rj (Fig 2C-D, Fig 3, bottom row), overlapping projected FNs show trials that had similar kinematic trajectories despite different target directions. Rj's kinematic trajectories towards the lower right targets were not straight toward the target (pink in Fig 2C and Fig 3 second row); Rj moves straight down and then right. We found that FN embeddings where the target is the lower right (pink) and the one straight down (violet), are correspondingly overlapping. Additionally, low-dimensional embeddings of temporal FNs separate into two main branches: temporal paths of the FNs for reach directions to the lower left targets (hand trajectories shown in Fig 2A and C) tended to be closer together forming a "branch" of paths, and the paths for the upper right targets form another. Specifically, in Rs (Figure 3, first row), the upper branch of paths corresponds to pulls towards the body. Conversely the lower branch corresponds to reaches that require the subject to push away from the body. This suggests that, while we have performed these analyses on data where the subject is performing an 8-direction center out task, FNs may be able to capture a wider range of movement directions and kinematic variability than explored here.

FNs are a useful tool to achieve insight into M1 network dynamics that correspond to motor behavior. FNs provides a tractable summary of population activity that is decodable and can provide insight into how the state of the system changes over the time course of a trial. The neural interactions summarized by FNs influence spiking activity of the population that can be, in turn,

read out by downstream agents [39]. Our results suggest that FNs reorganize according to motor goals and argue that a functional network examination of motor cortical FNs may provide insights into the underlying circuit mechanisms that drive these cortical population responses and ultimately motor behavior.

SUPPLEMENTARY FIGURES

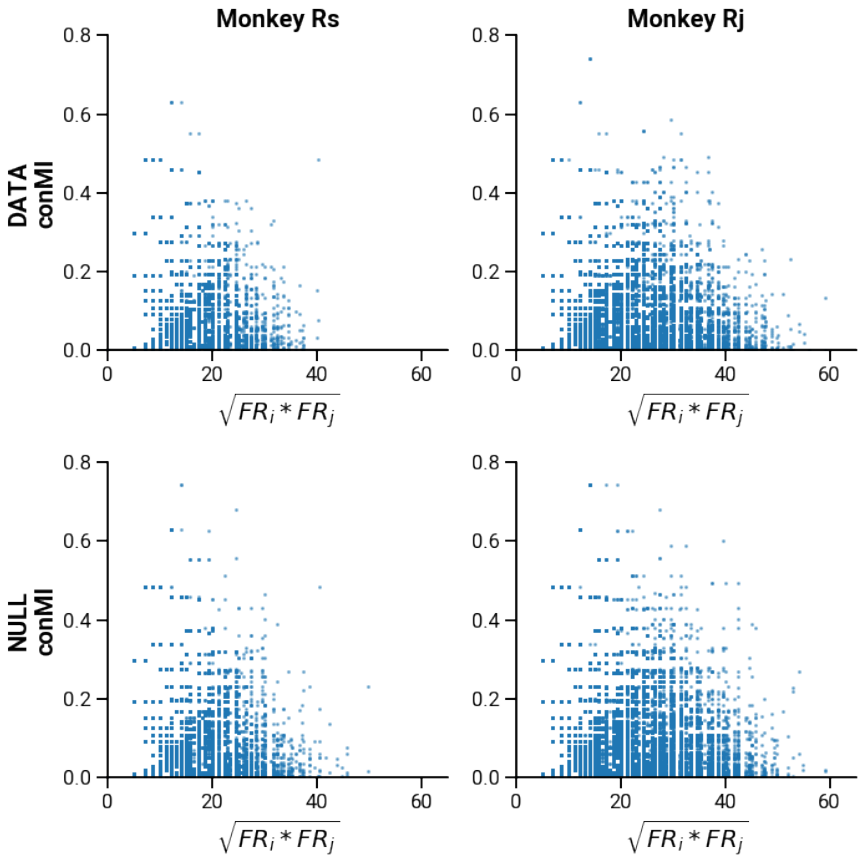

Supplementary Figure II-1 Confluent Mutual Information and firing rates are related.

Relationship between the geometric mean of two neurons and their measured conMI. Top row) data; Bottom row) null

[39] Levy, Sporns, and MacLean, "Network Analysis of Murine Cortical Dynamics Implicates Untuned Neurons in Visual Stimulus Coding."

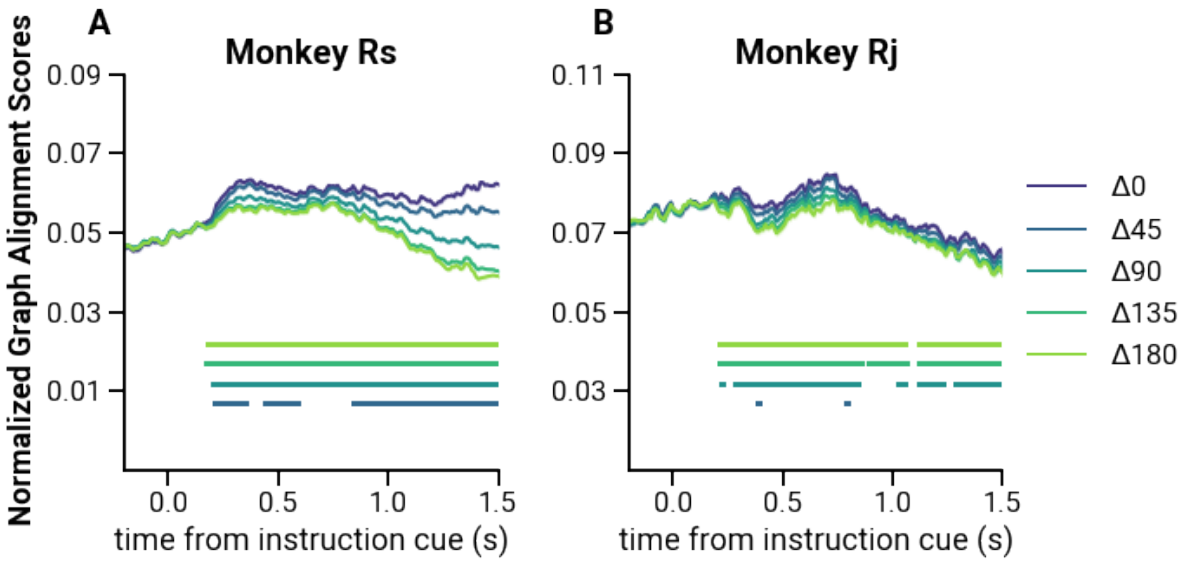

Supplementary Figure II-2 Normalized Graph Alignment Scores.

Normalized GAS as described in [40]

$$norm(GAS) = \frac{GAS - \widehat{GAS}}{1 - \widehat{GAS}}$$

Where $\widehat{GAS}$is the average GAS between two pairs of FNs for 45 rate-matched null FNs. **(A)** Mean normalized alignment scores between pairs of FNs at each sliding window aligned to the instruction cue. The shaded region, while very small, indicates the SEM of the GAS distribution. Alignment scores are separated based on reach target difference (in **Δ**degrees). Straight horizontal lines bottom plot indicate when the GAS scores from each **Δ**degree distribution become significantly different from the score distributions between FNs of the same direction ($p<0.01$ MWU two-sided test, Bonferroni corrected).

[40] Gemmetto et al., "Multiplexity and Multireciprocity in Directed Multiplexes"; Levy, Sporns, and MacLean, "Network Analysis of Murine Cortical Dynamics Implicates Untuned Neurons in Visual Stimulus Coding."

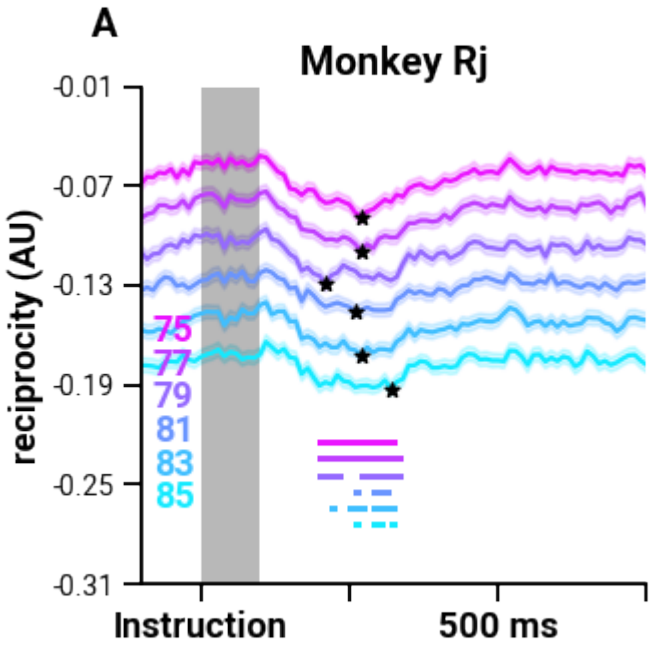

Supplementary Figure II-3 Significant decrease in reciprocity in Rj between upper quartile of edge weights.

Same as Fig 6 but for edge weights from the upper quartile and above.

CHAPTER III. Temporal functional network states reveal stereotypical behavioral sequences during artificial prey capture

INTRODUCTION

In Chapter 2, I found that the set of precise pairwise statistics between neurons across the population summarized as a Functional Network (FN) carries information about behavior (specifically, about the instructed reach direction) that is beyond what can be found from firing rates alone. These statistical relationships are temporally dynamic and, consequently, the decodable information changes during the trial in a systematic way. The experimental paradigm wherein I demonstrated these results required the trained subjects (2 male *Macaca mulatta*) to use an exoskeleton, which limited the movements to 1 dimension (horizontal plane), to control a cursor on the screen and perform 1 of 8 straight-line reaches from the center to an instructed peripheral target (center-out task, CO). In this current chapter, I investigated if these previous findings hold true for a free-behavior paradigm, the artificial prey capture task (PC), with the common marmoset (*Callithrix Jacchus)*. In this task, the marmoset is presented with a virtual prey that traverses a touchscreen and is rewarded upon the successful capture of the virtual prey. He can voluntarily engage with the task by self-initiating trials in an in-enclosure behavioral training apparatus [1]. I asked whether the structure of the FNs are related to different behaviors during this less constrained task.

Prey capture is a skill that juvenile marmosets learn from experience and repeated exposure. A study that compared locust catching behavior in juvenile and experienced marmosets showed that juveniles would lose almost half of their caught prey, while expert marmosets were

[1] Walker et al., "A Platform for Semiautomated Voluntary Training of Common Marmosets for Behavioral Neuroscience."

able to catch and consume most of their prey [2]. Thus prey capture is an ethologically relevant motor behavior that marmosets learn and engage in in the wild. The ability to recreate this in an experimentally repeatable and controllable way would therefore be complementary to the live-prey capture experimental paradigm (led by Jeff Walker), as well as beneficial to the study of motor control and skill acquisition of marmosets. I developed a parameterized prey capture task to present realistic and repeatable prey dynamics to the marmoset via a touchscreen. This allows us to test a wider range of "prey" tortuosities as well as investigate the emergence of strategies through the learning of new prey dynamics.

Early studies that quantified animal dispersal in unobstructed environments show persistence and bias in movement direction [3]. That is, an animal tends to move forward, and more likely would make small deviations from the forward direction rather than make large angle turns. This directional persistence results in, in theory, movement directions that are autocorrelated and the distribution of turning angles that are centered at 0°. The observation of directional persistence led to studies that modeled animal movements as correlated random walks [4]. I used a continuous-time correlated random walk to generate prey trajectories for the PC task [5]. I found that a marmoset (TY) voluntarily engaged in the task, performing up to 120 trials in one 90 min session. Marmoset TY exhibited evidence of learning by decreasing the average time it takes for him to capture the virtual prey over days when presented with prey moving in the same generated movement trajectory.

---

[2] Schiel et al., "Hunting Strategies in Wild Common Marmosets Are Prey and Age Dependent"; Schiel and Souto, "The Common Marmoset."
[3] Turchin, *Quantitative Analysis of Movement : Measuring and Modeling Population Redistribution in Animals and Plants*.
[4] Kareiva and Shigesada, "Analyzing Insect Movement as a Correlated Random Walk"; Turchin, *Quantitative Analysis of Movement : Measuring and Modeling Population Redistribution in Animals and Plants*.
[5] Johnson et al., "Continuous-Time Correlated Random Walk Model for Animal Telemetry Data"; Reynolds, "Bridging the Gulf between Correlated Random Walks and Lévy Walks."

In this chapter, I focused on one behavioral session. In ~65% of the trials he performed in this session, he captured the virtual prey within 1 second. The hand position was tracked using DeepLabCut (DLC, [6], and showed that for these sub-second trials, marmoset TY made stereotyped hand movements. I investigated whether the structure of the measured temporal FNs relate to aspects of the behavior during engagement with the task. I constructed temporal FNs in the same way described in Chapter 2. Briefly, pairwise confluent Mutual Information (conMI) is computed between all pairs of neurons within a short sliding window (200 ms) across a trial. The temporal FNs are projected into a low-dimensional subspace using UMAP (Methods) and a spline is fitted along the points to show the projected neural trajectory for each PC trial. In Chapter 2, I found that the similarity of the FNs were related to the similarity of the instructed reach target. I used the same similarity metric (graph alignment score, GAS) to show that FNs during PC task events such as trial start, target presentation, and target acquisition, are discriminable above chance levels by their nearest neighbors.

Taking advantage of these results, I created a meta-network of non-overlapping FNs in time by measuring their pairwise GAS as the edge weights of the meta-network. Many complex networks exhibit groups of nodes that have dense connections between them compared to the rest of the network [7]. This property can be quantified as the network's *modularity* and methods of finding partitions that maximize modularity can be used to detect these node groups or "communities". I used the Louvain community detection algorithm (Louvain, LCDA, [8]) to partition the meta-network. Therefore, LCDA can find a partition of the network where each

[6] Mathis and Mathis, "Deep Learning Tools for the Measurement of Animal Behavior in Neuroscience"; Mathis et al., "DeepLabCut: Markerless Pose Estimation of User-Defined Body Parts with Deep Learning"; Nath et al., "Using DeepLabCut for 3D Markerless Pose Estimation across Species and Behaviors"; Moore et al., "Validating Markerless Pose Estimation with 3D X-Ray Radiography."
[7] Girvan and Newman, "Community Structure in Social and Biological Networks."
[8] Blondel et al., "Fast Unfolding of Communities in Large Networks."

community is composed of times when the computed FNs are most similar. I hypothesized that FNs that are structurally similar (high GAS) that are consequently grouped into the same community will show similar behavioral states. Indeed, I found that temporal FN states correspond to certain behaviors, such as extension of the arm or licking, and that successful trials involve a stereotyped sequence of these states.

METHODS

Development of an artificial prey capture task: model and implementation

Generative model for prey trajectories

Correlated random walks (CRW) have been used to describe the dispersal patterns of individual animals [9] such as ovipositing cabbage butterflies [10]. These early studies showed that the distribution of the turning angles of movement paths was unimodal and centered on 0° [11]. However, turning angles and path lengths are subject to how one discretizes these movement patterns which are often continuous in nature [12]. The continuous-time CRW model mitigates this by modeling movement velocities as an Ornstein-Uhlenbeck process (OU),$x(t)$, where:

$$dx = \frac{-(x-\mu)}{\tau}dt + \sigma\sqrt{\frac{2}{\tau}}dW$$

and μ is the mean, σ is the standard deviation, τ is the autocorrelation timescale of the velocities, and W a Wiener process. This stochastic differential equation produces velocities that

[9] Turchin, *Quantitative Analysis of Movement : Measuring and Modeling Population Redistribution in Animals and Plants*.
[10] Kareiva and Shigesada, "Analyzing Insect Movement as a Correlated Random Walk."
[11] Kareiva and Shigesada; Reynolds, "Bridging the Gulf between Correlated Random Walks and Lévy Walks."
[12] Johnson et al., "Continuous-Time Correlated Random Walk Model for Animal Telemetry Data"; Reynolds, "Bridging the Gulf between Correlated Random Walks and Lévy Walks."

are Gaussian-distributed and exponentially correlated, comparable to velocity distributions that are observed empirically in *Tenebrio Molitor*, a beetle species that is a staple in marmosets' diet [13].

BeTL task: Behavioral Touchscreen Learning Task

I developed Behavioral Touchscreen Learning or BeTL (pronounced *beetle)*, a Processing-based software (Processing.org) that presents visually cued motor tasks to marmosets via a touchscreen. The software runs on a Raspberry Pi 3B, the details of the hardware are discussed in the next section.

In general, the marmoset is presented with a target on the screen and is given an Acacia Gum reward (15% dilution) through a reward tube, and is paired with a clicker sound (term *reward* in this chapter refers to both the liquid reward and the paired sound). The target can be set by the experimenter and is determined by the preference of the marmoset. During training, the marmoset is presented with images of a beetle, a mealworm, a dried mango, a circle, and a marmoset face. The location and behavior of the target is dictated by the program mode. The BeTL program has two main modes: "noisy beetle", and "prey capture".

The *noisy beetle* (NB) mode shows a moving target with a constant Y position, and moves on the X-axis using a Perlin Noise function [14] over time mapped over the width of the touchscreen. This noise function produces random positions that are normally distributed and centered on the middle of the touchscreen. This mode is used to train the marmoset to engage with the touchscreen or to assess attention or engagement level.

The *prey capture* (PC) mode uses the model described in the section above to generate artificial prey trajectories. The velocities for each dimension are independent (i.e. the x and y

[13] Reynolds, Leprêtre, and Bohan, "Movement Patterns of Tenebrio Beetles Demonstrate Empirically That Correlated-Random-Walks Have Similitude with a Lévy Walk."
[14] Perlin, "An Image Synthesizer."

velocities are generated from independent OU processes). The artificial prey capture task is structured as follows: A start screen is presented while on idle (no engagement). This shows a target on the screen on the side of the reaching arm (determined by the experimenter and can be toggled between left- and right-side within the software; usually contralateral to the hemisphere of the recording site). The marmoset can voluntarily initiate a trial by touching the start target. A small reward is given for initiating a trial. After about 550 ms delay (550.21 ± 29.67 ms), a target appears and begins to move in the generated path. The experimenter can load a previously generated path or generate a new prey trajectory during the session. If the marmoset is able to "capture" the moving target, a full reward is given (16x initial reward). A successful capture of the target is defined as touching within the boundaries of a circle circumscribing the target plus a 50 pixel buffer (about +9.53 mm). A trial is considered incorrect if the marmoset missed the target. Trials wherein the target was not captured within 15 seconds were not included in the analyses.

Because the prey trajectories are created programmatically, the task is flexible: we can present the same trajectory multiple times to assess the learning of individual trajectories, and we can generate a family of trajectories that are specified by the parameters of the model to study the emergence of strategies through the learning of new prey dynamics. The experiments presented in this Chapter are of the former kind.

I began each learning experiment by a few sessions of habituation to the apparatus and the touchscreen, if necessary. Despite being trained on engaging with the touchscreen, the marmoset sometimes requires an initial "priming" of the behavior between different behavior paradigms or experimental breaks (>2 weeks of no touchscreen tasks) so that any improvements that we see can be attributed to learning the prey trajectory and not from getting used to the touchscreen. During the habituation phase, the marmoset can freely enter the apparatus and engage with the

touchscreen. They are presented with the NB task and are rewarded for initiating trials and capturing the target. There are some instances where the marmoset is uninterested or unaware that the game is available, I play a few clicks to entice the marmoset and they are given a reward for entering the apparatus. The experiment does not begin until the marmoset shows consistent touchscreen engagement (e.g. performs more than 20 NB trials in one session). Before each experiment, I check whether the generated trajectory passes the criteria: 1) the trajectory does not begin too close to the start position or where the marmoset tends to rest their hand (close to the partition). 2) While this is already accounted for by the variable *wallAvoidanceFactor* in the code (this reflects the velocity by 1.5x when the target is at a boundary), I make sure that the artificial prey trajectory does not spend most of the time "hugging" the boundaries of the virtual arena. I show the marmoset the same artificial prey trajectory over a series of days until their time-to-target plateaus. The behavior data presented in this chapter consists of 4 learning experiments. For experiment 1 and 2, marmoset TY was shown the same trajectory 80 days apart (from the end of experiment 1 to the beginning of experiment 2). New trajectories were generated for experiment 3 and 4 separately. For all trajectories: σ= 0.01 m/s, τ = 10 s.

To screen potential subjects, I presented a video of moving insects to the marmoset on a tablet. I observed whether they look at the screen and reach for the target. Most marmosets readily reached for moving beetles on a screen however pairing the target to a reward needed incremental training. The marmoset is first presented with a preferred treat and when they reach for the treat, I play a clicker sound. Eventually the sound of the clicker will signal to the marmoset that there is a treat present. This is then paired with a physical target: the marmoset must reach the target before receiving the reward. The clicker sound is played and the marmoset is given a reward through a reward tube whenever they enter the apparatus (described in the next section, *marmoset-pi*). The

behavior is shaped by showing a marmoset a physical target and while the marmoset is holding the target, the experimenter can lead that hand to the touchscreen. A touchscreen training task (TTT) is then shown to the marmoset. This task has three modes: a still target in the middle of the screen, an NB mode, and a random target mode. I took a hybrid of two strategies: 1) daily training for <2 hours a day where I shape the behavior manually by a mixture of target and clicker training in the apparatus and presenting the TTT. 2) Leaving the apparatus and TTT available for the marmoset to voluntarily engage with throughout the day. I monitor the behavior via a webcam and control software via remoting into the Raspberry Pi.

Implementing this task on a touchscreen allows the flexibility to create and present new visually-cued motor tasks with minimal additional training.

Marmoset-Pi: using Raspberry Pi for capturing voluntary, goal-directed behaviors

Previous work by Walker et al [15] showed that marmosets will readily forage and self-train throughout the day in an in-enclosure behavioral training apparatus. This training apparatus is flexible and modular allowing multiple behavioral tasks to be presented in the apparatus by changing the "front end" while the base that is attached to the enclosure remains the same. We upgraded the front end of the behavioral apparatus to include a single-board computer (Raspberry Pi 3b, Raspberry Pi Foundation, UK) which has a touchscreen display (Raspberry Pi official 7 inch Touchscreen, Raspberry Pi Foundation, UK) to present visually cued motor tasks, IR break beam sensors (Adafruit Industries, New York, NY) to trigger behavior tracking (videos and engagement times) throughout the day, and a syringe pump (syringepumps.com, NE-500) to deliver acacia gum. In development, I also prototyped the inclusion of a Radio Frequency identification

[15] "A Platform for Semiautomated Voluntary Training of Common Marmosets for Behavioral Neuroscience."

(RFIDREAD-μRW 134 kHz, Priority1 Designs, Melbourne, AU) reader to allow for parallel training with multiple animals (microchipped with Datamars Slim Transponder 134.2 kHz, FDX-B, Datamars, Lamone, CH). However this was unreliable due to the reading distance and positioning of the reader. This could benefit from a different reader with a further and wider reading distance. The infrastructure for the behavioral apparatus is affordable and allows for rapid prototyping. The blueprint for the apparatus was designed in Fusion 360 detailed in Walker et al [16]. Panels are laser cut (Universal Laser Systems VLS4.60, Scottdale, AZ) acrylic sheets (McMaster Carr, Elmhurst, IL). A custom reward tube holder is 3D printed (Form3, Formlabs, Somerville, MA) and a PVC soft plastic tubing (McMaster Carr, Elmhurst, IL) is fitted into the holder. A thin laser-cut acrylic partition separates the task arena and where the marmoset stands while engaging in the task.

Marmoset-pi is a suite of Python scripts that allows for the control and reading of the included actuators and sensors via the Raspberry-Pi GPIO pins. A key script that was used in this chapter is beamBreaker.py. This script has two modes: sensor and manual. In sensor mode, the IR break beam sensors are read at 100 Hz, and if the receiver detects a beam break (subject possibly present and engaging), it sends a trigger to begin behavioral video recording. In manual mode, the state of the recording can be toggled on or off by the experimenter by pressing the Enter or Return key. In addition, the marmoset-pi also serves the BeTL task via the touchscreen (detailed above). The BeTL software controls the pump to deliver the reward, and sends out 5V pulses to an analog channel in the Cerebus Neural Signal Processor (BlackRock Microsystems, Salt Lake City, UT) during different task events: reward, clicker, trial start, and trial end. These trigger signals were used to align the data from the BeTL task to the neural data.

[16] Walker et al.

Neural and Behavioral recordings

A common marmoset, *Callithrix jacchus* (marmoset TY, Male, 10 years old, 368 g), was implanted with a 96-channel Utah Array (Blackrock Microsystems, Salt Lake City, UT) on the right hemisphere using stereotaxic coordinates [17] to target the forelimb area of the primary motor cortex (Fig 1A). Surgical procedure is described in detail in Walker et al [18]. This is marmoset TY's second array implantation and the titanium pedestal was reused for the new array (See "Alternative Outcomes" section and Fig 7 in [19]).

Marmoset Ty is pair-housed with another marmoset (female, 6 years old, 286 g) in an enclosure (height: 60 ft, width: 2 ft, depth: 2 ft) with free access to food, water, climbing branches, a foraging shelf, and a nest box. A hammock is also provided all day except during behavioral task sessions as it occludes parts of the enclosure.

The surgical and behavioral procedures involved in this study were approved by the University of Chicago Institutional Animal Care and Use Committee.

[17] Burman et al., "Anatomical and Physiological Definition of the Motor Cortex of the Marmoset Monkey"; Burman et al., "Patterns of Cortical Input to the Primary Motor Area in the Marmoset Monkey."
[18] "Chronic Wireless Neural Population Recordings with Common Marmosets."
[19] Walker et al.

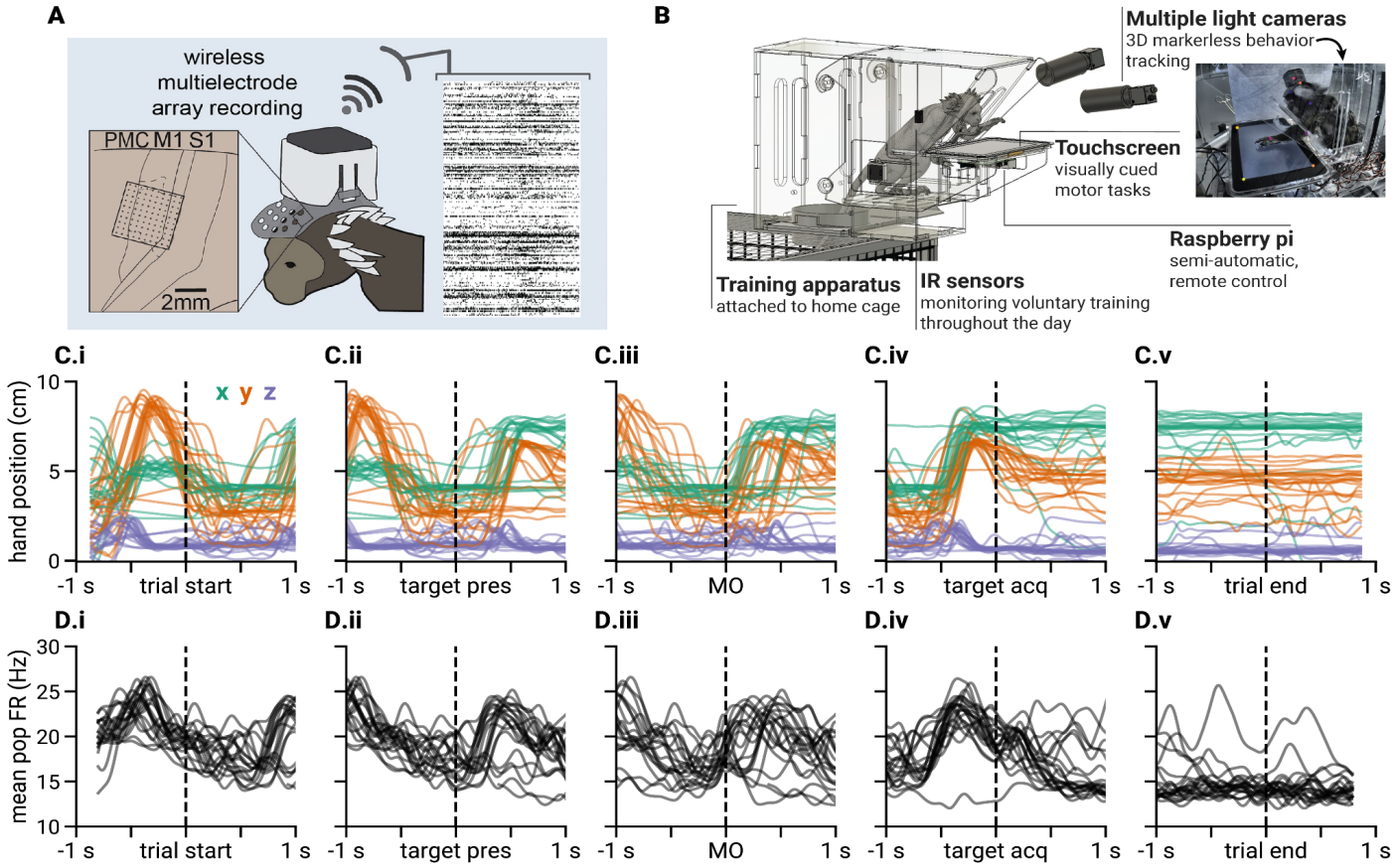

Figure III-1 Simultaneous neural and behavioral data during unconstrained voluntary goal-directed reaching.

(A) (from Walker et al. 2021) L-R Target location of the array according to stereotaxic coordinates, headstage for wireless recording, example raster from the array. **(B)** Behavioral training infrastructure. Inset: frame from a BeTL task with body parts tracked using a trained DLC model. **(C)** x- (green), y- (orange), z- (purple) 3D coordinates inferred from the DLC model centered on (i) Trial start, (ii) target presentation, (iii) movement onset, (iv) target acquisition, (v) trial end for 27 trials **(D)** Mean instantaneous firing rate across 155 neurons for the same trials and centered on the same times as in C.

Neural Data recording and pre-processing

Neural data was collected using a Blackrock Cereplex Exilis, which combines a digital amplifier and a wireless transmitter in a compact headstage (9.87 g, height: 14 mm, width: 25 mm, depth: 23 mm). The headstage has a built-in Li-ion rechargeable battery (3.7 V, 200 mAh) that allows us to collect neural data for around 90 minutes. A quick-connect solution designed by Jeff Walker facilitated the removal/attachment and charging cycle with minimal experimenter intervention and disruption to the marmosets' natural behaviors (Fig 1A, [20] elaborates on a similar quick-connect system). Data is transmitted to 8 receiving antennas placed strategically around the enclosure to minimize signal drop-off. The antennas are attached to the wireless receiver which amplifies and decodes the signal, before it is transmitted into a digital hub, which then converts the digital signal into an optic-digital format to be processed by the Cerebus Neural Signal Processor (Blackrock Microsystems, Salt Lake City, UT). Finally, the signal is visualized, and stored using Blackrock's Central Software running on a processing computer. The maximum sampling rate of the Cereplex Exilis is 24.5 kHz, however the signal up-sampled to 30 kHz using an up-sampled buffering process and band pass filtered. The waveforms that crossed the root mean square (RMS) multiplier threshold (-6.25x RMS voltage) were roughly sorted online using the Hoops method wherein the experimenter defines a unit by placing a series of "hoops" that a waveform has to pass through in order to be considered as a spike from that unit. After the experimental session, sorting rules were verified and if needed, threshold crossings were re-sorted using the scanning Valley-seeking method using Plexon Offline sorter (Plexon, Dallas, TX).

[20] Walker et al.

Behavioral Recording and Pose Estimation

Four high-speed cameras were used to capture both spontaneous behavior in the enclosure and voluntary, goal-directed behavior while engaging in the task in the apparatus (FLIR Blackfly S, 200 frames s−1, 1440×1080, FLIR, Wilsonville, OR). The cameras were positioned to minimize occlusion from the enclosure furniture and apparatus infrastructure (Fig 1B). The enclosure cameras record throughout the entire experimental session at 30 frames per second. The cameras that are pointed at the apparatus are triggered by the breaking of the IR beam or manually by the experimenter (see marmoset-pi section above) and records videos at 150 frames per second. Calibration frames were recorded before each experimental session to use to triangulate the two pairs of camera views for the enclosure and the apparatus. The contrast of the videos is improved using contrast limited adaptive histogram equalization (CLAHE, OpenCV, [21]). The filtered videos are then labeled using a DeepLabCut (DLC)[22] model trained on videos from previous experimental sessions (Fig 1B inset). Details of the network training and validation of the model can be found in Moore et al [23]. The output of the DLC model was refined using a set of XMALab tools for DLC ([24], with custom code from Jeff Walker). Specifically, marker jumps and reprojection errors were corrected on XMALab then triangulated into 3D coordinates using the calibration images.

[21] Bradski, "The OpenCV Library."
[22] Mathis et al., "DeepLabCut: Markerless Pose Estimation of User-Defined Body Parts with Deep Learning"; Nath et al., "Using DeepLabCut for 3D Markerless Pose Estimation across Species and Behaviors."
[23] "Validating Markerless Pose Estimation with 3D X-Ray Radiography."
[24] Laurence-Chasen et al., "Integrating XMALab and DeepLabCut for High-Throughput XROMM."

Network Analysis

Temporal functional network (FN) construction

The spike times for the isolated units are binned into 10 ms bins where the bin is assigned a value of 1 if at least one spike occurred during that window and 0 otherwise. For every trial I computed the pairwise confluent mutual information (conMI) within a 200 ms sliding window for all pairs of putative neurons (see Chapter 2, [25]). conMI tells us how much information we gain from the firing state of a source neuron i at time t about the firing state of target neuron j in the same time bin t and the consecutive bin, t+1:

$$conMI = \sum_{i(t)\in\{0,1\}} \sum_{j(\widehat{t})\in\{0,1\}} p(i(t), j(\widehat{t})) \cdot log_2 \left[\frac{p(i(t), j(\widehat{t}))}{p(i(t)) \cdot p(j(\widehat{t}))} \right]$$

$$where\ j(\widehat{t}) = \begin{cases} 1, & \text{if } j(t) = 1 \text{ OR } \ j(t+1) = 1 \\ 0, & \text{otherwise} \end{cases}$$

The functional network (FN) constructed using this measure is weighted and directed. Each trial can be represented as a temporal FN: a set of FNs where, FN = (V,E,T) where V are the nodes, E are the edges, and T is the time dimension (definition adapted from [26]. The time point, T, that I associate with the temporal FNs is the last time bin of the 200ms window from which we compute the edge weights. For example, the binarized spike train used to compute the FN at a specific time includes 19 bins before instruction and the bin aligned to that time.

I generated FNs from short interval rate-matched Poisson neurons (rate-matched FN, FN_{rm}) in order to distinguish between the second order structure that results from firing rates alone and that which is the result of precise spike timing. First, the instantaneous firing rate of each neuron

[25] Chambers et al., "Ensemble Stacking Mitigates Biases in Inference of Synaptic Connectivity."
[26] Thompson, Brantefors, and Fransson, "From Static to Temporal Network Theory: Applications to Functional Brain Connectivity."

was estimated by convolving the spike train of each neuron with a Gaussian kernel (σ= 20 ms) over each trial. Then a rate-matched spike train is generated from an inhomogeneous Poisson process using the estimated instantaneous firing rate profile as the probability of observing a spike for that neuron within a sampling period (10 ms).

Low-dimensional embedding and evaluation measures

Non-overlapping temporal FNs from all trials were vectorized and used as samples to create a low-dimensional manifold using Uniform Manifold Approximation and Projection (UMAP, [27] with the following parameters: n_neighbors=30, min_dist=0, metric='cosine'. Horizontal and vertical univariate cubic splines were fitted through the set of low-dimensional projected points that represent the temporal FN in order to visualize a single trajectory through the constructed low-dimensional manifold.

I used a precision-at-k metric to evaluate whether the embedding and the FNs are separable at specific task events. Specifically, the trial initiation, target presentation, movement onset, target acquisition, and trial end. Briefly, precision-at-k measures the fraction of a point's k nearest neighbors that belong to the same category. In this work I looked at the fraction of the top 5 nearest neighbors of each point that represents a task event. I performed this evaluation on both the low-dimensional embedding and the FNs themselves. For the low-dimensional embedding, I used the Euclidean distance between the projected points in order to rank the neighbors. To compare the similarity of the FNs, I used the Graph Alignment Score between pairs of FNs (see Chapter 2, [28]):

[27] Mcinnes, Healy, and Melville, "UMAP : Uniform Manifold Approximation and Projection for Dimension Reduction ArXiv : 1802 . 03426v2 [Stat . ML] 6 Dec 2018."
[28] Levy, Sporns, and MacLean, "Network Analysis of Murine Cortical Dynamics Implicates Untuned Neurons in Visual Stimulus Coding"; Gemmetto et al., "Multiplexity and Multireciprocity in Directed Multiplexes."

$$GAS = \frac{2\sum_{i=1}^{k}\sum_{j=1}^{k} min(M_{ij}, N_{ij})}{\sum_{i=1}^{k}\sum_{j=1}^{k} M_{ij} + Nij}$$

GAS measures the ratio of similar edges over the total number of edges. In the weighted case, the numerator represents the sum of the minimum edge weight between each pair of nodes, and the denominator is the total sum of the edge weights.

Detecting states of temporal FNs using graph alignment

In order to detect temporal FN states, I took advantage of the separability of the FNs via graph alignment scores demonstrated in Chapter 2 and in this current work. State detection methods for temporal networks used here were introduced contemporaneously by Masuda and Holme [29], and Cao and Sayama [30], In both methods a similarity matrix across time was computed. This similarity matrix between the time-varying networks was then clustered via hierarchical clustering [31] or community detection [32]. In this work, I constructed a meta-network where in the nodes are non-overlapping FNs in time (FN_t) and the edge weights are their pairwise GAS. This network is undirected and weighted, since GAS is a commutative operation. I chose to use a non-overlapping time window for the FN_t to avoid high GAS scores between FNs computed from overlapping time windows despite different latent states.

The meta-network was then partitioned into "communities" or groups of FN_t that are more connected *within the group* versus *between groups*, a property of a network partition described as its *modularity*. The Louvain Community Detection Algorithm [33], finds such partitions by optimizing modularity:

[29] "Detecting Sequences of System States in Temporal Networks."
[30] "Detecting Dynamic States of Temporal Networks Using Connection Series Tensors."
[31] Masuda and Holme, "Detecting Sequences of System States in Temporal Networks."
[32] Cao and Sayama, "Detecting Dynamic States of Temporal Networks Using Connection Series Tensors."
[33] Blondel et al., "Fast Unfolding of Communities in Large Networks."

$$\Delta Q = \frac{k_{i,in}}{2m} - \gamma \frac{\Sigma_{tot} \cdot k_i}{2m^2}$$

All the communities with less than 10 members were not included in the rest of the analysis. I computed the probability of the temporal FN being in a specific state centered on the following task events: trial initiation, target presentation, movement onset, target acquisition, reward, and trial end.

In order to visualize the behavior during the detected states, I created composite frames from the behavioral videos during each state. First, I superimposed 25 random frames during the detected state. This shows in general what marmoset TY is doing during this state. I observed that many of the elements of the frame remained the same (the apparatus, touchscreen, background). Since I am interested in capturing motor behavior during these states, I am interested in the pixels that are changing over time. To isolate these pixels, I computed the mean for each pixel during each state which represents the pixels that were stable across the frames, and subtracted this mean to each frame. The sum of the absolute pixel values are shown in the second row of (Fig 5). This shows the pixels that are changing relative to the mean which captures movements in the frame during the state. Finally, I wanted to isolate the pixels that were changing the most (again, if the pixel values were stable it is likely that it is a stationary element in the environment). I computed the variance across time for each pixel and thresholded the frame to keep the top 25% of pixels that were varying the most.

RESULTS

Marmoset engaged with a virtual prey capture task

In 4 separate multi-day learning experiments, marmoset TY self-trained in the PC task. Marmoset TY readily engaged with the task, performing 70.74 ± 33.96 trials per day. Each valid

trial requires at least 2 reaches (to begin the trial and to capture the target), therefore the number of reaches exceeds the number of trials per day. This suggests that this task can be used to assay reaching behavior. On average, his performance (correct captures) across all the sessions is 74.39 ± 0.07 %. This stable performance shows that any improvements in the time-to-target is due to learning of the trajectory and not the task itself. The slope for time-to-target across sessions is negative for all experiments exhibiting improvements in time-to-target across sessions (Fig 2A). Moreover, marmoset TY was shown the same trajectory for experiment 1 and 2, 80 days apart (Methods). Although not significantly different, the initial mean time-to-target on the first day of the experiment was lower for experiment 2 (n.s., $p=0.082$, Welch's t-test). This may indicate that marmoset TY has some familiarity with the trajectory he was previously exposed to.

Since the generative model was validated on movement paths that were in the order of minutes and marmoset TY was able to capture the target within ≤9.51 s, the distribution of target velocities that the marmoset engaged with does not fully reflect what is expected from the model (Fig 2B). Considerations needed to be taken into account when using generative models are talked about in the Discussion. An interesting consequence of this discrepancy between model and output is that the generated velocities for experiment 3 were slower than the others (mean tangential velocity 0.018 ± 0.011 m/s) despite the identical model parameters. Indeed, the slope for the time-to-target across sessions was lowest for experiment 3 (slope = -0.006 s/days).

I have shown that marmoset TY readily engaged with the task without any behavioral modifications such as food restriction or isolating him from his pair-housed partner.

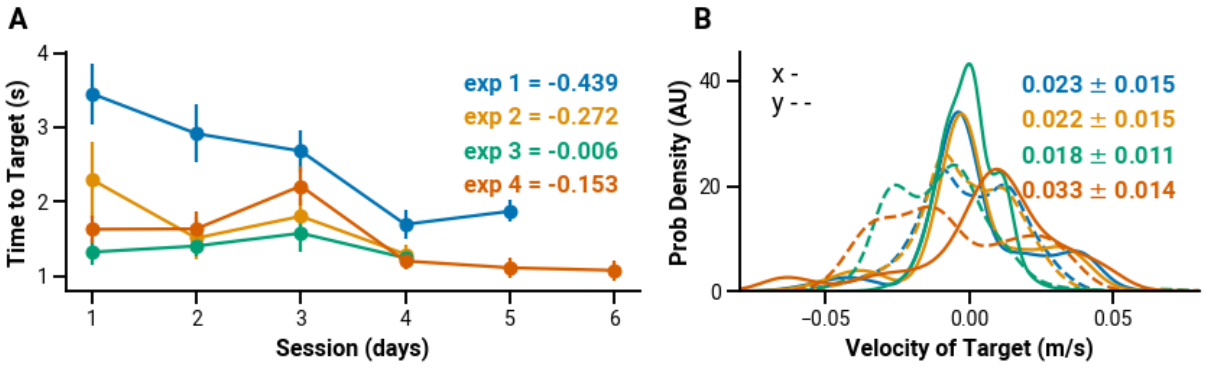

Figure III-2 A marmoset exhibits learning across days in an artificial prey capture task.

(A) Mean time to target over daily sessions for 4 separate learning experiments. Error bars indicated the standard error of the mean. The slope of the mean across sessions is indicated in the top right legend. **(B)** Distribution of x (solid line) and y (broken line) velocities of the presented targets across sessions for the 4 learning experiments. Color legend is the same as A. Mean (and standard deviation) tangential velocities for each experiment are indicated on the top right.

Temporal FNs are informative of task events

For the neural data analysis, I focused on the second session of the fourth experiment (TY20210329). The distribution of time to target in dataset TY20210329 shows that in 64.79% of the PC trials marmoset TY captured the target within 1 second of target presentation (Fig S2). The tracked hand position shows that for these correct trials that were completed within 1 second, marmoset TY performs this reaching strategy in a stereotyped manner. Is this reflected in the neural activity? In Chapter 2, I showed that similar target reach directions invoked similar trajectories of temporal FNs in low-dimensional space.

I constructed temporal FNs for each BeTL trial (neurons = 155, trials = 79). A low-dimensional subspace was created using non-overlapping FNs for all 79 trials. In Fig 3A, I show example neural trajectories of correct trials that were completed within 1 second (n trials = 16). It also shows the points in the trajectory when the following task events happen: 1 second before

trial start (gray circle), trial initiation (blue square), target appearance (orange triangle), movement onset (brown hexagon), target acquired (red cross), reward (violet star), trial end (green circle) and 1 second after the trial (black arrow head). These event types occur close together in low-dimensional space. Additionally, events from trial initiation to target capture occur within the same area forming a sequential "loop" during the trial. Interestingly, two trials start separately from the other trials (blue squares are outlined in red in Fig 3A). In these trials, marmoset TY initiated the trials with his right hand. The end of the trial (indicated by green circles in Fig 3A, also taken to mean that the full reward was delivered) lies in a different part of the subspace. This time also usually coincides with marmoset TY consuming the reward (manifested as licking behavior, facial movements were not tracked by DLC).

In order to quantify whether trial events are separable from each other, I computed the precision of the embedding for the top 5 nearest neighbors for each embedded task event (precision-at-5, Methods, for 5 event types: trial start, target presentation, movement onset, target acquired, trial end). Incorrect and long trials were also included in this quantification. For the low dimensional embedding, the mean fraction of the top 5 nearest neighbors of an embedded point belonging to the same task event is 0.46 ± 0.33 (mean ± sd), which is above chance (0.2). I investigated whether this is true for the full dimension of the networks themselves. I performed the same precision analysis above using the graph alignment scores (GAS, Methods), which compares two FNs edge by edge. The precision-at-5 for the task event FNs is 0.47 ± 0.30. I also measured the precision-at-5 for 25 realizations of FN_{rm}s to compare the distribution of fraction hits that might arise from chance correlations due to firing rates. I found that this is significantly lower than the empirical FNs with a precision-at-k 0.39 ± 0.28 (p=2.689e-03, MWW two sided test) for all the task events. I next looked at the fraction hits by task event to uncover if there are specific

events that are more easily discriminable than others. As expected from the low-dimensional embedding (Fig 3), the fraction hits for projected points and empirical FNs is highest for the end of the trial (0.65 ± 0.41 and 0.68 ± 0.36, respectively). Again, the end of the trial is defined as the time either all of the reward has been delivered (correct trials), or 500 ms after the trial timed out (incorrect reach or maximum time reached). At this point, marmoset TY has completed the reaching epoch of the trial, and specifically for correct trials, he is licking the reward tube. Note that the distribution of fraction of hits for the FN_{rm} at the end of the trial are significantly lower than the empirical FNs (0.39 ± 0.28, p = 3.260e-05, MWW two sided test). There is no significant difference between the FNs and FN_{rm}s during trial start, target presentation, movement onset, and target acquisition.

These results show that the structure of temporal FNs have information about events during engagement with the task. Specifically, for trials completed within 1 second, marmoset TY employed a stereotyped sequence of movements and the dynamics of the population structure during the trial showed stereotypy as well.

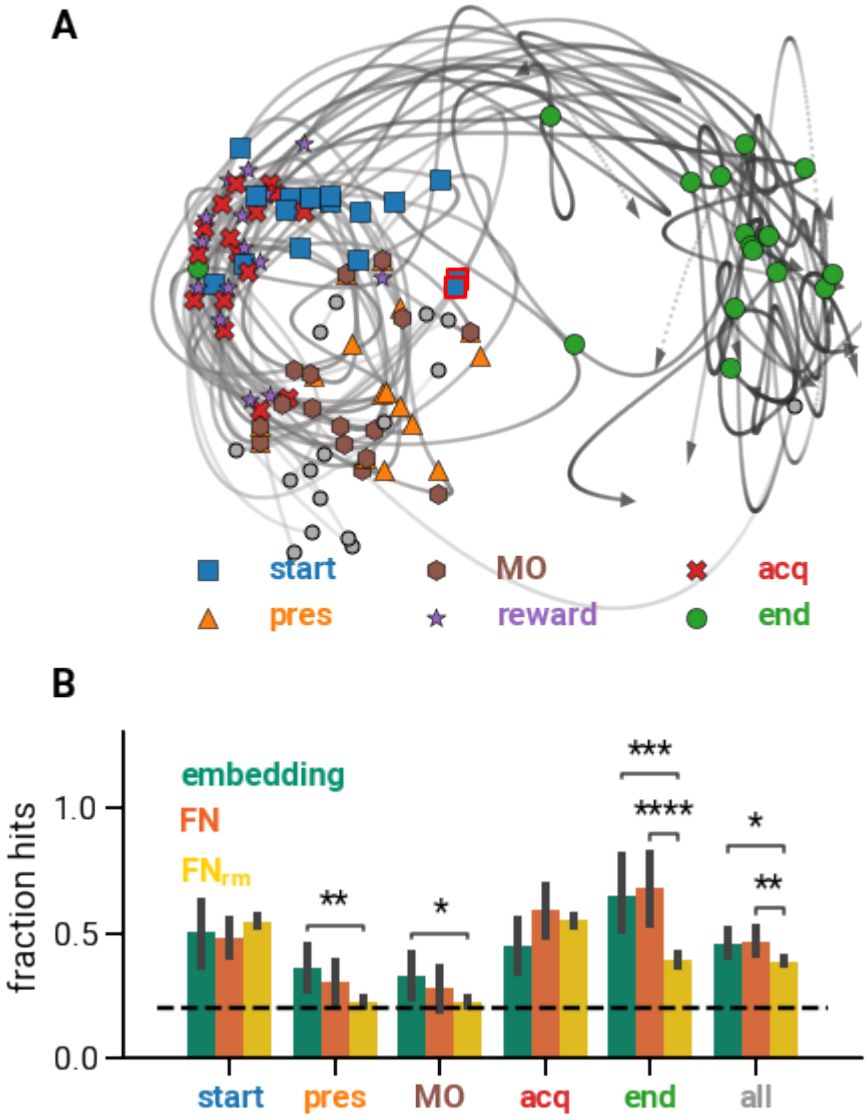

Figure III-3 Temporal FNs are informative of task events.

(A) Temporal FN paths through a low-dimensional (UMAP) embedding. Light to dark color of the path indicates early to late times in the trial, respectively. Markers across the path indicate: 1 second before trial start (gray circle), trial initiation (blue square), target appearance (orange triangle), movement onset (brown hexagon), target acquired (red cross), reward (violet star), trial end (green circle) and 1 second after the trial (black arrow head). **(B)** Precision-at-5 fraction hits for embedding (green), empirical FNs (orange), and 25 rate matched FNs (yellow). Dashed line indicates the chance level (0.20). P-value annotation under MWU test two-sides: *: 1.00e-02 < p <= 5.00e-02, **: 1.00e-03 < p <= 1.00e-02, ***: 1.00e-04 < p <= 1.00e-03, ****: p <= 1.00e-04

Detecting states of temporal FNs via alignment scores

In chapter 2, I showed that graph alignment scores between trials correlated with the similarity of the instructed reach. That is, trials with the same or neighboring instructed reach targets have higher alignment scores than those with opposite target reaches. In the results above, I demonstrated that FN structure is related to trial events like initiating a trial or receiving rewards. The same graph alignment score measure in Chapter 2 was used to show that these trial events are discriminable above chance from the FNs.

I utilized the similarity in the FN structure that was demonstrated by the low-dimensional embedding and the precision scores in order to detect dynamic states of the temporal FN (Fig 4A). I hypothesized that these states corresponded to specific task events. I constructed a meta-network wherein the nodes of the network are non-overlapping snapshots of the temporal FNs across trials in the TY20210329 dataset, and the edges between them are their pairwise alignment scores (GAS). This would mean that times with FNs that are more similar (higher GAS) will have stronger edges between them. Using Louvain Community Detection Algorithm (LCDA), the graph can be partitioned into "communities" where network modularity is optimized. Network modularity, simply put, measures the density of edges *within a community* versus *between communities*. Therefore, LCDA finds a partition of the network where each community is composed of times when the computed FNs are most similar.

LCDA detected 9 communities or "states" (Fig 4B Methods) however all communities that had less than 10 time points were not included in the analysis. This leaves us with 6 states which I will refer to using the original state numbers given by LCDA. In the same trials as in Fig 3A (correct trials that were completed within 1 second), I observe that the temporal FNs roughly followed a sequence of states across the trial (Fig 4H). These trials often begin at

state 5, then transition to state 8. Indeed, the probability of the FN being at state 5 peaks before trial start, and the probability of being in state 8 has a peak that is aligned to the beginning of the trial (Fig 4C). The temporal FNs are then likely transitions to state 2: a peak in probability is observed close to target presentation (Fig 4D). Notably, this is only true for the correct, stereotypical trials; there is no peak at this time for both the long trials and the incorrect trials (Fig S3). Shortly after movement onset, the temporal FNs transition back to state 5 followed by state 8 again when the target is acquired (Fig 4F). Finally the temporal FNs transition to state 6 (Fig 4G).

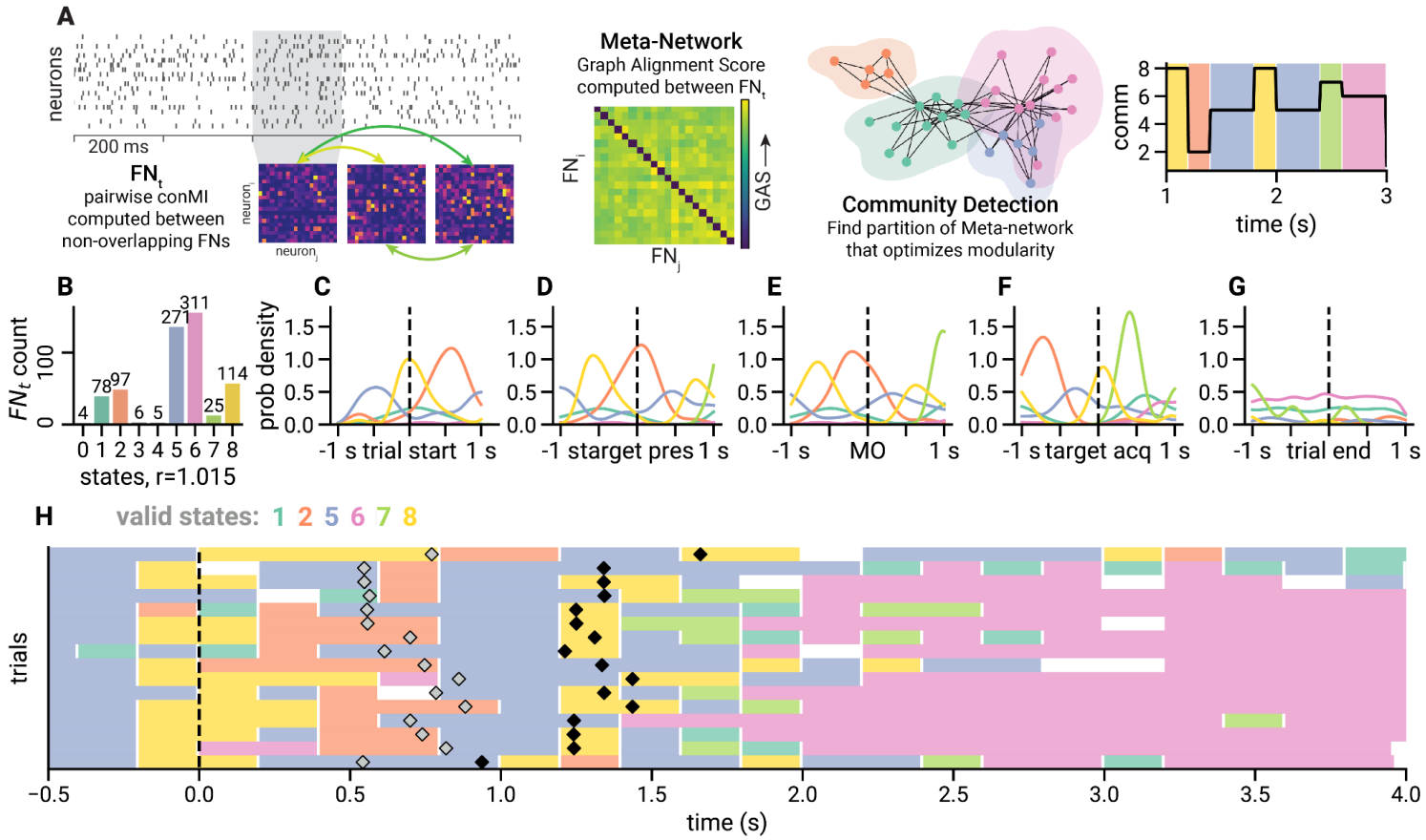

Figure III-4 Detecting states of temporal FNs via alignment scores.

(A) Procedure for creating the meta-network to detect structurally similar FNs. **(B)** Membership counts for each detected state. **(C)** Probability density of states aligned to trial start, **(D)** target presentation, **(E)** movement onset, **(F)** target acquisition, **(G)** trial end. **(H)** States over time for the 16 trials (whose trajectories were also shown in Fig 3A) arranged according to time-to-target (bottom is fastest). Gray diamond shows movement onset, and black diamond shows target acquisition.

In order to further relate the detected states with behavior, I looked at composite frames from the behavioral video during each state (Fig 5). Both states 5 and 8 show arm extension, signifying a relationship to reaching behavior which is supported by the evidence shown in Fig 4C and F (probability densities). When the FN is in state 2, most of the movement happens behind the partition. The peak in probability of this state during target presentation and right before the reaching sequences (transitions from states 5 then 8, Fig 4D), may point to this state corresponding to marmoset TY searching for the target. This may also be related to torso movements as he is searching from behind the partition. The frames during states 7, 6, and 1 show marmoset TY's head close to the reward tube suggesting that these states are related to licking behavior. The amount of arm extension is different between the three states. State 7, which only has 25 frames, has peaks following target acquisition and before the probability of state 6 and 1 rises. Frames during state 7 also show an extended arm while receiving the reward, which suggests that it may be linked to the earlier phase of licking for the reward. Towards the end of the trial the probability is dominated by state 6. Here, marmoset TY still has an extended arm. State 1 seems to correspond to licking behavior while the arm is behind the partition.

I showed that temporal FNs can be partitioned into structurally similar states and that these states show correspondence to similar behaviors. Moreover, successful trials completed within 1 second showed a systematic progression of temporal FN states.

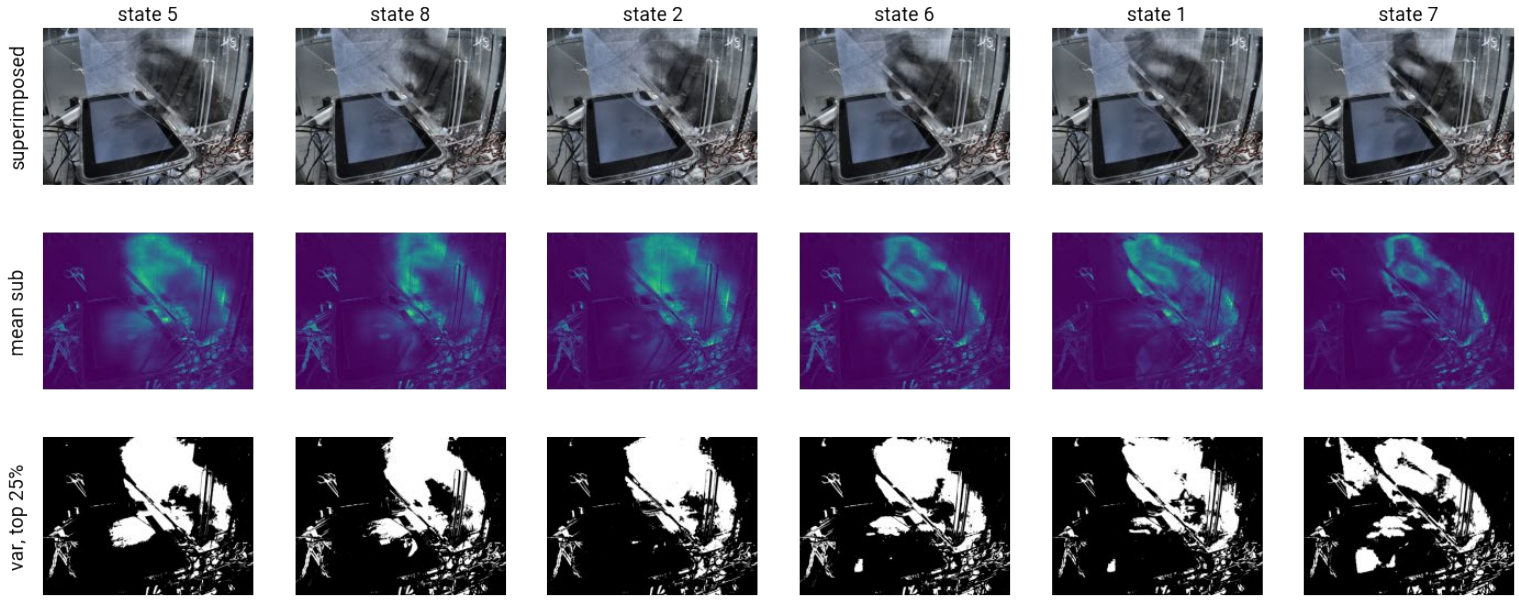

Figure III-5 Composite video frames for each detected state.

(Columns) Detected states, **(Rows) superimposed:** 25 random frames from each state are (continued) plotted on top of each other at 20% opacity. **Mean sub:** Shows the summed absolute value of all the mean-subtracted frames in the state. The mean frame is constructed by taking the mean value for each pixel. **Var, top 25%:** shows the top 25% of pixels with the highest variance during each state.

DISCUSSION

In this work, I have shown that the structure of short interval FNs may be related to aspects of behavior. First, I visualized the networks using a low-dimensional embedding. I show that temporal FN trajectories of successful trials in a voluntary, goal-directed artificial prey capture task are stereotyped echoing the stereotypy in the hand position trajectories. I observed that the top 5 nearest neighbors of FNs in both the low-dimensional space and in network space are likely to be from the same task events. This suggests that FN structure is discriminable by behavior. Interestingly, the same precision-at-5 metric for networks wherein the precise spike time correlations are disrupted (FN_{rm}), showed above chance precision-at-5, however it is significantly lower than the data overall. During the reaching phases of the trials (from start to target acquisition), the differences in task events can be explained by first order firing rates of the recorded units; the FN_{rm} are not significantly different from the empirical FNs. Notably, the mean population firing rate across the array, which was stereotaxically targeted to encompass the forelimb region of M1 [34], is high during the reaching epochs (peaks around 25 Hz). At the end of the trial, however, there is significantly more information from the second order interactions of the population that is not explained by chance correlations arising from the firing rates alone. In fact, the precision-at-k for the empirical FNs is highest at the end of the trial showing that the structure of pairwise correlations may be able to provide additional information about the behavior and may be able to detect state changes even when firing rates are low (firing rates are around 10 Hz during the end of the trial and he typically not moving his arm). These results are in line with the findings in Chapter 2 wherein there is additional information in the pairwise correlations that consequently allows different behavior contexts to be more decodable.

[34] Walker et al., "Chronic Wireless Neural Population Recordings with Common Marmosets."

Because the graph alignment score metric can discriminate between discrete task events above chance, I used this to create a meta-network wherein the nodes are non-overlapping FNs in time, and the edges are their pairwise alignment scores. I then partitioned the network to optimize modularity, a property of a partitioning wherein the nodes within a partition are more densely connected with each other than outside of the partition. This produces "communities" of FNs in time that are structurally similar. I hypothesized that the behavior during times that are assigned to the same communities will be similar as well. I found that the probability of observing specific states were aligned to the discrete task events and that a stereotyped sequence of states unfolded during successful trials. Other studies, using alternative methods, have also shown that neural population activity can be decomposed into "states" that align with kinematics [35] and timing of self-initiated behaviors [36]. The meta-network community detection framework corroborates these findings. Fig S4 shows that relative to trial start and target acquisition (end points of a reach), when the probability of state 8 surpases state 5 (i.e. a likely state transition from state 5 to 8), the velocity of the hand begins to decelerate. Additionally, this analysis suggests that the structure of the precise spike time statistics is important to identifying these states. Indeed, Recanatesi et al [37], using a Hidden Markov Model to infer latent states of the neural population in single trials, showed that destroying pairwise correlations by shifting spike trains circularly, lowers pattern confidence and does not detect stereotyped pattern sequences that were evident in the data. Future work to compare the found temporal FN states to the FN_{rm} controls would benefit in substantiating these results. From the precision-at-k analysis above, we might predict that states during the reach may be detected from FN_{rm} since discriminability between task events are comparable to the data FNs.

[35] Kadmon Harpaz et al., "Movement Decomposition in the Primary Motor Cortex."
[36] Recanatesi et al., "Metastable Attractors Explain the Variable Timing of Stable Behavioral Action Sequences."
[37] Recanatesi et al.

In behaviors that are not dominated by the firing rates (ie end of the trial), the data FNs showed higher precision-at-k and may add an additional axis of information to state detection especially for behaviors that do not give rise to high modulated firing rates across the recorded population (such as in reaching). It would be also be worthwhile to investigate whether the sequences found in the empirical FNs were more stable than FN_{rm} by looking at their respective state transition matrices. Moreover, one can generate a meta-network using normalized GAS (as described in Chapter 2 Supplementary Figure 2) to look at FN similarity and states beyond what is observed from chance interactions from firing rates alone

In this chapter, I also introduced the BeTL task as a paradigm to assay motor behavior. The dynamics of the prey was modeled as having velocities that followed an Ornstein-Uhlenbeck process. This is based on the observation that many animals show directional persistence and early work showing the utility of using correlated random walks to model animal dispersal [38]. The generative model should, in theory, produce velocities that are Gaussian-distributed centered on the mean, and exponentially correlated. In experimental conditions, however, the presented velocities do not match the expected velocity distributions from the model (Fig 2B). This is due to the fact that marmoset TY captures the target within 10 seconds whereas Reynolds et al [39] described the movement paths of *Tenebrio molitor* beetles during the span of 10 minutes. Moreover, these theoretical models of animal movement paths often assume a featureless unbounded environment. In the BeTL task, the beetle is bounded within the reaching distance of the marmoset. I also observed that despite the similar model parameters, the prey trajectories that the marmoset actually

[38] Turchin, *Quantitative Analysis of Movement : Measuring and Modeling Population Redistribution in Animals and Plants*; Kareiva and Shigesada, "Analyzing Insect Movement as a Correlated Random Walk"; Reynolds, "Bridging the Gulf between Correlated Random Walks and Lévy Walks"; Reynolds, Leprêtre, and Bohan, "Movement Patterns of Tenebrio Beetles Demonstrate Empirically That Correlated-Random-Walks Have Similitude with a Lévy Walk."
[39] "Movement Patterns of Tenebrio Beetles Demonstrate Empirically That Correlated-Random-Walks Have Similitude with a Lévy Walk."

sees may have different dynamics because of the short interval of the path that is presented. It is important to consider this when choosing prey trajectories and model parameters, especially when comparing different prey dynamics and movement strategies. An additional complexity in prey behavior that can be explored is their dynamic escape response [40]. Recent advancements in real time markerless pose estimation [41] may be able to aid in the development of a closed-loop virtual prey capture task to study hunting strategies when the prey exhibits evasive maneuvers.

The BeTL task has the potential to be used as a learning task. I observed improvements in time to capture the moving target over sessions during each experiment. It is worthwhile to investigate how the stereotypy in hand kinematics and temporal FNs emerge through learning. Previous studies have shown that possible activity patterns of a population in M1 are constrained within a low-dimensional "intrinsic manifold" [42] and that learning re-associates patterns within the intrinsic manifold to the new intended output within a brain computer interface (BCI) control paradigm [43]. This would suggest that the set of possible FN structures that could produce these within manifold patterns are also constrained. We can postulate from comparing incorrect or long trials with the correct trials that were completed within 1 second, that the ability to perform the BeTL task correctly and quickly requires the linking of temporal states into a strategic sequence. The correct linking and timing of behavior sequence require downstream circuits such as pre-supplementary area and supplementary motor areas, as well as the premotor cortex [44]. Eventually, performing this motor sequence many times over days may improve time to target, and may rely less on external inputs [45]. An advantage of a network representation of neural populations not used

[40] Card, "Escape Behaviors in Insects."
[41] Kane et al., "Real-Time, Low-Latency Closed-Loop Feedback Using Markerless Posture Tracking."
[42] Sadtler et al., "Neural Constraints on Learning."
[43] Golub et al., "Learning by Neural Reassociation."
[44] Kadmon Harpaz, Hardcastle, and Ölveczky, "Learning-Induced Changes in the Neural Circuits Underlying Motor Sequence Execution."
[45] Kadmon Harpaz, Hardcastle, and Ölveczky.

here but would be beneficial to studying learning-dependent changes, is that one can create sub-networks from existing FNs. Due to the marmosets' lissencephalic cortex, a single Utah array can span multiple motor and sensory areas (Fig 1A). A stimulation experiment could be performed to confirm the electrode placement and assign nodes into a sub-FN based on functional area. Learning-dependent FN changes can then be attributed to interactions between or within specific regions.

Over longer learning periods (in the order of days), researchers have observed that when the BCI mappings were outside of the intrinsic manifold, new neural patterns emerged to perform the task [46]. Moreover, in a different BCI learning paradigm, emergent coordination within the recorded population was observed [47] and network density was shown to be dynamic across days of BCI exposure [48]. One might postulate that perhaps during training to use the touchscreen, new associations regarding the capturing of a 2-dimensional prey (versus a live one), touching to capture (versus grasping), and licking the reward tube (versus bringing the prey to the mouth) would have to have happened. While outside the scope of the work presented in this chapter, it would be interesting to compare the detected states between touchscreen engagement and live prey capture and whether they make use of the same temporal FN states. Additionally, it would also be worthwhile to investigate how the temporal FN states emerge during training to engage with the touchscreen, and how sequences of temporal FN states are linked and refined when learning a new prey trajectory (within known prey dynamics) versus when the marmoset encounters new prey dynamics.

[46] Oby et al., "New Neural Activity Patterns Emerge with Long-Term Learning."
[47] Vaidya et al., "Emergent Coordination Underlying Learning to Reach to Grasp with a Brain-Machine Interface."
[48] Balasubramanian et al., "Changes in Cortical Network Connectivity with Long-Term Brain-Machine Interface Exposure after Chronic Amputation."

SUPPLEMENTARY FIGURES

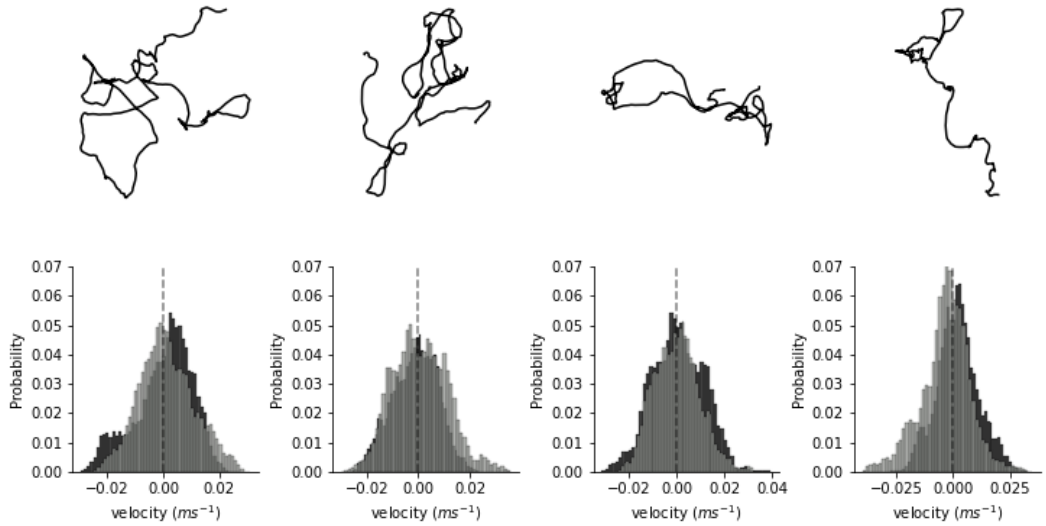

Supplementary Figure III-1 Example 10 minute prey trajectories from generative model.

Bottom row: x (black) and y (gray) velocity probability distributions

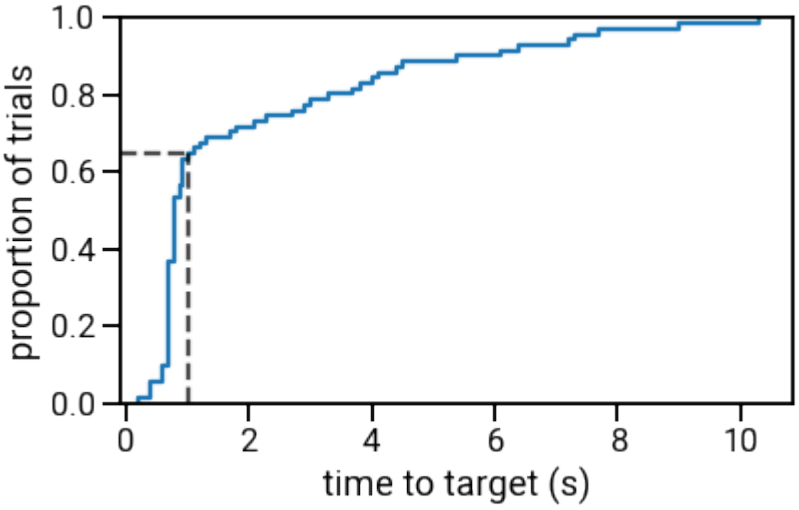

Supplementary Figure III-2 Cumulative distribution of time-to-target times for dataset TY20210329

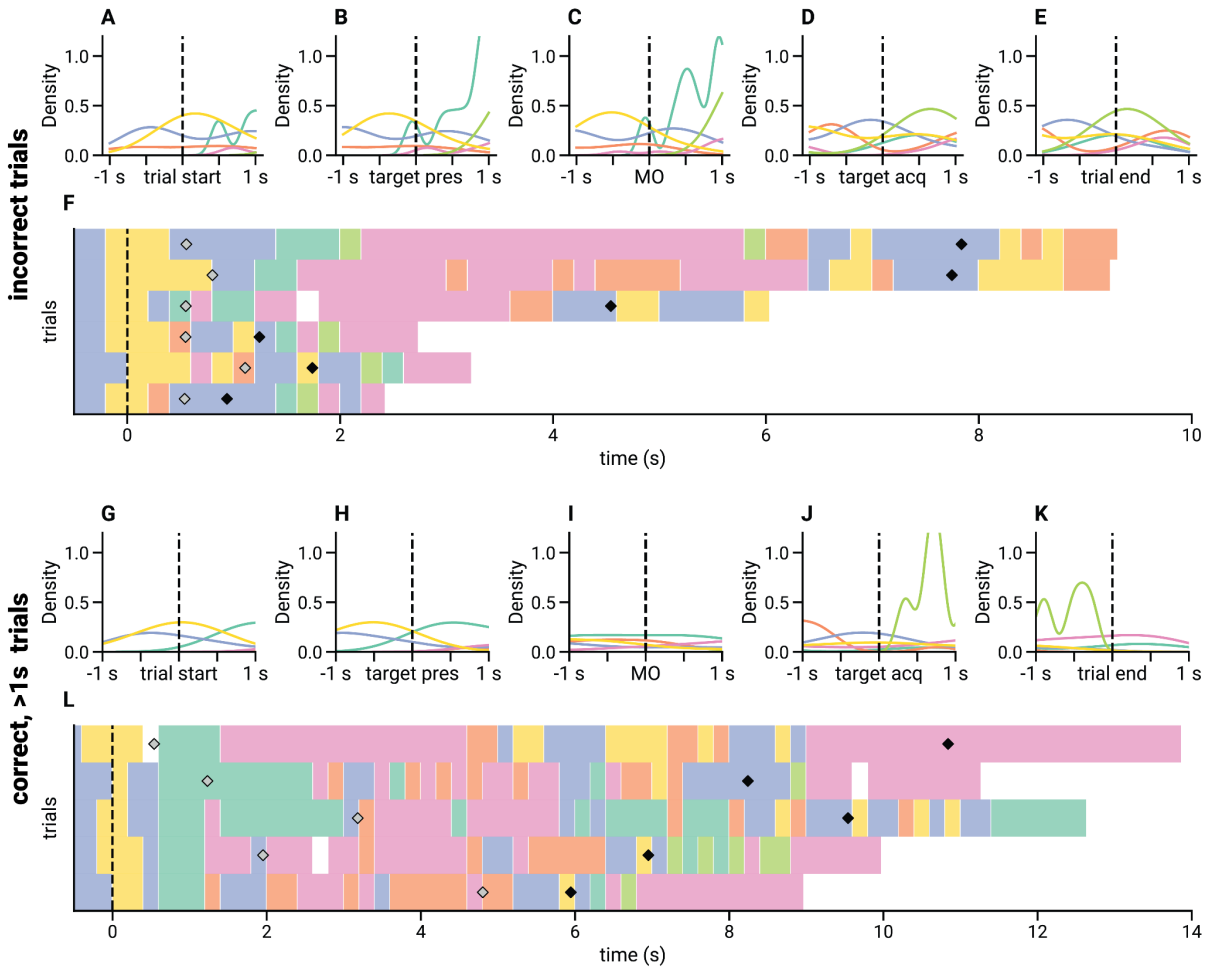

Supplementary Figure III-3 State plot and probabilities for incorrect and long trials.

(A-F) The same as Fig 4C-H but for incorrect trials. **(G-L)** The same as Fig 4C-H but for trials where marmoset TY captured the target >1s after target presentation.

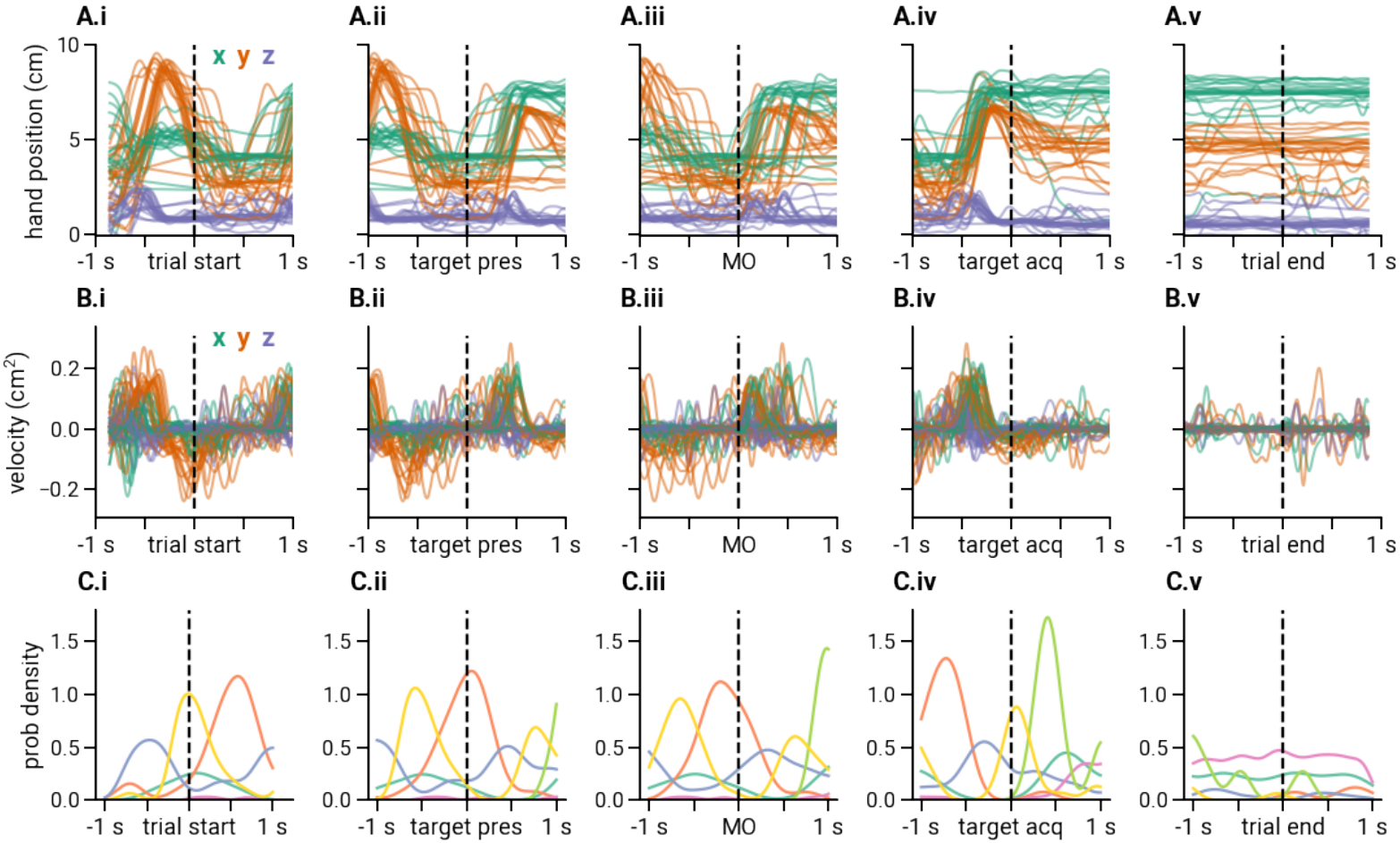

Supplementary Figure III-4 Hand position, velocity, and state probabilities centered on trial events.

A) is the same as Fig 3-1C, **(B)** shows the velocity from inferred hand positions from the DLC model centered on (i) Trial start, (ii) target presentation, (iii) movement onset, (iv) target acquisition, (v) trial end. **(C)** the same as Fig 3-4C-G.

CHAPTER IV. General Discussion

How does the brain flexibly perform multiple neural computations that enable us to interact with the world? In order to gain insight on how the motor cortex drives voluntary behaviors, it is important to describe single neuron activity relative to movement and also neuronal activity relative to other neurons; i.e. the circuit. Throughout this thesis, I describe neural population dynamics as a functional network (FN), and assert that pairwise precise spike time (measured using confluent mutual information) structure in the population provides an additional source of information about behavior beyond what is carried by chance correlations due to firing rates alone.

In chapter 2, I show evidence that the pairwise structural similarity (measured using graph alignment score, GAS) of FNs constructed from whole single trials is related to the distance of their instructed reaches. In order to investigate the dynamics of the statistical dependencies between the recorded population, I constructed temporal FNs, which is a set of FNs where the edges are computed over a 200 ms sliding window. Using this method, I was able to show that reach-specific structural differences in FNs emerge shortly after instruction and consequently become decodable. Moreover, I observed a transient decrease in reciprocal interactions between the top percentile weights following instruction, providing evidence for this reorganization. Interestingly, decoding performance peaks after the reciprocity minima and performance persists even after the FN reciprocity returns to baseline.

Motivated by the results in chapter 2, I utilized the same FN analysis to study the dynamics of spike time statistics during a less constrained task with a free-behaving marmoset. First, I developed a self-initiated artificial prey capture task. A virtual prey traverses a touchscreen (with a trajectory generated according to a parameterized model), and presented to the marmoset over the course of multiple days. A marmoset engaged with this task and showed evidence of learning.

In the session analyzed for chapter 3, the marmoset completed 70% of the trials within 1 second. In these short and successful trials, the marmoset developed a stereotyped strategy of performing the task. While there is variability in timing in this self-initiated task, FNs at specific task events (ie trial initiation, target presentation, movement onset, target acquisition, trial end) can be discriminated based on its nearest neighbors using both a low-dimensional metric (euclidean distance in an embedding space) and the full graph (GAS). Building on this result, I created a meta-network from FNs across task engagement (nodes of the meta-network) and their pairwise GAS (edges). Using a community detection approach to partition the network according to FN structural similarity, I found 6 distinct communities that corresponded well to specific behavioral states such as licking, and accelerative and decelerative reach velocity. This highlights that FNs may be able to provide insight on the statistical regularities of precise spike time statistics that produce neural population dynamics during voluntary goal-directed behaviors.

Future directions

Functional network dynamics at different temporal and behavioral hierarchies

The focus of this thesis was to investigate the dynamics of precise spike time correlation dynamics within a reaching trial or epoch. In the experimental paradigm that I employed with marmosets in chapter 3, I also record spontaneous behavior video data within their housing enclosure along with simultaneous recording of neural and behavioral data during engagement with the task [1]. Previously, Walker et al [2] manually annotated a single 1 hour session, and found that within this session, marmosets engaged in a rich set of behaviors such as grooming of self and

[1] Walker et al., "Chronic Wireless Neural Population Recordings with Common Marmosets."
[2] Walker et al.

of others, climbing, scent marking, sitting, and vertical clinging to name a few. With the rapid innovations that we have witnessed over the past few years in computer vision and markerless pose tracking [3], quantifying natural, spontaneous behavior is within reach. This rich dataset has the ability to place the dynamics observed during task engagement within the context of broader behavior. Animal behaviors can be organized in a hierarchical structure [4]: activities (the highest level) can be made up of behavioral sequences, which are then made up of shorter actions. In chapter 3, we are observing the activity of engagement with the task which, in successful trials, is made up of the behavioral sequence that includes the following actions: a reach outside of the partition to initiate a trial, retracting the arm behind the partition, searching for the virtual prey, reaching towards the prey, and then receiving the reward. In Fig 1, I show a density map of the embedding of non-overlapping temporal FNs across all behavioral episodes in the apparatus in gray, the red overlay shows the density of the FNs from the trials analyzed in Chapter 3. We can observe that the temporal FNs while performing the BeTL task occupy only a part of the subspace and that there are possibly many more states that the neural population could assume within that behavioral episode . It would be interesting to investigate where behavioral episodes in the apparatus lie in the subspace that includes the longer timescale of the entire session (and of multiple sessions). If the temporal FN state sequence during the BeTL task appears outside of the context of the apparatus, this would further validate the BeTL task as an appropriate assay for reaching behaviors. Meaning we are sampling behaviors that the marmoset engages in naturalistically. However, there is evidence that learned movement sequences may be represented differently than

[3] Mathis et al., "DeepLabCut: Markerless Pose Estimation of User-Defined Body Parts with Deep Learning"; Nath et al., "Using DeepLabCut for 3D Markerless Pose Estimation across Species and Behaviors"; Pereira, Shaevitz, and Murthy, "Quantifying Behavior to Understand the Brain"; Mathis and Mathis, "Deep Learning Tools for the Measurement of Animal Behavior in Neuroscience."
[4] Mazzucato, "Neural Mechanisms Underlying the Temporal Organization of Naturalistic Animal Behavior."

its more flexible constituent actions [5]. Either way, contextualizing the actions within behavioral sequences within the realm of naturalistic behavior is important to understanding the underlying neural mechanisms that produce them [6].

I mentioned in Chapter 3 that the session that was analyzed was part of a learning experiment and I speculated about the possible changes in sequences of temporal FN states during learning sessions in the BeTL task. It would be worthwhile to investigate FN dynamics within and across days during skill acquisition to get at how functional connectivity structure changes during different timescales of learning. In addition to collecting neural and behavioral datasets of spontaneous and goal-directed behaviors across days of learning a generated virtual prey trajectory, I also collected neural data during sleep [7]. Memory consolidation during sleep has been shown to have behavioral gains in learning paradigms [8], and reactivation of circuit activity during sleep has been implicated in memory consolidation [9]. A preliminary study with a macaque shows that static FNs from different behavioral states (task, non-task, and sleep) that a subset of sleep FNs and task FNs overlap in a low-dimensional projection of all FNs (UMAP, similar to the methods in Chapter 2 for the static networks) indicating low dimensional structure that are similar, and consistent with task-related reactivation during sleep (unpublished results). A complementary preliminary study to this was conducted in the marmoset to identify cell assembly structure [10] and reactivation events across the array (which could possibly include PMC, M1, and somatosensory

[5] Kadmon Harpaz, Hardcastle, and Ölveczky, "Learning-Induced Changes in the Neural Circuits Underlying Motor Sequence Execution."
[6] Krakauer et al., "Neuroscience Needs Behavior."
[7] Walker et al., "Chronic Wireless Neural Population Recordings with Common Marmosets."
[8] Brawn and Margoliash, "A Bird's Eye View of Sleep-Dependent Memory Consolidation"; Brawn, Nusbaum, and Margoliash, "Sleep-Dependent Reconsolidation after Memory Destabilization in Starlings."
[9] Ramanathan, Gulati, and Ganguly, "Sleep-Dependent Reactivation of Ensembles in Motor Cortex Promotes Skill Consolidation."
[10] Watanabe et al., "Unsupervised Detection of Cell-Assembly Sequences by Similarity-Based Clustering."

areas, [11]). Patterns produced by a putative cell assembly were identified using this method from the awake activity (using the same dataset in Chapter 3), and were found to reactivate during sleep (Moore, unpublished personal communication). The BeTL task and Marmoset-pi toolkit, along with the behavioral infrastructure [12] and wireless neural recording developments [13] with marmosets, presents a potential experimental paradigm to study learning and sleep.

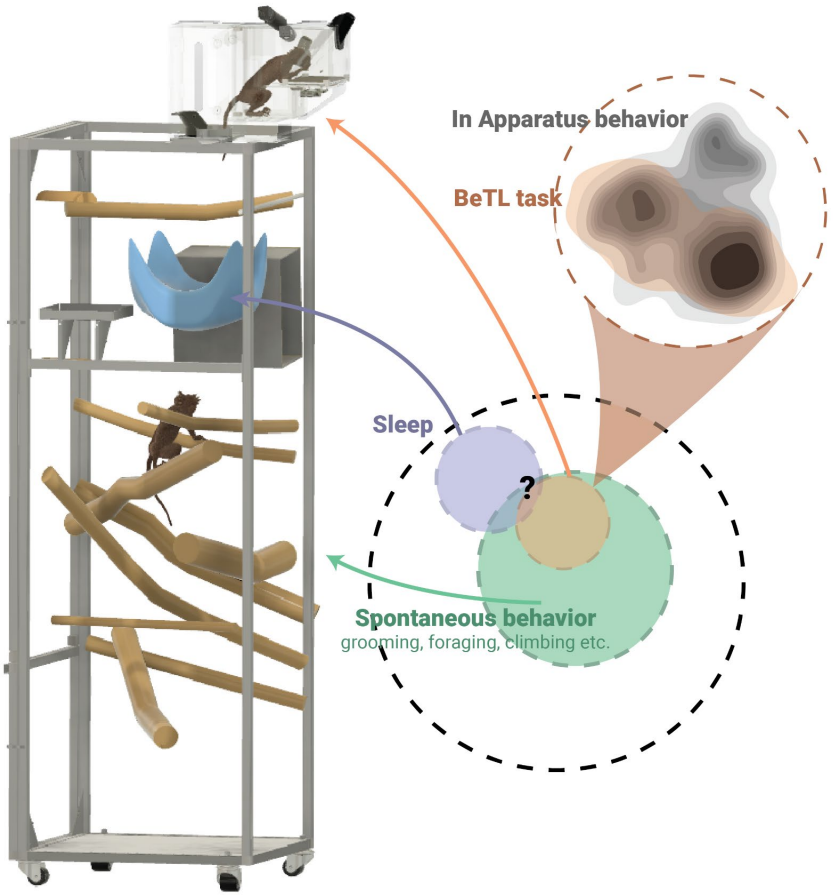

Figure IV-1 Behavioral and neural recording infrastructure has the potential for studying complex natural behaviors.

[11] Walker et al., "Chronic Wireless Neural Population Recordings with Common Marmosets."
[12] Walker et al., "A Platform for Semiautomated Voluntary Training of Common Marmosets for Behavioral Neuroscience."
[13] Walker et al., "Chronic Wireless Neural Population Recordings with Common Marmosets."

Spatial information across areas, lamina, and recording resolutions

An advantage of representing complex systems as networks is the ability to contextualize an element within the system as a whole, as well as isolate specific sub-networks from a larger network. For example, the array in Chapter 3 encompasses multiple functional areas due to the marmosets' lissencephalic cortex [14]. Through stimulation, we can confirm each electrode location and assign nodes based on their location in the array and likely functional area in the cortex (for example in Figure S4 in [15] show stimulation results for Marmoset TY's first array). We can then segregate sub-networks by area and examine the contribution of each sub-network to the overall FN dynamics during reaching. Furthermore, with this FN framework, one can dissect node interactions within and between areas during the course of the reach. Dann et al revealed that in a multi-region FN of the grasping circuit (ventral premotor, M1, anterior intraparietal cortex) in macaques performing a grasping task, a modular organization emerged that was not predicted by anatomical area. Moreover, they showed evidence that a rich-club of oscillatory neurons may be involved in synchronizing the network to generate grasping behavior [16].

Electrophysiology and imaging techniques now allow recording of neural population activity across layers, for example, using customizable N-Form arrays (Modular Bionics, Berkeley, CA) and prism probes (Inscopix, Mountain View, CA), respectively. I have developed and optimized surgical protocols to perform viral injections in mice and marmosets (unpublished methods) to deliver genetically encoded calcium indicators (a tetracycline-inducible system: AAV5-TRE3-GCaMP6f 1.41E+12 GC/mL and AAV5-mThy1PSs-tTAad 3.07E+11 GC/mL, [17])

[14] Walker, MacLean, and Hatsopoulos, "The Marmoset as a Model System for Studying Voluntary Motor Control."
[15] Walker et al., "Chronic Wireless Neural Population Recordings with Common Marmosets."
[16] Dann et al., "Uniting Functional Network Topology and Oscillations in the Fronto-Parietal Single Unit Network of Behaving Primates," August 15, 2016.
[17] Watakabe et al., "Comparative Analyses of Adeno-Associated Viral Vector Serotypes 1, 2, 5, 8 and 9 in Marmoset, Mouse and Macaque Cerebral Cortex"; Watakabe et al., "Application of Viral Vectors to the Study of

to image across cortical lamina through a prism probe via a miniature 1-photon microscope (Inscopix, Mountain View, CA). In preliminary analysis of 1-photon calcium imaging data from mouse's caudal forelimb area, I found that, in this recording resolution and experimental paradigm, there is evidence that that FN structure may have reach direction information similar to what was found in Chapter 2 (unpublished results, data collected by Elizabeth de Laittre) however layer and cell type specificity of these relationships during behavior is yet to be explored. Kondo et al [18] similarly showed that in marmosets performing a bimanual reaching task, movement direction can be decoded from calcium transients. Additionally, they found that only a small fraction of the recorded population in the deep layer of the arm region were movement selective during pre-movement, movement, and post-movement (in one marmoset: 3.42%, 9.76%, and 3.90%, respectively) and that decoding from movement selective neurons was sufficient to maintain decoding accuracy. Interestingly, they found that these movement selective neurons were anatomically distributed in the recording field, and also report that neurons were exclusively selective for specific movement epochs only. Exploring the structure of the functional relationships between the recorded population may reveal novel insight neural dynamics at this temporal and spatial resolution. Moreover, it would be interesting to investigate how the non-movement-selective neurons in the study participate in the control of movement. Building on the foundational work described in Walker et al [19], development in the use of N-form arrays with recording sites along electrode shanks to record in superficial and deep layers of marmoset M1 is under way (Moore, unpublished). Layer-specific changes during learning have been reported in rodents [20].

Neural Connectivities and Neural Circuits in the Marmoset Brain."; Sadakane et al., "Long-Term Two-Photon Calcium Imaging of Neuronal Populations with Subcellular Resolution in Adult Non-Human Primates."

[18] "Calcium Transient Dynamics of Neural Ensembles in the Primary Motor Cortex of Naturally Behaving Monkeys."

[19] "Chronic Wireless Neural Population Recordings with Common Marmosets."

[20] Masamizu et al., "Two Distinct Layer-Specific Dynamics of Cortical Ensembles during Learning of a Motor Task"; Papale and Hooks, "Circuit Changes in Motor Cortex During Motor Skill Learning."

Indeed, marmoset M1 receives input from many brain areas [21], project to other cortical, thalamocortical, and spinal cord regions [22], as well as have connections within itself. Moreover, these connections are heterogeneous across layers [23] thus there is reason to believe that the changes that occur during learning may be layer-specific and, thus, have unique consequences. Again, a network perspective provides a useful framework for studying systems with emergent dynamics but heterogeneous element-wise properties. Moreover, both electrophysiology and calcium imaging have benefits and drawbacks, and probing a system using both techniques may be able to mitigate these limitations and may reveal novel macro- and micro-circuit computations that underlie complex behaviors [24].

Cell type Information

Recent advances in mapping anatomical and functional connectivity in the primary motor cortex of the mouse, marmoset, and human [25] illustrate the potential for an analytical strategy like FNs that can take into account both single cell information and network dynamics. In this current work, all recorded neurons were not classified into functional or biophysical cell types. Future work to incorporate cell type would benefit in the understanding of neural dynamics and computation. In an ongoing collaboration with the Özdinler group in Northwestern University, we are investigating the use of a viral vector to target large pyramidal cells [26] in layer 5 in the macaque. This shows promising developments towards using viral vectors to target specific cell-types in

[21] Bakola, Burman, and Rosa, "The Cortical Motor System of the Marmoset Monkey (Callithrix Jacchus)"; Burman et al., "Anatomical and Physiological Definition of the Motor Cortex of the Marmoset Monkey"; Burman et al., "Patterns of Cortical Input to the Primary Motor Area in the Marmoset Monkey."
[22] Kondo et al., "Histological and Electrophysiological Analysis of the Corticospinal Pathway to Forelimb Motoneurons in Common Marmosets."
[23] Burman et al., "Patterns of Cortical Input to the Primary Motor Area in the Marmoset Monkey."
[24] O'Shea et al., "The Need for Calcium Imaging in Nonhuman Primates."
[25] Bakken et al., "Comparative Cellular Analysis of Motor Cortex in Human, Marmoset and Mouse."
[26] Jara et al., "AAV2 Mediated Retrograde Transduction of Corticospinal Motor Neurons Reveals Initial and Selective Apical Dendrite Degeneration in ALS."

research as well as a therapeutic approach for diseases caused by upper motor neuron degeneration[27].

It was shown in the murine orbitofrontal cortex in vivo and in vitro, that the proportion of inhibitory neurons participating in rich club structures (highly connected hub neurons) was higher compared to the overall FN or the non-rich sub-FN. Furthermore, these rich-club inhibitory neurons were found to be more synchronous with each other compared to with other cell types within and outside the rich-club [28]. A recent study using a network science approach to study the relative influence of excitatory and inhibitory neurons in a somato-motor slice recording that inhibitory neurons have high network centralities compared to excitatory neurons revealing their possible role in maintaining the balance in excitatory-inhibitory networks [29]. Additionally, subclasses of excitatory and inhibitory neurons have different biophysical properties and synaptic targets, and therefore have different internal dynamics and roles in shaping the dynamics of the population, and consequently of behavior [30]. This points to the importance of considering cell types in studying neural population dynamics.

[27] Jara et al., "Retrograde Labeling, Transduction and Genetic Targeting Allow Cellular Analysis of Corticospinal Motor Neurons"; Jara et al., "Healthy and Diseased Corticospinal Motor Neurons Are Selectively Transduced upon Direct AAV2-2 Injection into the Motor Cortex."
[28] Hafizi et al., "Inhibition-Dominated Rich-Club Shapes Dynamics in Cortical Microcircuits."
[29] Kajiwara et al., "Inhibitory Neurons Exhibit High Controlling Ability in the Cortical Microconnectome."
[30] Abbas et al., "Somatostatin Interneurons Facilitate Hippocampal-Prefrontal Synchrony and Prefrontal Spatial Encoding."

BIBLIOGRAPHY

Abbas, Atheir I., Marina J. M. Sundiang, Britt Henoch, Mitchell P. Morton, Scott S. Bolkan, Alan J. Park, Alexander Z. Harris, Christoph Kellendonk, and Joshua A. Gordon. "Somatostatin Interneurons Facilitate Hippocampal-Prefrontal Synchrony and Prefrontal Spatial Encoding." *Neuron* 100, no. 4 (November 21, 2018): 926-939.e3. https://doi.org/10.1016/j.neuron.2018.09.029.

Aertsen, A. M., G. L. Gerstein, M. K. Habib, and G. Palm. "Dynamics of Neuronal Firing Correlation: Modulation of 'Effective Connectivity.'" *Journal of Neurophysiology* 61, no. 5 (1989). https://doi.org/10.1152/jn.1989.61.5.900.

———. "Dynamics of Neuronal Firing Correlation: Modulation of 'Effective Connectivity.'" *Journal of Neurophysiology* 61, no. 5 (May 1, 1989): 900–917. https://doi.org/10.1152/jn.1989.61.5.900.

Aertsen, Amhj, E. Vaadia, M. Abeles, M. Ahissar, H. Bergman, B. Karmon, Y. Lavner, E. Margalit, I. Nelken, and S. Rotter. "Neural Interactions in the Frontal Cortex of a Behaving Monkey: Signs of Dependence on Stimulus Context and Behavioral State." *Journal Für Hirnforschung* 32, no. 6 (November 1991): 735–43.

Afshar, Afsheen, Gopal Santhanam, Byron M. Yu, Stephen I. Ryu, Maneesh Sahani, and Krishna V. Shenoy. "Single-Trial Neural Correlates of Arm Movement Preparation." *Neuron* 71, no. 3 (August 11, 2011): 555–64. https://doi.org/10.1016/J.NEURON.2011.05.047.

Ahissar, Ehud, Eilon Vaadia, Merav Ahissar, Hagai Bergman, Amos Arieli, and Moshe Abeles. "Dependence of Cortical Plasticity on Correlated Activity of Single Neurons and on Behavioral Context." *Science* 257, no. 5075 (September 4, 1992): 1412–15. https://doi.org/10.1126/science.1529342.

Baker, Bowen, Ilge Akkaya, Peter Zhokhov, Joost Huizinga, Jie Tang, Adrien Ecoffet, Brandon Houghton, Raul Sampedro, and Jeff Clune. "Video PreTraining (VPT): Learning to Act by Watching Unlabeled Online Videos." arXiv, June 23, 2022. https://doi.org/10.48550/arXiv.2206.11795.

Bakken, Trygve E., Nikolas L. Jorstad, Qiwen Hu, Blue B. Lake, Wei Tian, Brian E. Kalmbach, Megan Crow, et al. "Comparative Cellular Analysis of Motor Cortex in Human, Marmoset and Mouse." *Nature* 598, no. 7879 (October 2021): 111–19. https://doi.org/10.1038/s41586-021-03465-8.

Bakola, Sophia, Kathleen J. Burman, and Marcello G.P. Rosa. "The Cortical Motor System of the Marmoset Monkey (Callithrix Jacchus)." *Neuroscience Research* 93 (April 1, 2015): 72–81. https://doi.org/10.1016/J.NEURES.2014.11.003.

Balasubramanian, Karthikeyan, Mukta Vaidya, Joshua Southerland, Islam Badreldin, Ahmed Eleryan, Kazutaka Takahashi, Kai Qian, et al. "Changes in Cortical Network Connectivity with Long-Term Brain-Machine Interface Exposure after Chronic Amputation." *Nature Communications* 8, no. 1 (December 1, 2017): 1–10. https://doi.org/10.1038/s41467-017-01909-2.

Baskerville, Edward B., Andy P. Dobson, Trevor Bedford, Stefano Allesina, T. Michael Anderson, and Mercedes Pascual. "Spatial Guilds in the Serengeti Food Web Revealed by a Bayesian Group Model." Edited by Lauren Ancel Meyers. *PLoS Computational Biology* 7, no. 12 (December 29, 2011): e1002321. https://doi.org/10.1371/journal.pcbi.1002321.

Bassett, Danielle S., and Olaf Sporns. "Network Neuroscience." *Nature Neuroscience* 20, no. 3 (February 23, 2017): 353–64. https://doi.org/10.1038/nn.4502.

Bassett, Danielle S, and Olaf Sporns. "Network Neuroscience." *Nature Neuroscience* 20, no. 3 (March 1, 2017): 353–64. https://doi.org/10.1038/nn.4502.

Betzel, Richard F., Katherine C. Wood, Christopher Angeloni, Maria Neimark Geffen, and Danielle S. Bassett. "Stability of Spontaneous, Correlated Activity in Mouse Auditory Cortex." *PLOS Computational Biology* 15, no. 12 (2019): e1007360. https://doi.org/10.1371/JOURNAL.PCBI.1007360.

Blondel, Vincent D., Jean-Loup Guillaume, Renaud Lambiotte, and Etienne Lefebvre. "Fast Unfolding of Communities in Large Networks." *Journal of Statistical Mechanics: Theory and Experiment* 2008, no. 10 (October 2008): P10008. https://doi.org/10.1088/1742-5468/2008/10/P10008.

Bojanek, Kyle, Yuqing Zhu, and Jason MacLean. "Cyclic Transitions between Higher Order Motifs Underlie Sustained Asynchronous Spiking in Sparse Recurrent Networks." Edited by Daniele Marinazzo. *PLoS Computational Biology* 16, no. 9 (September 30, 2020): e1007409. https://doi.org/10.1371/journal.pcbi.1007409.

Bradski, G. "The OpenCV Library." *Dr. Dobb's Journal of Software Tools*, 2000.

BRAIN Initiative Cell Census Network (BICCN). "A Multimodal Cell Census and Atlas of the Mammalian Primary Motor Cortex." *Nature* 598 (2021): 86–102. https://doi.org/10.1038/s41586-021-03950-0.

Brawn, Timothy P., and Daniel Margoliash. "A Bird's Eye View of Sleep-Dependent Memory Consolidation," 207–37. Springer, Berlin, Heidelberg, 2014. https://doi.org/10.1007/7854_2014_349.

Brawn, Timothy P., Howard C. Nusbaum, and Daniel Margoliash. "Sleep-Dependent Reconsolidation after Memory Destabilization in Starlings." *Nature Communications* 9, no. 1 (December 6, 2018): 3093. https://doi.org/10.1038/s41467-018-05518-5.

Bullmore, Ed, and Olaf Sporns. “Complex Brain Networks: Graph Theoretical Analysis of Structural and Functional Systems.” *Nature Reviews Neuroscience* 10, no. 3 (March 4, 2009): 186–98. https://doi.org/10.1038/nrn2575.

———. “Complex Brain Networks: Graph Theoretical Analysis of Structural and Functional Systems.” *Nature Reviews Neuroscience* 10, no. 3 (March 4, 2009): 186–98. https://doi.org/10.1038/nrn2575.

Burman, Kathleen J., Sophia Bakola, Karyn E. Richardson, David H. Reser, and Marcello G.P. Rosa. “Patterns of Cortical Input to the Primary Motor Area in the Marmoset Monkey.” *Journal of Comparative Neurology* 522, no. 4 (March 2014): 811–43. https://doi.org/10.1002/cne.23447.

Burman, Kathleen J., Susan M. Palmer, Michela Gamberini, Matthew W. Spitzer, and Marcello G.P. Rosa. “Anatomical and Physiological Definition of the Motor Cortex of the Marmoset Monkey.” *The Journal of Comparative Neurology* 506, no. 5 (February 10, 2008): 860–76. https://doi.org/10.1002/cne.21580.

Cao, Shun, and Hiroki Sayama. “Detecting Dynamic States of Temporal Networks Using Connection Series Tensors.” arXiv, August 19, 2020. https://doi.org/10.48550/arXiv.2007.12756.

Card, Gwyneth M. “Escape Behaviors in Insects.” *Current Opinion in Neurobiology* 22, no. 2 (April 1, 2012): 180–86. https://doi.org/10.1016/J.CONB.2011.12.009.

Chambers, Brendan, Maayan Levy, Joseph B. Dechery, and Jason N. Maclean. “Ensemble Stacking Mitigates Biases in Inference of Synaptic Connectivity.” *Network Neuroscience* 2, no. 1 (March 26, 2018): 60–85. https://doi.org/10.1162/netn_a_00032.

Chambers, Brendan, and Jason N. MacLean. “Higher-Order Synaptic Interactions Coordinate Dynamics in Recurrent Networks.” *PLOS Computational Biology* 12, no. 8 (August 19, 2016): e1005078. https://doi.org/10.1371/journal.pcbi.1005078.

Cheney, P. D., and E. E. Fetz. “Functional Classes of Primate Corticomotoneuronal Cells and Their Relation to Active Force.” *Journal of Neurophysiology* 44, no. 4 (October 1980): 773–91. https://doi.org/10.1152/jn.1980.44.4.773.

Churchland, Mark M., John P. Cunningham, Matthew T. Kaufman, Justin D. Foster, Paul Nuyujukian, Stephen I. Ryu, and Krishna V. Shenoy. “Neural Population Dynamics during Reaching.” *Nature* 487, no. 7405 (July 3, 2012): 51–56. https://doi.org/10.1038/nature11129.

Churchland, Mark M., and Krishna V. Shenoy. “Temporal Complexity and Heterogeneity of Single-Neuron Activity in Premotor and Motor Cortex.” *Https://Doi.Org/10.1152/Jn.00095.2007* 97, no. 6 (June 2007): 4235–57. https://doi.org/10.1152/JN.00095.2007.

Churchland, Mark M., Byron M. Yu, Stephen I. Ryu, Gopal Santhanam, and Krishna V. Shenoy. "Neural Variability in Premotor Cortex Provides a Signature of Motor Preparation." *Journal of Neuroscience* 26, no. 14 (April 5, 2006): 3697–3712. https://doi.org/10.1523/JNEUROSCI.3762-05.2006.

Cunningham, John P., and Byron M. Yu. "Dimensionality Reduction for Large-Scale Neural Recordings." *Nature Neuroscience* 17, no. 11 (October 28, 2014): 1500–1509. https://doi.org/10.1038/nn.3776.

Dann, Benjamin, Jonathan A. Michaels, Stefan Schaffelhofer, and Hansjörg Scherberger. "Uniting Functional Network Topology and Oscillations in the Fronto-Parietal Single Unit Network of Behaving Primates." *ELife* 5, no. AUGUST (August 15, 2016). https://doi.org/10.7554/eLife.15719.

Dann, Benjamin, Jonathan A Michaels, Stefan Schaffelhofer, and Hansjörg Scherberger. "Uniting Functional Network Topology and Oscillations in the Fronto-Parietal Single Unit Network of Behaving Primates." *ELife* 5 (August 15, 2016): e15719. https://doi.org/10.7554/eLife.15719.

De Robertis, Eduardo D. P., and H. Stanley Bennett. "SOME FEATURES OF THE SUBMICROSCOPIC MORPHOLOGY OF SYNAPSES IN FROG AND EARTHWORM." *The Journal of Biophysical and Biochemical Cytology* 1, no. 1 (January 25, 1955): 47–58.

Dechery, Joseph B., and Jason N. MacLean. "Functional Triplet Motifs Underlie Accurate Predictions of Single-Trial Responses in Populations of Tuned and Untuned V1 Neurons." Edited by Jeff Beck. *PLoS Computational Biology* 14, no. 5 (May 4, 2018): e1006153. https://doi.org/10.1371/journal.pcbi.1006153.

Denker, M., A. Yegenoglu, and S. Grün. "Collaborative HPC-Enabled Workflows on the HBP Collaboratory Using the Elephant Framework." In *Neuroinformatics 2018*, P19, 2018. https://doi.org/10.12751/incf.ni2018.0019.

Denker, Michael, Cristiano Köhler, Aitor Morales-Gregorio, Alexander Kleinjohann, Peter Bouss, Alessandra Stella, Regimantas Jurkus, et al. "Elephant 0.11.2." Zenodo, November 9, 2022. https://doi.org/10.5281/zenodo.7307401.

Elsayed, Gamaleldin F., Antonio H. Lara, Matthew T. Kaufman, Mark M. Churchland, and John P. Cunningham. "Reorganization between Preparatory and Movement Population Responses in Motor Cortex." *Nature Communications* 7, no. 1 (October 27, 2016): 1–15. https://doi.org/10.1038/ncomms13239.

Evarts, Edward V. "Pyramidal Tract Activity Associated with a Conditioned Hand Movement in the Monkey." *Journal of Neurophysiology* 29, no. 6 (November 1966): 1011–27. https://doi.org/10.1152/jn.1966.29.6.1011.

———. “Relation of Discharge Frequency to Conduction Velocity in Pyramidal Tract Neurons.” *Journal of Neurophysiology* 28, no. 2 (March 1965): 216–28. https://doi.org/10.1152/jn.1965.28.2.216.

———. “Relation of Pyramidal Tract Activity to Force Exerted during Voluntary Movement.” *Journal of Neurophysiology* 31, no. 1 (January 1968): 14–27. https://doi.org/10.1152/jn.1968.31.1.14.

Faskowitz, Joshua, Richard F. Betzel, and Olaf Sporns. “Edges in Brain Networks: Contributions to Models of Structure and Function.” *Network Neuroscience* 6, no. 1 (February 1, 2022): 1–28. https://doi.org/10.1162/NETN_A_00204.

Fetz, Eberhard E. “Are Movement Parameters Recognizably Coded in the Activity of Single Neurons?” *Behavioral and Brain Sciences* 15, no. 4 (December 1992): 679–90. https://doi.org/10.1017/S0140525X00072599.

Garlaschelli, Diego, and Maria I. Loffredo. “Patterns of Link Reciprocity in Directed Networks.” *Physical Review Letters* 93, no. 26 I (April 21, 2004). https://doi.org/10.1103/PhysRevLett.93.268701.

Gemmetto, Valerio, Tiziano Squartini, Francesco Picciolo, Franco Ruzzenenti, and Diego Garlaschelli. “Multiplexity and Multireciprocity in Directed Multiplexes.” *Physical Review E* 94, no. 4 (October 27, 2016): 042316. https://doi.org/10.1103/PhysRevE.94.042316.

Georgopoulos, A P, J F Kalaska, R Caminiti, and J T Massey. “On the Relations between the Direction of Two-Dimensional Arm Movements and Cell Discharge in Primate Motor Cortex.” *The Journal of Neuroscience : The Official Journal of the Society for Neuroscience* 2, no. 11 (November 1, 1982): 1527–37. https://doi.org/10.1523/JNEUROSCI.02-11-01527.1982.

Gerstein, G. L., P. Bedenbaugh, and A. M Aertsen. “Neuronal Assemblies.” *IEEE Transactions on Biomedical Engineering* 36, no. 1 (January 1989): 4–14. https://doi.org/10.1109/10.16444.

Gerstein, G. L., and W. A. Clark. “Simultaneous Studies of Firing Patterns in Several Neurons.” *Science* 143, no. 3612 (March 20, 1964): 1325–27. https://doi.org/10.1126/science.143.3612.1325.

Gerstein, G. L., and D. H. Perkel. “Simultaneously Recorded Trains of Action Potentials: Analysis and Functional Interpretation.” *Science* 164, no. 3881 (1969): 828–30.

Gerstein, G. L., D. H. Perkel, and Je Dayhoff. “Cooperative Firing Activity in Simultaneously Recorded Populations of Neurons: Detection and Measurement.” *The Journal of Neuroscience* 5, no. 4 (April 1, 1985): 881–89. https://doi.org/10.1523/JNEUROSCI.05-04-00881.1985.

Girvan, M, and M E J Newman. “Community Structure in Social and Biological Networks.” *Proceedings of the National Academy of Sciences of the United States of America* 99, no. 12 (June 11, 2002): 7821–26. https://doi.org/10.1073/pnas.122653799.

Golub, Matthew D., Patrick T. Sadtler, Emily R. Oby, Kristin M. Quick, Stephen I. Ryu, Elizabeth C. Tyler-Kabara, Aaron P. Batista, Steven M. Chase, and Byron M. Yu. “Learning by Neural Reassociation.” *Nature Neuroscience* 21, no. 4 (April 12, 2018): 607–16. https://doi.org/10.1038/s41593-018-0095-3.

Hafizi, Hadi, Sunny Nigam, Josh Barnathan, Naixin Ren, Ian H. Stevenson, Sotiris C. Masmanidis, Ehren L. Newman, Olaf Sporns, and John M. Beggs. “Inhibition-Dominated Rich-Club Shapes Dynamics in Cortical Microcircuits.” bioRxiv, August 20, 2022. https://doi.org/10.1101/2021.05.07.443074.

Harris, Kenneth D. “Neural Signatures of Cell Assembly Organization.” *Nature Reviews Neuroscience* 6, no. 5 (May 1, 2005): 399–407. https://doi.org/10.1038/nrn1669.

Hatsopoulos, N. G., C. L. Ojakangas, L. Paninski, and J. P. Donoghue. “Information about Movement Direction Obtained from Synchronous Activity of Motor Cortical Neurons.” *Proceedings of the National Academy of Sciences of the United States of America* 95, no. 26 (December 22, 1998): 15706–11. https://doi.org/10.1073/pnas.95.26.15706.

Hatsopoulos, N. G., Q. Xu, and Y. Amit. “Encoding of Movement Fragments in the Motor Cortex.” *Journal of Neuroscience* 27, no. 19 (2007): 5105–14. https://doi.org/10.1523/JNEUROSCI.3570-06.2007.

Hatsopoulos, Nicholas G., Jignesh Joshi, and John G. O’Leary. “Decoding Continuous and Discrete Motor Behaviors Using Motor and Premotor Cortical Ensembles.” *Journal of Neurophysiology* 92, no. 2 (August 2004): 1165–74. https://doi.org/10.1152/jn.01245.2003.

Hebb, D. O. (Donald Olding). *The Organization of Behavior; a Neuropsychological Theory.* A Wiley Book in Clinical Psychology. New York,: Wiley, 1949.

Hepp-Reymond, M. C., U. R. Wyss, and R. Anner. “Neuronal Coding of Static Force in the Primate Motor Cortex.” *Journal De Physiologie* 74, no. 3 (1978): 287–91.

Holme, Petter, and Jari Saramäki. “Temporal Networks.” *Physics Reports* 519, no. 3 (October 1, 2012): 97–125. https://doi.org/10.1016/j.physrep.2012.03.001.

Hubel, David H. “Tungsten Microelectrode for Recording from Single Units.” *Science* 125, no. 3247 (March 22, 1957): 549–50. https://doi.org/10.1126/science.125.3247.549.

Humphries, Mark D. “Dynamical Networks: Finding, Measuring, and Tracking Neural Population Activity Using Network Science.” *Network Neuroscience* 1, no. 4 (December 31, 2017): 324–38. https://doi.org/10.1162/NETN_a_00020.

Humphries, Mark D. “Strong and Weak Principles of Neural Dimension Reduction,” 2020.

Insanally, Michele N., Ioana Carcea, Rachel E. Field, Chris C. Rodgers, Brian DePasquale, Kanaka Rajan, Michael R. DeWeese, Badr F. Albanna, and Robert C. Froemke. “Spike-Timing-Dependent Ensemble Encoding by Non-Classically Responsive Cortical Neurons.” *ELife* 8 (January 28, 2019). https://doi.org/10.7554/eLife.42409.

Jara, Javier H, Baris Genc, Jodi Klessner, and Hande Ozdinler. “Retrograde Labeling, Transduction and Genetic Targeting Allow Cellular Analysis of Corticospinal Motor Neurons: Implications in Health and Disease.” *Frontiers in Neuroanatomy* 8 (2014). https://www.frontiersin.org/articles/10.3389/fnana.2014.00016.

Jara, Javier H, M. J. Stanford, Y. Zhu, M. Tu, W. W. Hauswirth, M. C. Bohn, S. H. DeVries, and P. H. Özdinler. “Healthy and Diseased Corticospinal Motor Neurons Are Selectively Transduced upon Direct AAV2-2 Injection into the Motor Cortex.” *Gene Therapy* 23, no. 3 (March 2016): 272–82. https://doi.org/10.1038/gt.2015.112.

Jara, Javier H, Stephanie R. Villa, Nabil A. Khan, Martha C. Bohn, and P. Hande Özdinler. “AAV2 Mediated Retrograde Transduction of Corticospinal Motor Neurons Reveals Initial and Selective Apical Dendrite Degeneration in ALS.” *Neurobiology of Disease* 47, no. 2 (August 1, 2012): 174–83. https://doi.org/10.1016/J.NBD.2012.03.036.

Johnson, Devin S, Joshua M London, Mary-Anne Lea, and John W Durban. “Continuous-Time Correlated Random Walk Model for Animal Telemetry Data.” *Source: Ecology* 89, no. 5 (2008): 1208–15.

Ju, Harang, and Danielle S. Bassett. “Dynamic Representations in Networked Neural Systems.” *Nature Neuroscience*, June 15, 2020, 1–10. https://doi.org/10.1038/s41593-020-0653-3.

———. “Dynamic Representations in Networked Neural Systems.” *Nature Neuroscience*, June 15, 2020, 1–10. https://doi.org/10.1038/s41593-020-0653-3.

Kadmon Harpaz, Naama, Kiah Hardcastle, and Bence P. Ölveczky. “Learning-Induced Changes in the Neural Circuits Underlying Motor Sequence Execution.” *Current Opinion in Neurobiology* 76 (October 1, 2022): 102624. https://doi.org/10.1016/j.conb.2022.102624.

Kadmon Harpaz, Naama, David Ungarish, Nicholas G Hatsopoulos, and Tamar Flash. “Movement Decomposition in the Primary Motor Cortex.” *Cerebral Cortex* 29, no. 4 (April 1, 2019): 1619–33. https://doi.org/10.1093/cercor/bhy060.

Kajiwara, Motoki, Ritsuki Nomura, Felix Goetze, Masanori Kawabata, Yoshikazu Isomura, Tatsuya Akutsu, and Masanori Shimono. “Inhibitory Neurons Exhibit High Controlling Ability in the Cortical Microconnectome.” *PLOS Computational Biology* 17, no. 4 (April 8, 2021): e1008846. https://doi.org/10.1371/journal.pcbi.1008846.

Kalaska, J. F. “Emerging Ideas and Tools to Study the Emergent Properties of the Cortical Neural Circuits for Voluntary Motor Control in Non-Human Primates.” *F1000Research* 8 (May 29, 2019): 749. https://doi.org/10.12688/f1000research.17161.1.

———. “From Intention to Action: Motor Cortex and the Control of Reaching Movements.” In *Progress in Motor Control: A Multidisciplinary Perspective*, edited by Dagmar Sternad, 139–78. Advances in Experimental Medicine and Biology. Boston, MA: Springer US, 2009. https://doi.org/10.1007/978-0-387-77064-2_8.

Kalaska, J. F., D. A. Cohen, M. L. Hyde, and M. Prud’homme. “A Comparison of Movement Direction-Related versus Load Direction-Related Activity in Primate Motor Cortex, Using a Two-Dimensional Reaching Task.” *The Journal of Neuroscience: The Official Journal of the Society for Neuroscience* 9, no. 6 (June 1989): 2080–2102. https://doi.org/10.1523/JNEUROSCI.09-06-02080.1989.

Kane, Gary A, Gonçalo Lopes, Jonny L Saunders, Alexander Mathis, and Mackenzie W Mathis. “Real-Time, Low-Latency Closed-Loop Feedback Using Markerless Posture Tracking.” Edited by Gordon J Berman, Timothy E Behrens, Gordon J Berman, and Tiago Branco. *ELife* 9 (December 8, 2020): e61909. https://doi.org/10.7554/eLife.61909.

Kareiva, P. M., and N. Shigesada. “Analyzing Insect Movement as a Correlated Random Walk.” *Oecologia* 56, no. 2–3 (February 1983): 234–38. https://doi.org/10.1007/BF00379695.

Kaufman, Matthew T., Mark M. Churchland, Stephen I. Ryu, and Krishna V. Shenoy. “Cortical Activity in the Null Space: Permitting Preparation without Movement.” *Nature Neuroscience* 17, no. 3 (March 2014): 440–48. https://doi.org/10.1038/nn.3643.

Kaufman, Matthew T, Mark M Churchland, Stephen I Ryu, Krishna V Shenoy, and Nat Neurosci Author. “Cortical Activity in the Null Space: Permitting Preparation without Movement HHS Public Access Author Manuscript.” *Nat Neurosci* 17, no. 3 (2014): 440–48. https://doi.org/10.1038/nn.3643.

Kondo, Takahiro, Risa Saito, Masaki Otaka, Kimika Yoshino-Saito, Akihiro Yamanaka, Tetsuo Yamamori, Akiya Watakabe, et al. “Calcium Transient Dynamics of Neural Ensembles in the Primary Motor Cortex of Naturally Behaving Monkeys.” *Cell Reports* 24, no. 8 (August 21, 2018): 2191-2195.e4. https://doi.org/10.1016/J.CELREP.2018.07.057.

Kondo, Takahiro, Yamato Yoshihara, Kimika Yoshino-Saito, Tomofumi Sekiguchi, Akito Kosugi, Yuta Miyazaki, Yukio Nishimura, et al. “Histological and Electrophysiological Analysis of the Corticospinal Pathway to Forelimb Motoneurons in Common Marmosets.” *Neuroscience Research* 98 (September 1, 2015): 35–44. https://doi.org/10.1016/J.NEURES.2015.05.001.

Kotekal, Subhodh, and Jason N. MacLean. “Recurrent Interactions Can Explain the Variance in Single Trial Responses.” Edited by Leyla Isik. *PLoS Computational Biology* 16, no. 1 (January 30, 2020): e1007591. https://doi.org/10.1371/journal.pcbi.1007591.

Krakauer, John W., Asif A. Ghazanfar, Alex Gomez-Marin, Malcolm A. MacIver, and David Poeppel. “Neuroscience Needs Behavior: Correcting a Reductionist Bias.” *Neuron* 93, no. 3 (2017): 480–90. https://doi.org/10.1016/j.neuron.2016.12.041.

———. “Neuroscience Needs Behavior: Correcting a Reductionist Bias.” *Neuron* 93, no. 3 (February 8, 2017): 480–90. https://doi.org/10.1016/j.neuron.2016.12.041.

Laurence-Chasen, J.D., Armita R. Manafzadeh, Nicholas G. Hatsopoulos, Callum F. Ross, and Fritzie I. Arce-McShane. “Integrating XMALab and DeepLabCut for High-Throughput XROMM.” *The Journal of Experimental Biology* 223, no. 17 (September 4, 2020): jeb226720. https://doi.org/10.1242/jeb.226720.

Levy, Eliott R.J., Eun Hye Park, William T. Redman, and André A. Fenton. “A Neuronal Code for Space in Hippocampal Coactivity Dynamics Independent of Place Fields.” *SSRN Electronic Journal*, April 5, 2021, 2021.07.26.453856. https://doi.org/10.2139/ssrn.3928087.

Levy, Maayan, Olaf Sporns, and Jason N. MacLean. “Network Analysis of Murine Cortical Dynamics Implicates Untuned Neurons in Visual Stimulus Coding.” *Cell Reports* 31, no. 2 (April 14, 2020): 107483. https://doi.org/10.1016/j.celrep.2020.03.047.

Li, Choh-Luh, and Herbert Jasper. “Microelectrode Studies of the Electrical Activity of the Cerebral Cortex in the Cat.” *The Journal of Physiology* 121, no. 1 (July 28, 1953): 117–40.

López-Muñoz, Francisco, Jesús Boya, and Cecilio Alamo. “Neuron Theory, the Cornerstone of Neuroscience, on the Centenary of the Nobel Prize Award to Santiago Ramón y Cajal.” *Brain Research Bulletin* 70, no. 4 (October 16, 2006): 391–405. https://doi.org/10.1016/j.brainresbull.2006.07.010.

Magrans de Abril, Ildefons, Junichiro Yoshimoto, and Kenji Doya. “Connectivity Inference from Neural Recording Data: Challenges, Mathematical Bases and Research Directions.” *Neural Networks* 102 (June 1, 2018): 120–37. https://doi.org/10.1016/J.NEUNET.2018.02.016.

Malonis, Peter J, Nicholas G Hatsopoulos, Jason N Maclean, Matthew T Kaufman, Josh Coles, Zach Haga, Jignesh Joshi, et al. “M1 Dynamics Share Similar Inputs for Initiating and Correcting Movement.” *BioRxiv*, October 19, 2021, 2021.10.18.464704. https://doi.org/10.1101/2021.10.18.464704.

Masamizu, Yoshito, Yasuhiro R Tanaka, Yasuyo H Tanaka, Riichiro Hira, Fuki Ohkubo, Kazuo Kitamura, Yoshikazu Isomura, Takashi Okada, and Masanori Matsuzaki. “Two Distinct Layer-Specific Dynamics of Cortical Ensembles during Learning of a Motor Task.” *Nature Neuroscience* 17, no. 7 (July 1, 2014): 987–94. https://doi.org/10.1038/nn.3739.

Masuda, Naoki, and Petter Holme. “Detecting Sequences of System States in Temporal Networks.” *Scientific Reports* 9, no. 1 (January 28, 2019): 795. https://doi.org/10.1038/s41598-018-37534-2.

Mathis, Alexander, Pranav Mamidanna, Kevin M. Cury, Taiga Abe, Venkatesh N. Murthy, Mackenzie Weygandt Mathis, and Matthias Bethge. “DeepLabCut: Markerless Pose

Estimation of User-Defined Body Parts with Deep Learning." *Nature Neuroscience*, August 20, 2018, 1. https://doi.org/10.1038/s41593-018-0209-y.

Mathis, Mackenzie Weygandt, and Alexander Mathis. "Deep Learning Tools for the Measurement of Animal Behavior in Neuroscience." *Current Opinion in Neurobiology*, Neurobiology of Behavior, 60 (February 1, 2020): 1–11. https://doi.org/10.1016/j.conb.2019.10.008.

Maynard, E. M., N. G. Hatsopoulos, C. L. Ojakangas, B. D. Acuna, J. N. Sanes, R. A. Normann, and J. P. Donoghue. "Neuronal Interactions Improve Cortical Population Coding of Movement Direction." *Journal of Neuroscience* 19, no. 18 (September 15, 1999): 8083–93. https://doi.org/10.1523/jneurosci.19-18-08083.1999.

Mazzucato, Luca. "Neural Mechanisms Underlying the Temporal Organization of Naturalistic Animal Behavior." Edited by Gordon J Berman and Timothy E Behrens. *ELife* 11 (July 6, 2022): e76577. https://doi.org/10.7554/eLife.76577.

McInnes, Leland, John Healy, and James Melville. "UMAP: Uniform Manifold Approximation and Projection for Dimension Reduction," February 9, 2018. http://arxiv.org/abs/1802.03426.

Mcinnes, Leland, John Healy, and James Melville. "UMAP : Uniform Manifold Approximation and Projection for Dimension Reduction ArXiv : 1802 . 03426v2 [Stat . ML] 6 Dec 2018," 2018.

Moore, Dalton D., Jeffrey D. Walker, Jason N. MacLean, and Nicholas G. Hatsopoulos. "Validating Markerless Pose Estimation with 3D X-Ray Radiography." *Journal of Experimental Biology* 225, no. 9 (May 1, 2022): jeb243998. https://doi.org/10.1242/jeb.243998.

Moran, Daniel W., and Andrew B. Schwartz. "Motor Cortical Representation of Speed and Direction During Reaching." *Journal of Neurophysiology* 82, no. 5 (November 1999): 2676–92. https://doi.org/10.1152/jn.1999.82.5.2676.

Nardin, Michele, Jozsef Csicsvari, Gašper Tkačik, Tkaˇ Tkačik, and Cristina Savin. "The Structure of Hippocampal CA1 Interactions Optimizes Spatial Coding across Experience." *BioRxiv*, September 29, 2021, 2021.09.28.460602. https://doi.org/10.1101/2021.09.28.460602.

Nath, Tanmay, Alexander Mathis, An Chi Chen, Amir Patel, Matthias Bethge, and Mackenzie W. Mathis. "Using DeepLabCut for 3D Markerless Pose Estimation across Species and Behaviors." *BioRxiv*, November 24, 2018, 476531. https://doi.org/10.1101/476531.

Newman, M. E. J. "Spread of Epidemic Disease on Networks." *Physical Review. E, Statistical, Nonlinear, and Soft Matter Physics* 66, no. 1 Pt 2 (July 2002): 016128. https://doi.org/10.1103/PhysRevE.66.016128.

Oby, Emily R., Matthew D. Golub, Jay A. Hennig, Alan D. Degenhart, Elizabeth C. Tyler-Kabara, Byron M. Yu, Steven M. Chase, and Aaron P. Batista. "New Neural Activity Patterns Emerge with Long-Term Learning." *Proceedings of the National Academy of Sciences*, June 10, 2019, 201820296. https://doi.org/10.1073/PNAS.1820296116.

O'Leary, John G., and Nicholas G. Hatsopoulos. "Early Visuomotor Representations Revealed from Evoked Local Field Potentials in Motor and Premotor Cortical Areas." *Journal of Neurophysiology* 96, no. 3 (2006): 1492–1506. https://doi.org/10.1152/jn.00106.2006.

OpenAI, Christopher Berner, Greg Brockman, Brooke Chan, Vicki Cheung, Przemysław Dębiak, Christy Dennison, et al. "Dota 2 with Large Scale Deep Reinforcement Learning." arXiv, December 13, 2019. http://arxiv.org/abs/1912.06680.

O'Shea, Daniel J., Eric Trautmann, Chandramouli Chandrasekaran, Sergey Stavisky, Jonathan C. Kao, Maneesh Sahani, Stephen Ryu, Karl Deisseroth, and Krishna V. Shenoy. "The Need for Calcium Imaging in Nonhuman Primates: New Motor Neuroscience and Brain-Machine Interfaces." *Experimental Neurology* 287, no. Pt 4 (January 2017): 437–51. https://doi.org/10.1016/j.expneurol.2016.08.003.

Palay, Sanford L. "SYNAPSES IN THE CENTRAL NERVOUS SYSTEM." *The Journal of Biophysical and Biochemical Cytology* 2, no. 4 (July 25, 1956): 193–202.

Palay, Sanford L., and George E. Palade. "THE FINE STRUCTURE OF NEURONS." *The Journal of Biophysical and Biochemical Cytology* 1, no. 1 (January 25, 1955): 69–88.

Papale, Andrew E., and Bryan M. Hooks. "Circuit Changes in Motor Cortex During Motor Skill Learning." *Neuroscience*, Barrel Cortex Function, 368 (January 1, 2018): 283–97. https://doi.org/10.1016/j.neuroscience.2017.09.010.

Pedreschi, Nicola, Christophe Bernard, Wesley Clawson, Pascale Quilichini, Alain Barrat, and Demian Battaglia. "Dynamic Core Periphery Structure of Information Sharing Networks in Entorhinal Cortex and Hippocampus." *Network Neuroscience*, April 28, 2020, 1–42. https://doi.org/10.1162/netn_a_00142.

Pereira, Talmo D., Joshua W. Shaevitz, and Mala Murthy. "Quantifying Behavior to Understand the Brain." *Nature Neuroscience* 23, no. 12 (December 1, 2020): 1537–49. https://doi.org/10.1038/s41593-020-00734-z.

Perkel, D. H., G. L. Gerstein, and G. P. Moore. "Neuronal Spike Trains and Stochastic Point Processes. II. Simultaneous Spike Trains." *Biophysical Journal* 7, no. 4 (July 1967): 419–40. https://doi.org/10.1016/S0006-3495(67)86597-4.

Perlin, Ken. "An Image Synthesizer." *ACM SIGGRAPH Computer Graphics* 19, no. 3 (July 1, 1985): 287–96. https://doi.org/10.1145/325165.325247.

Ramanathan, Dhakshin S., Tanuj Gulati, and Karunesh Ganguly. "Sleep-Dependent Reactivation of Ensembles in Motor Cortex Promotes Skill Consolidation." *PLOS Biology* 13, no. 9 (September 18, 2015): e1002263. https://doi.org/10.1371/journal.pbio.1002263.

Recanatesi, Stefano, Gabriel Koch Ocker, Michael A. Buice, and Eric Shea-Brown. "Dimensionality in Recurrent Spiking Networks: Global Trends in Activity and Local Origins in Connectivity." Edited by Jörn Diedrichsen. *PLOS Computational Biology* 15, no. 7 (July 12, 2019): e1006446. https://doi.org/10.1371/journal.pcbi.1006446.

Recanatesi, Stefano, Ulises Pereira, Masayoshi Murakami, Zachary Mainen, and Luca Mazzucato. "Metastable Attractors Explain the Variable Timing of Stable Behavioral Action Sequences," 2020.

Reimer, Jacob, and Nicholas G. Hatsopoulos. "Periodicity and Evoked Responses in Motor Cortex." *Journal of Neuroscience* 30, no. 34 (2010): 11506–15. https://doi.org/10.1523/JNEUROSCI.5947-09.2010.

———. "The Problem of Parametric Neural Coding in the Motor System." *Advances in Experimental Medicine and Biology* 629 (2009): 243–59. https://doi.org/10.1007/978-0-387-77064-2_12.

Reynolds, Andy M. "Bridging the Gulf between Correlated Random Walks and Lévy Walks: Autocorrelation as a Source of Lévy Walk Movement Patterns." *Journal of the Royal Society Interface* 7, no. 53 (December 6, 2010): 1753–58. https://doi.org/10.1098/rsif.2010.0292.

Reynolds, Andy M., Lisa Leprêtre, and David A. Bohan. "Movement Patterns of Tenebrio Beetles Demonstrate Empirically That Correlated-Random-Walks Have Similitude with a Lévy Walk." *Scientific Reports* 3, no. 1 (December 7, 2013): 3158. https://doi.org/10.1038/srep03158.

Riehle, A., S. Grün, M. Diesmann, and A. Aertsen. "Spike Synchronization and Rate Modulation Differentially Involved in Motor Cortical Function." *Science (New York, N.Y.)* 278, no. 5345 (December 12, 1997): 1950–53. https://doi.org/10.1126/science.278.5345.1950.

Rubinov, Mikail, and Olaf Sporns. "Complex Network Measures of Brain Connectivity: Uses and Interpretations." *NeuroImage* 52, no. 3 (September 2010): 1059–69. https://doi.org/10.1016/j.neuroimage.2009.10.003.

Ruda, Kiersten, Joel Zylberberg, and Greg D. Field. "Ignoring Correlated Activity Causes a Failure of Retinal Population Codes." *Nature Communications* 11, no. 1 (December 1, 2020). https://doi.org/10.1038/s41467-020-18436-2.

Sadakane, Osamu, Yoshito Masamizu, Akiya Watakabe, Shin-Ichiro Terada, Masanari Ohtsuka, Masafumi Takaji, Hiroaki Mizukami, et al. "Long-Term Two-Photon Calcium Imaging of Neuronal Populations with Subcellular Resolution in Adult Non-Human Primates." *Cell Reports* 13, no. 9 (December 1, 2015): 1989–99. https://doi.org/10.1016/j.celrep.2015.10.050.

Sadtler, Patrick T., Kristin M. Quick, Matthew D. Golub, Steven M. Chase, Stephen I. Ryu, Elizabeth C. Tyler-Kabara, Byron M. Yu, and Aaron P. Batista. "Neural Constraints on

Learning." *Nature* 512, no. 7515 (August 28, 2014): 423–26. https://doi.org/10.1038/nature13665.

Saxena, Shreya, and John P. Cunningham. "Towards the Neural Population Doctrine." *Current Opinion in Neurobiology* 55 (April 1, 2019): 103–11. https://doi.org/10.1016/J.CONB.2019.02.002.

Schiel, Nicola, and Antonio Souto. "The Common Marmoset: An Overview of Its Natural History, Ecology and Behavior." *Developmental Neurobiology* 77, no. 3 (March 1, 2017): 244–62. https://doi.org/10.1002/dneu.22458.

Schiel, Nicola, Antonio Souto, Ludwig Huber, and Bruna M. Bezerra. "Hunting Strategies in Wild Common Marmosets Are Prey and Age Dependent." *American Journal of Primatology* 72, no. 12 (December 1, 2010): 1039–46. https://doi.org/10.1002/ajp.20860.

Schmidt, Dominik, and Thomas Schmied. "Fast and Data-Efficient Training of Rainbow: An Experimental Study on Atari." arXiv, November 19, 2021. http://arxiv.org/abs/2111.10247.

Scott, Stephen H. "Inconvenient Truths about Neural Processing in Primary Motor Cortex." *The Journal of Physiology* 586, no. 5 (2008): 1217–24. https://doi.org/10.1113/jphysiol.2007.146068.

Shenoy, Krishna V., Maneesh Sahani, and Mark M. Churchland. "Cortical Control of Arm Movements: A Dynamical Systems Perspective." *Annual Review of Neuroscience* 36, no. 1 (July 8, 2013): 337–59. https://doi.org/10.1146/annurev-neuro-062111-150509.

Sherrington. *Man On His Nature*, 1940. http://archive.org/details/in.ernet.dli.2015.188837.

Silver, David, Thomas Hubert, Julian Schrittwieser, Ioannis Antonoglou, Matthew Lai, Arthur Guez, Marc Lanctot, et al. "A General Reinforcement Learning Algorithm That Masters Chess, Shogi, and Go through Self-Play." *Science* 362, no. 6419 (December 7, 2018): 1140–44. https://doi.org/10.1126/science.aar6404.

Squartini, Tiziano, Francesco Picciolo, Franco Ruzzenenti, and Diego Garlaschelli. "Reciprocity of Weighted Networks." *Scientific Reports* 3, no. 1 (September 23, 2013): 2729. https://doi.org/10.1038/srep02729.

Stevenson, Ian H., Brian M. London, Emily R. Oby, Nicholas A. Sachs, Jacob Reimer, Bernhard Englitz, Stephen V. David, et al. "Functional Connectivity and Tuning Curves in Populations of Simultaneously Recorded Neurons." *PLoS Computational Biology* 8, no. 11 (2012): e1002775. https://doi.org/10.1371/journal.pcbi.1002775.

Taylor, Charlotte S.R., and Charles G. Gross. "Twitches versus Movements: A Story of Motor Cortex." *Neuroscientist*, 2003. https://doi.org/10.1177/1073858403257037.

Thach, W. T. "Correlation of Neural Discharge with Pattern and Force of Muscular Activity, Joint Position, and Direction of Intended next Movement in Motor Cortex and

Cerebellum." *Journal of Neurophysiology* 41, no. 3 (May 1, 1978): 654–76. https://doi.org/10.1152/jn.1978.41.3.654.

Thompson, William Hedley, Per Brantefors, and Peter Fransson. "From Static to Temporal Network Theory: Applications to Functional Brain Connectivity." *Network Neuroscience* 1, no. 2 (June 30, 2017): 69–99. https://doi.org/10.1162/NETN_a_00011.

Turchin, 1957-, Peter. *Quantitative Analysis of Movement : Measuring and Modeling Population Redistribution in Animals and Plants*. Sunderland, Mass.: Sinauer, 1998.

Vaadia, E., I. Haalman, M. Abeles, and H. Bergman. "Dynamics of Neuronal Interactions in Monkey Cortex in Relation to Behavioural Events." *Nature* 373, no. 6514 (February 9, 1995): 515–18. https://doi.org/10.1038/373515a0.

Vaidya, Mukta, Karthikeyan Balasubramanian, Joshua Southerland, Islam Badreldin, Ahmed Eleryan, Kelsey Shattuck, Suchin Gururangan, et al. "Emergent Coordination Underlying Learning to Reach to Grasp with a Brain-Machine Interface." *Journal of Neurophysiology* 119, no. 4 (April 1, 2018): 1291–1304. https://doi.org/10.1152/jn.00982.2016.

Vyas, Saurabh, Matthew D. Golub, David Sussillo, and Krishna V. Shenoy. "Computation Through Neural Population Dynamics." *Annual Review of Neuroscience* 43, no. 1 (July 8, 2020): 249–75. https://doi.org/10.1146/annurev-neuro-092619-094115.

Walker, Jeffrey D., Jason MacLean, and Nicholas G. Hatsopoulos. "The Marmoset as a Model System for Studying Voluntary Motor Control." *Developmental Neurobiology* 77, no. 3 (2017): 273–85. https://doi.org/10.1002/dneu.22461.

Walker, Jeffrey D., Friederice Pirschel, Nicholas Gidmark, Jason N. MacLean, and Nicholas G. Hatsopoulos. "A Platform for Semiautomated Voluntary Training of Common Marmosets for Behavioral Neuroscience." *Journal of Neurophysiology* 123, no. 4 (April 1, 2020): 1420–26. https://doi.org/10.1152/JN.00300.2019.

Walker, Jeffrey D., Friederice Pirschel, Marina Sundiang, Marek Niekrasz, Jason N. MacLean, and Nicholas G. Hatsopoulos. "Chronic Wireless Neural Population Recordings with Common Marmosets." *Cell Reports* 36, no. 2 (July 2021): 109379. https://doi.org/10.1016/j.celrep.2021.109379.

Watakabe, Akiya, Masanari Ohtsuka, Masaharu Kinoshita, Masafumi Takaji, Kaoru Isa, Hiroaki Mizukami, Keiya Ozawa, Tadashi Isa, and Tetsuo Yamamori. "Comparative Analyses of Adeno-Associated Viral Vector Serotypes 1, 2, 5, 8 and 9 in Marmoset, Mouse and Macaque Cerebral Cortex." *Neuroscience Research* 93 (April 1, 2015): 144–57. https://doi.org/10.1016/J.NEURES.2014.09.002.

Watakabe, Akiya, Osamu Sadakane, Katsusuke Hata, Masanari Ohtsuka, Masafumi Takaji, and Tetsuo Yamamori. "Application of Viral Vectors to the Study of Neural Connectivities and Neural Circuits in the Marmoset Brain." *Developmental Neurobiology* 77, no. 3 (2017): 354–72. https://doi.org/10.1002/dneu.22459.

Watanabe, Keita, Tatsuya Haga, Masami Tatsuno, David R. Euston, and Tomoki Fukai. "Unsupervised Detection of Cell-Assembly Sequences by Similarity-Based Clustering." *Frontiers in Neuroinformatics* 13 (2019): 39. https://doi.org/10.3389/fninf.2019.00039.

Wolpert, Daniel M., Jörn Diedrichsen, and J. Randall Flanagan. "Principles of Sensorimotor Learning." *Nature Reviews Neuroscience* 12, no. 12 (2011): 739–51.

Wu, Wei, and Nicholas Hatsopoulos. "Evidence against a Single Coordinate System Representation in the Motor Cortex." *Experimental Brain Research* 175, no. 2 (November 2006): 197–210. https://doi.org/10.1007/s00221-006-0556-x.

Yuste, Rafael. "From the Neuron Doctrine to Neural Networks." *Nature Reviews Neuroscience* 16, no. 8 (August 8, 2015): 487–97. https://doi.org/10.1038/nrn3962.

Zylberberg, Joel. "The Role of Untuned Neurons In Sensory Information Coding." *BioRxiv*, May 30, 2018, 134379. https://doi.org/10.1101/134379.